

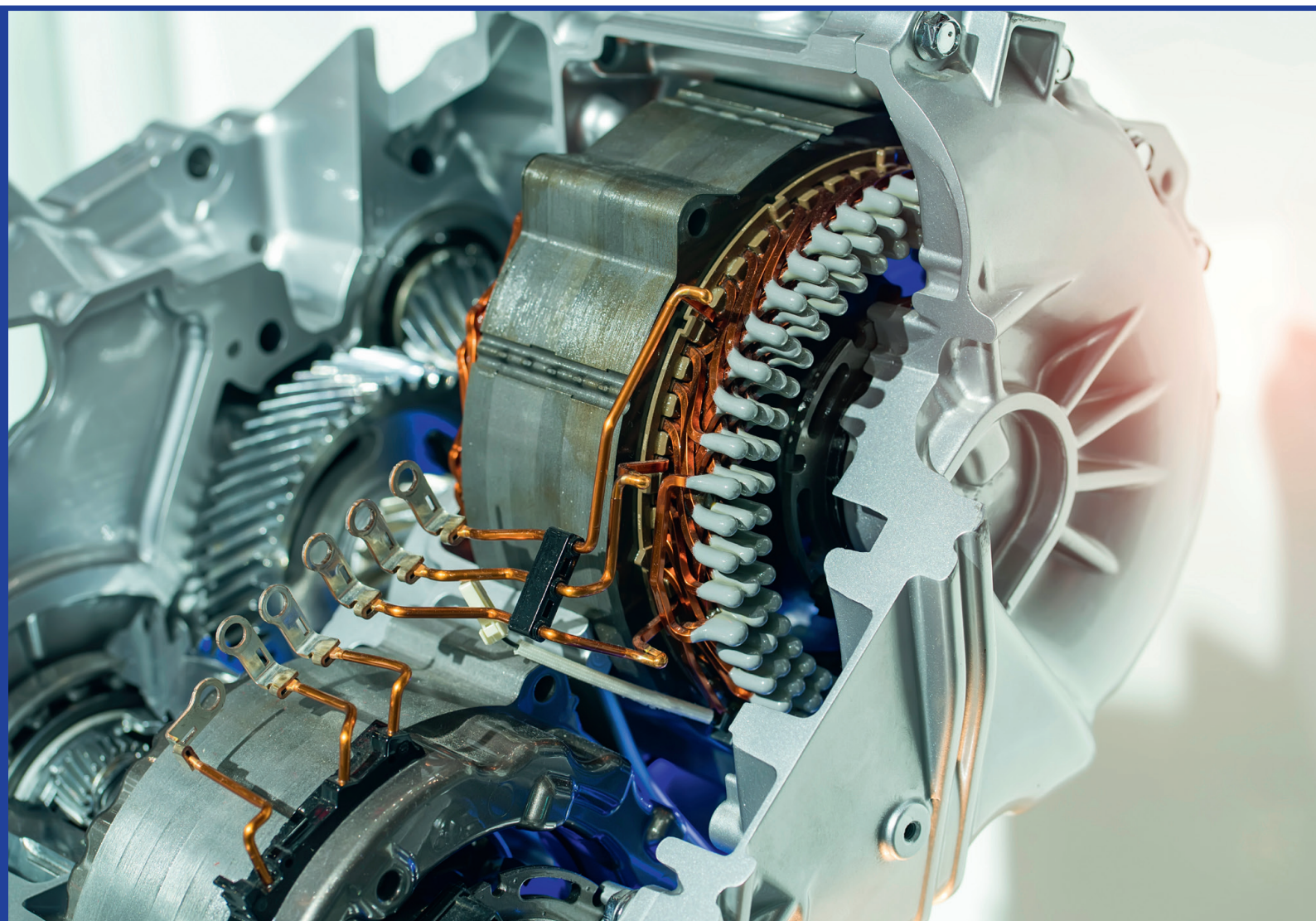


RIGA TECHNICAL  
UNIVERSITY

**Jaroslavs Zarembo**

**RESEARCH AND DEVELOPMENT  
OF THE SYNCHRONOUS RELUCTANCE  
MOTOR TRACTION DRIVE**

Doctoral Thesis



RTU Press  
Riga 2022

**RIGA TECHNICAL UNIVERSITY**

Faculty of Electrical and Environmental Engineering

Institute of Industrial Electronics and Electrical Engineering

**Jaroslavs Zarembo**

Doctoral Student of Study Program “Computerized Control of Electrical Technologies”

**RESEARCH AND DEVELOPMENT OF THE SYNCHRONOUS  
RELUCTANCE MOTOR TRACTION DRIVE**

**Doctoral Thesis**

Scientific Supervisor  
Professor *Dr. habil. sc. ing.*  
LEONĪDS RIBICKIS

RTU Press

Rīga 2022

Zarebo, J. Research and Development of The Synchronous Reluctance Motor Traction Drive. Doctoral Thesis. – Riga: RTU Press, 2022. – 80 p.

Published in accordance with the decision of the Promotion Council “RTU P-14” of 21 April 2022, Minutes No. 210.11.

# Contents

Introduction .....	5
1. Analysis of Trolleybus Traction Requirements .....	8
1.1. Trolleybus Dynamics Requirements .....	8
1.2. Construction of Reference Traction Characteristic .....	9
2. Design of the SynRM Traction Drive .....	12
2.1. Working Principle of SynRM .....	12
2.2. SynRM Design Prerequisites .....	13
2.3. Main Parameters and Design Limitations .....	13
2.4. Stator Design .....	14
2.5. Rotor Design .....	14
2.6. Parameters of the Designed Motor .....	15
2.7. Traction Characteristic of the Designed Motor .....	18
3. Development of Control Algorithm and Model .....	21
3.1. Mathematical Model of the SynRM .....	21
3.2. Implementation of Embedded Motor Control .....	23
3.3. SynRM Control Algorithm .....	27
3.3.1. Constant $i_d$ control .....	28
3.3.2. Maximum Rate of Change of Torque Control .....	28
3.3.3. Maximum Power Factor Control .....	29
3.3.4. Maximum Torque per Ampere Control .....	29
3.4. Simulink Model of the Electric Drive .....	29
3.4.1. High-level Overview of Algorithm .....	30
3.4.2. Field-Oriented Controller Algorithm .....	32
3.4.3. Mathematical Model of the Trolleybus .....	34
4. Experimental Investigation of SynRM Traction Drive .....	37
4.1. Production Process of the SynRM Traction Drive .....	37

4.2.	Laboratory Testing of the Developed SynRM Traction Drive .....	41
4.2.1.	Laboratory Equipment .....	41
4.2.2.	Traction Characteristic of SynRM.....	45
4.3.	Laboratory Investigation of SynRM Parameters.....	49
4.3.1.	Mechanical Losses .....	50
4.3.2.	Stator Winding Resistance.....	51
4.3.3.	D- and q-axis Inductances.....	51
4.3.4.	Thermal testing of SynRM .....	53
5.	Verification of SynRM Control System Performance in Traction Drive .....	55
5.1.	Investigation of SynRM and IM Performance in Traction .....	55
5.1.1.	Comparison of Maximum Torque Capabilities .....	55
5.1.2.	Comparison of Efficiency Indicators .....	56
5.1.3.	Distribution of IM and SynRM losses .....	59
5.1.4.	Comparison of Power Factor .....	60
5.1.5.	Summary of the comparison .....	61
5.2.	Performance of the SynRM Traction Drive Simulink Model.....	61
5.2.1.	The rated rotational speed test .....	61
5.2.2.	Test at different speeds .....	63
5.2.3.	Acceleration till the maximum speed .....	64
5.2.4.	Performance of the model.....	66
	Conclusions .....	70
	List of References.....	72
A1.	Appendix.....	76
A2.	Appendix.....	77
A3.	Appendix.....	78

## Introduction

The problem of ecology and greenhouse emissions has become critical in the modern world. In cities, transport is the largest source of CO<sub>2</sub> and other emissions. The solution to the problem should be the transfer of the transport system of a large city to an electric drive. Electric transport reduces noise levels, eliminates exhaust pollution, and helps to overcome dependence on oil by allowing electricity to be used for power, which in turn can be obtained from alternative sources. Addressing the issue a special-purpose EU programme on reducing greenhouse gas emissions in urban transport by 60% by 2050 has been adopted [1].

One of the existing transport types that can be used to achieve the set goal is a trolleybus. The trolleybus was first introduced in 1882, when Dr Ernst Werner ran his bus in Berlin suburbs. Already in 1901 the world's first passenger-carrying trolleybus operated in Bielathal, in Germany. However, later with abundant amount of oil and lack of environmental regulations urban electric transport became less economically viable and eventually in many cities stopped being used. Fossil fuel was cheap and overhead traction grid wires were thought to spoil the view and require expensive maintenance [2]. Nowadays trolley bus infrastructure remains in approximately 300 cities in the world, but due to environmental policy has changed over the past decades and trolleybuses can again find their place in the infrastructure of the new green community.

Many studies have been carried out to find new solutions to improve the performance of a trolleybus. The main trends were focusing on ensuring the ability to drive autonomously on some route sections and saving energy by installing on-board energy storage devices. Storage systems based on supercapacitors or batteries have proven their efficiency, however, their installation leads to a significant rise in the cost of a set of electrical equipment [3]. An alternative could be a complete replacement of trolleybuses with electric buses, but this entails a complete restructuring of the city's infrastructure to ensure fast charging. Another solution could be a hybrid trolleybus system with in motion charging on a limited section of the track [4]. Thus, the general trend in the development of the trolleybus is the installation of on-board energy storage devices.

With the emergence of vehicles with on-board energy sources, the issue of power reserve comes to the forefront. Portable energy storage devices with high capacity such as lithium-ion batteries, fuel cells, and supercapacitors are the most expensive part of an electric drive, therefore the most important task of a traction system is high efficiency rates. Regardless of

the used energy source, total consumed energy for the movement of the vehicle directly depends on the efficiency of the motor in a whole working range.

In most of modern trolleybus traction systems conventional induction motors (IM) are used. The advantages of the IM drive are reliability, relatively low cost of the set and the robust and proven control system. Though, nowadays high efficiency demands are hardly met by this type of drive system. Another solution is permanent magnet synchronous motor (PMSM) drive that provides the best indicators of power-to-mass ratio, as well as the best possible efficiency [5]. Drawbacks of PMSM are high cost of permanent magnets, as well as the dependence on a monopoly supplier. Both mentioned options are already well known and widely used in traction. However, introduction of alternative traction motor drive topologies could lead to optimisation of working parameters for a specific use case.

Potentially promising solution is the use of synchronous electric motors without active elements in the rotor. This approach reduces material costs, increases efficiency due to the absence of resistive losses in the rotor, and simplifies the manufacturing process. The most commonly topologies are switched reluctance motor (SRM) and synchronous reluctance motor (SynRM).

SRM is gaining popularity nowadays but has several disadvantages such as relatively low torque density, higher torque ripple and acoustic noise [6]. Acoustic noise and torque ripple are restraining factors in the development of this type of electric motors. SynRM is less prone to the inherent disadvantages of SRM. In addition, the electric motor uses a distributed winding, which is classical for IM, which makes it possible to retain the topology of the power inverter [7]. However, due to nonlinearity of the characteristics, the design process of SynRM and the development of control system for such machines are more complex tasks.

In traction applications, SynRM is a good alternative for induction motors. While it was introduced in 1923, only nowadays due to improvements in computational power of microprocessors, and more sophisticated computer aided analysis methods it is becoming more widespread [8].

The main aim of the Doctoral Thesis is the design, development and testing of an electric drive based on SynRM and a two-level frequency inverter for traction application. Within the work an electric motor in the overall dimensions of an existing serial IM for a trolleybus was developed, manufactured, and investigated. At the time of the start of the research, JSC “RER” produced only traction asynchronous electric motors. The result of the work was the development and testing of a new model of traction SynRM with control system for trolleybus drive. The fulfilment of the set goals made it possible for the company to gain experience in

the production technology of a new type of electric motors. Work on the topic was carried out within the framework of a European project at JSC “RER”.

The tasks are:

- analysis of of the electric motor design;
- production of electric motor prototype;
- creation of control system in a Matlab Simulink environment;
- development and deployment of embedded control software;
- testing of the produced electric motor with deployed control system on a laboratory setup.

The Doctoral Thesis has been written in English. It consists of Introduction, 5 chapters, Conclusions, 58 figures, 12 tables, and 2 appendices; the total number of pages is 80, including appendices. The Bibliography contains 40 titles.

# 1. Analysis of Trolleybus Traction Requirements

Design process of the electric drive requires understanding dynamics of the vehicle under consideration, for it to properly set criteria for the traction at different speeds. This chapter describes underlying requirements for the dynamics of the trolleybus and construction of the traction characteristic.

## 1.1. Trolleybus Dynamics Requirements

In the case of this research, the vehicle under consideration is trolleybus. The trolleybus technical specification is provided by the manufacturer and is shown in Table 1.1. Trolleybus is 12 m single section.

Table 1.1  
Trolleybus Parameters

Parameter	Unit	Value
Laden mass	[ton]	18.9
Gearbox number		9.84
Gearbox efficiency	%	97
Wheel diameter	[m]	0.88 (275/70R22.5)
Maximum working speed, at least	[km/h]	60
Acceleration till 45 km/h, at most	[s]	18
Maximum acceleration, at most	[m/s <sup>2</sup> ]	1.2
Maximum deceleration, at most	[m/s <sup>2</sup> ]	0.8
Rated voltage of overhead lines	[VDC]	550
Minimal voltage of overhead lines	[VDC]	400
Maximum voltage of overhead lines	[VDC]	700

In addition to the requirements in Table 1.1, trolleybus should abide by the following additional requirements to the dynamics:

- Electric drive should be able to sustain constant rated torque up to rated frequency of 50 Hz.
- Trolleybus should be able to sustain and reach speed of 45 km/h at 12 % of road inclination.
- At maximum speed of 60 km/h electric drive should have residual force of at least 10% above resistive force.

Based on all mentioned requirements to the dynamics of the vehicle traction characteristic is constructed, to be used for the design process and laboratory validation of the electric drive with SynRM.

## 1.2. Construction of Reference Traction Characteristic

In general, traction characteristic consists of three regions: constant torque, constant power ( $T_{elm} \cdot \omega_m \cong const.$ ), and  $T_{elm} \cdot \omega_m^2 \cong const.$ , separation of regions is shown in Fig. 1.1 [9]. From this knowledge, traction characteristic for the trolleybus is constructed based on dynamic requirements and two transition points, one is 50 Hz, and the other is chosen so that at maximum speed residual torque requirement is fulfilled. Equations for the calculation are derived from the linear model of the vehicle. Approach to the traction characteristic calculation is described further.

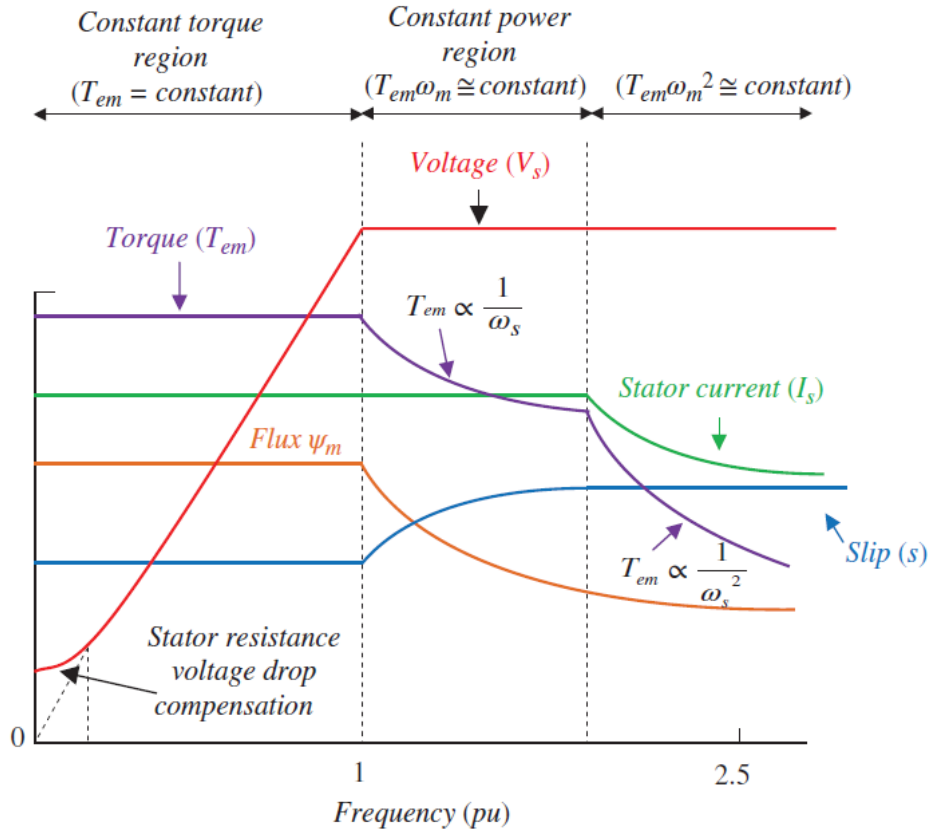


Fig. 1.1. Operating regions of the motor.

Calculation algorithm input data: trolleybus parameters, region 1 to 2 transition point (50 Hz), region 2 to 3 initial transition point, reference time up to 45 km/h, maximum allowable acceleration, initial value of constant power.

$$\begin{aligned}
 P_{1^{st} \text{ region}} &= P_{cnst} \cdot \frac{\omega_m}{\omega_{1to2}} \\
 P_{2^{nd} \text{ region}} &= P_{cnst} \\
 P_{3^{rd} \text{ region}} &= P_{cnst} \cdot \frac{\omega_{2to3}}{\omega_m}
 \end{aligned} \tag{1.1.}$$

where  $\omega_m$  is mechanical speed, is set to be range from 0 to max speed with some predetermined step  $dv$ .

Curve based on initially set transition point from 2 to 3, and constant power is constructed from three pieces as shown above:

$$P_{shaft} = \begin{cases} P_{1^{st} region}, & \omega_m = [0, \omega_{1to2}) \\ P_{2^{nd} region}, & \omega_m = [\omega_{1to2}, \omega_{2to3}) \\ P_{3^{rd} region}, & \omega_m = [\omega_{2to3}, \omega_{max}] \end{cases} \quad (1.2)$$

$$T_{shaft} = \frac{P_{shaft}}{\omega_m}$$

$$F_{wheel} = T_{shaft} \cdot \frac{\mu}{D/2} \cdot \eta_{gbx}$$

where  $\mu$  is gearbox ratio,  $D$  is wheel diameter, and  $\eta_{gbx}$  is gearbox efficiency.

Next step is calculation of force used for movement of the trolleybus, by subtracting resistive force and force due to slope. Per unit or relative resistance force is generalised for the trolleybus and is in  $N/kN$  units. Approach to the calculation is described in the model of electric drive chapter.

$$w_{res pu} = 12 + 0.004 \cdot v^2$$

$$F_{res} = w_{res pu} \cdot mg$$

$$F_{slope} = \sin\left(\text{atan}\frac{\alpha}{1000}\right) \cdot mg \quad (1.3)$$

$$F_{move} = F_{shaft} - F_{res} - F_{slope}$$

where  $\alpha$  is the slope in permille.

Last step in the calculation is determination of acceleration, and travel time.

$$a = \frac{F_{move}}{m \cdot (1 + \gamma)}$$

$$dt = \frac{dv}{a} \quad (1.4)$$

$$t_{total} = \sum dt$$

$$a_{mean} = \frac{v_{max}}{t_{total}}$$

Algorithm is repeated until requirement of time till 45 km/h being at most 18 seconds, and  $\frac{F_{wheel} - F_{res}}{F_{res}} \geq 10\%$ . At each iteration value of constant power and value of region 2 to 3 transition are adjusted. In the end both values are chosen approximately, with some safety margin.

As the requirement for the acceleration is not very strict, there are several appropriate for the provided dynamics requirements. Two optimal solutions are presented in Table 1.2. The

first one provides a more agile movement for the trolleybus at the cost of higher output power, the second proposed solution has lower acceleration of the vehicle and a possibility to reduce the size of the motor.

Table 1.2  
Proposed solutions for traction characteristic

	Solution 1	Solution 2
$P_{cnst}$ [kW]	180	170
Horizontal road		
Time to 45 km/h, s	16.24	17.42
$a_{max}$ [ $m/s^2$ ]	1.02	0.96
Residual force at 60 km/h	26.3%	19.3%
Top speed, km/h	64.6	63.4
12 % Inclination		
Time to 45 km/h, s	19.27	20.99
$a_{max}$ [ $m/s^2$ ]	0.92	0.86
Residual force at 54 km/h	23.2%	13.6%
Top speed, km/h	56.9	55.7

Both solutions fulfil the requirements for movement. Solution 1 has higher reserve for operation, even being able to accelerate to 45 km/h in just under 18 seconds at inclined road, while Solution 2 has much less of a reserve.

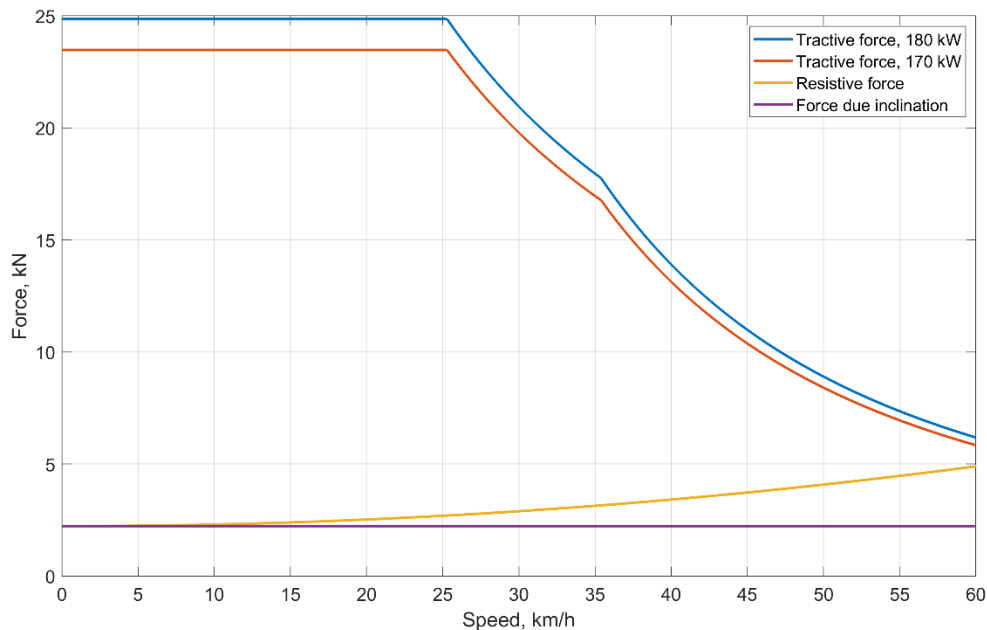


Fig. 1.2. Graphical representation of proposed traction characteristics.

Fig. 1.2 is a graphical representation of proposed traction characteristics with resistive force and gravitational forces due to inclination.

## 2. Design of the SynRM Traction Drive

Design and production of the SynRM prototype is done as a part within the frame of the European Project. The design process has been published in a The Latvian journal of physics and technical sciences [10]. Full description of the design and testing process was presented at the 23<sup>rd</sup> European Conference on Power Electronics and Applications [11]. This chapter gives a brief description of the design process with input data and results.

### 2.1. Working Principle of SynRM

The operation of a SynRM is based on the difference between the inductances of the direct and quadrature axes. This idea can be explained using Fig. 2.1 [12]. In this figure object “a” with anisotropic magnetic material has different (geometric) reluctances in the  $d$ -axis and  $q$ -axis. Whereas the isotropic magnetic material geometry in object “b” has similar in all directions.

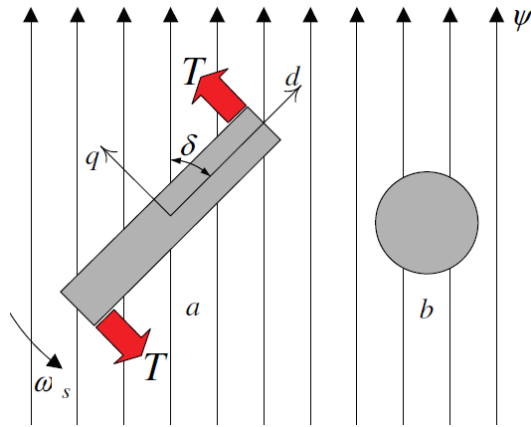


Fig. 2.1. An object with anisotropic (a) and isotropic (b) geometry.

Magnetic field  $\psi$  which is applied to the anisotropic object, produces torque if there is an angle difference between the  $d$ -axis and the field ( $\delta \neq 0$ ), or if the  $d$ -axis of object “a” is not aligned with the field [12].

In the SynRM field  $\psi$  is produced by a sinusoidally distributed winding in a slotted stator and it links the stator and rotor through a small airgap, exactly as in a traditional induction motor. The field is rotating at synchronous speed,  $\omega_s$ , and can be assumed to have a sinusoidal distribution. In this situation there will always be a torque which acts to reduce the potential energy of the whole system by reducing the distortion field in the  $q$ -axis, ( $\delta \rightarrow 0$ ). If  $\delta$ , the load angle, is kept constant then electromagnetic energy will be continuously converted into mechanical energy.

Therefore, the two most important parameters are: inductances  $L_d$  and  $L_q$  the direct and quadrature axes respectively. The power of a synchronous reluctance machine is obtained from the load angle equation (0.1.) [13].

$$P = 3U_s^2 \frac{L_d - L_q}{2\omega_s L_d L_q} \sin 2\delta = \frac{3U_s^2}{2\omega_s} \left( \frac{1 - \frac{L_q}{L_d}}{L_q} \right) \sin 2\delta, \quad (0.1.)$$

where

$U_s$  – stator phase voltage;

$L_d$  and  $L_q$  – d- and q-axis inductances;

$\delta$  – load angle;

$\omega_s$  – synchronous angular velocity.

As it can be seen in (0.1.) that the smaller the quadrature-axis synchronous inductance and the higher the direct-axis inductance, the higher is the power and torque at a certain load angle. In practice, the limiting value for  $L_q$  is the stator leakage inductance  $L_{s\sigma}$ ; consequently,  $L_q > L_{s\sigma}$ . It is the task of the designer to maximize the inductance ratio  $L_d/L_q$  to achieve a good performance.

The equation (0.1.) suggests that  $L_d - L_q$ , the difference of the d-axis and q-axis synchronous inductances, should be as large as possible, and  $L_d L_q$  should be as small as possible to produce maximum power. In practice, the target is to maximize the d-axis inductance and to minimize the q-axis synchronous inductance.

In principle, the machine can yield its maximum torque at load angle  $\delta = 45^\circ$ . Saturation and other phenomena may cause apparent deviation from this value [14].

## 2.2. SynRM Design Prerequisites

The target application of the developed SynRM is a trolleybus. Trolleybus under consideration already exists and has been in use with the induction traction motor. Replacement of IM with the SynRM is a part of research of different possibilities on motor variants for this application. Based on that, the most crucial constraint for the design of SynRM is outer case sizing, which should fit the predetermined place of the IM in the trolleybus.

Optimisation factor chosen for the design process of SynRM is highest efficiency at the rated point.

## 2.3. Main Parameters and Design Limitations

Sizing is based on the in-production induction motor for the trolleybus application (made by JSC “RER”). As SynRM was developed to replace IM, the casing size, electrical supply

parameters, mechanical parameters, and construction possibilities of the manufacturer (airgap width  $\delta$ ) had to be considered.

The rated point for SynRM is chosen the same as for the induction motor, as it is well suited for the chosen traction characteristic. The rated point and sizing constraints are presented in Table 2.1.

Table 2.1  
Rated Point and Sizing Limitations of SynRM

Parameter	Unit	Value
Rated output power	$P_n$ [kW]	180
Rated voltage	$U_n$ [V]	420
Rated frequency	$f_1$ [Hz]	50
Number of pole pairs		2
Number of phases		3
Operating regime		S2-60 min
Stator outer diameter	$D_{os}$ [mm]	493
Stator stack length	$L$ [mm]	290
Airgap width	$\delta$ [mm]	1.2

## 2.4. Stator Design

The stator was designed by performing calculations described in literature sources [15], [16], [13], and [17] with the addition of mathematical modelling of the magnetic field using the finite element modelling method (FEM). For stator parameter optimization, all FEM was performed by solving a magnetostatic model with defined three-phase currents in windings. Computations were for a non-linear model with electrotechnical steel SURA M470-50HP described by  $B(H)$  curve, which was used for the manufactured prototype.

## 2.5. Rotor Design

The rotor was designed by FEM magnetic field modelling for various rotor models. Important parameters were chosen from recommendations in the literature. The number of flux barriers and their positioning were chosen by the method described in [18], and [19]. The width of the rotor barriers and flux paths were chosen from recommendations in [20]. Arch and trapezoid types of flux barriers were considered. The designed rotor with the main geometrical parameters is presented in the Fig. 2.2.

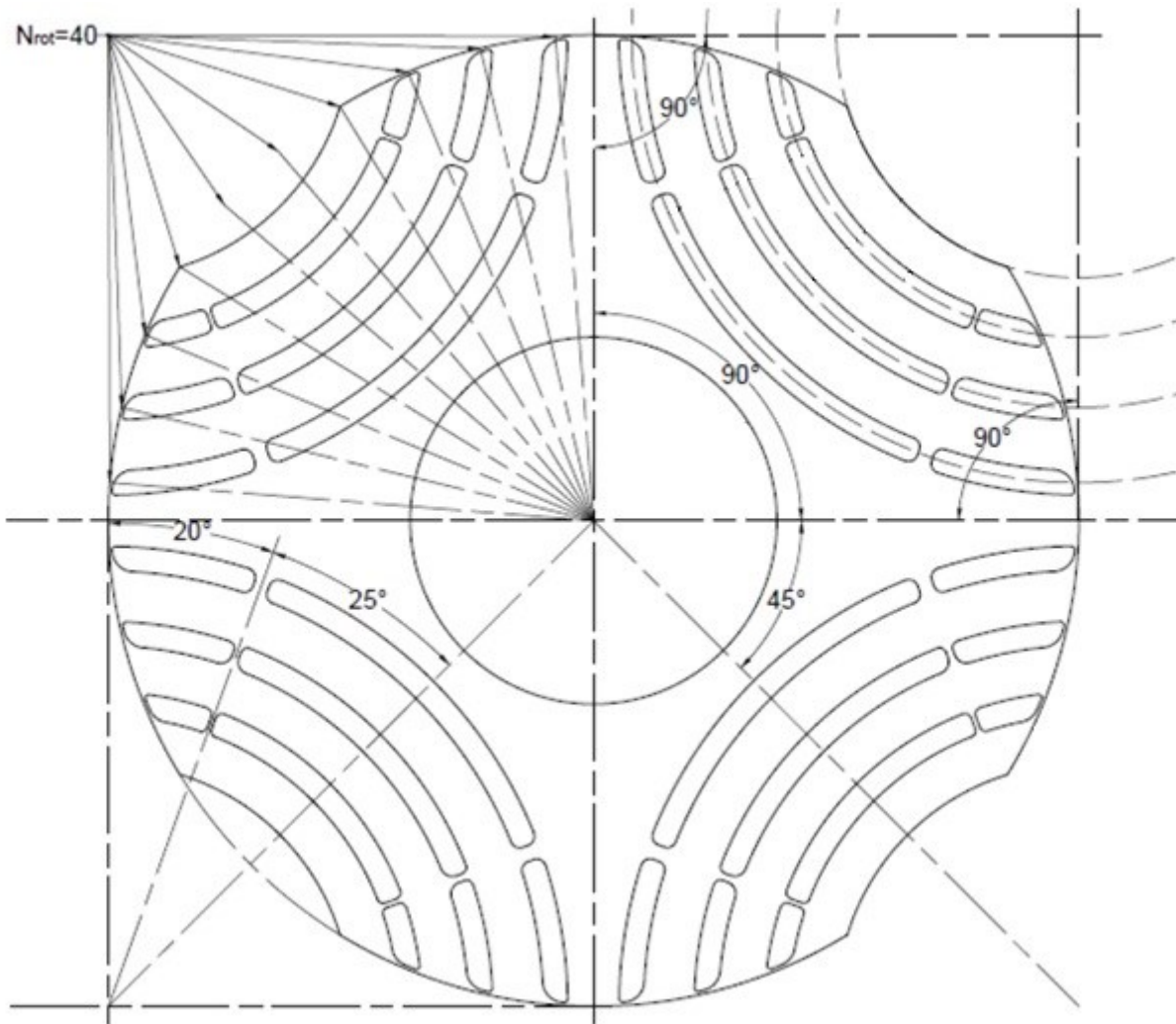


Fig. 2.2 SynRM rotor sheet geometry.

To guarantee the mechanical strength of the rotor it is necessary to create bridges – sections of steel left to physically connect adjacent flux paths across the flux barriers. Bridges reduce magnetic asymmetry by forming a path for quadrature axis flux, but they are essential for the structural integrity of the rotor. For designed machine bridges reduce the maximum torque by 7 %.

## 2.6. Parameters of the Designed Motor

To evaluate the design process, losses were split into their components. Winding losses were calculated from stator winding resistance at 75 °C, iron and mechanical losses were calculated from the no-load experiment. In reported data, additional load losses include frequency converter supply related losses, harmonic losses introduced by voltage waveform of the frequency converter. Reported values are at a constant 50 Hz frequency. Table 2.2 presents the comparison between designed SynRM and IM test results.

Table 2.2  
Comparison of SynRM (FEM modelling) and IM test results

Parameter	Unit	Design	IM
Supply current	$I_1 [A]$	392.4	309
Supply voltage	$U_1 [A]$	420	420
Power factor	$\cos \varphi$	0.663	0.85
Supply power	$P_{in} [W]$	189200	191400
Mechanical power	$P_{out} [W]$	179144	177989
Rotor angular velocity	$n [RPM]$	1500	1471
Mechanical torque	$T_{out} [W]$	1141	1156
Stator winding losses	$\Delta P_{el1} [W]$	5637	5017
Rotor winding losses	$\Delta P_{el2} [W]$	-	3580
Iron losses	$\Delta P_{mag} [W]$	2873	1940
Mechanical losses	$\Delta P_{mech} [W]$	544	960
Additional load losses	$\Delta P_{add} [W]$	1002	1914
Total losses	$\Sigma \Delta P [W]$	10056	13411
Efficiency	$\eta [\%]$	94.69	92.99

SynRM power factor (0.663) is low compared to IM (0.89) consequently the current is higher. When designing SynRM a trade-off between the power factor and torque capacity is unavoidable. The primary goal of the research was to obtain the required torque and efficiency reducing possibility for power factor optimization.

The designed synchronous motor overload capacity is 1.15. Maximum efficiency of the motor is  $\eta = 94.69 \%$ , in rated load mode. The developed motor has a high efficiency factor, but low overload capacity. The motor has been developed for the purposes of getting maximum power at set outer sizes, voltage, and preferable efficiency factor. With the given outer sizes and the selected rotor design, the maximum torque may be increased only by reducing the efficiency factor. Overload capacity can be increased by creating a longer machine, which increases magnetic flux.

Winding temperature rise for rated load mode is  $73.6 \text{ }^\circ\text{C}$ . The calculated temperature rise in the rate load mode is considerably lower than the maximum permissible temperature than that of the selected slot insulation thermal class.

Inner stator diameter and slot width values were selected in the course of the work, which ensure higher ratio of impedances at the set parameters.

The rotor design has been created based on the information available in literature on the design, which ensures minimum electromagnetic torque oscillations.

The magnetic field pictures are shown in Fig. 2.3 and Fig. 2.4. Field distribution shows that the motor in rated mode is saturated, induction on teeth is up to 2 T and in the stator yoke up to 1.6 T.

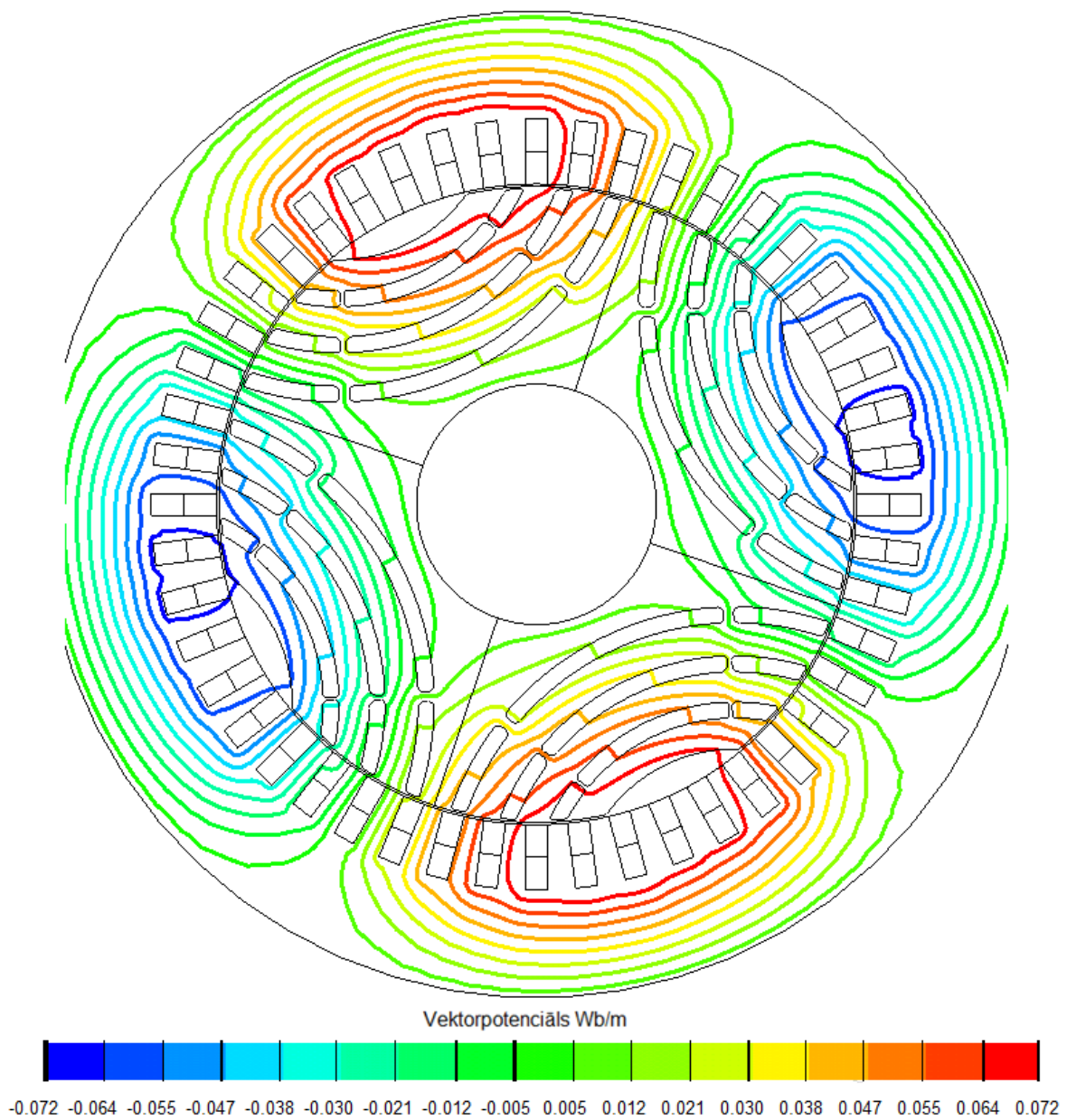
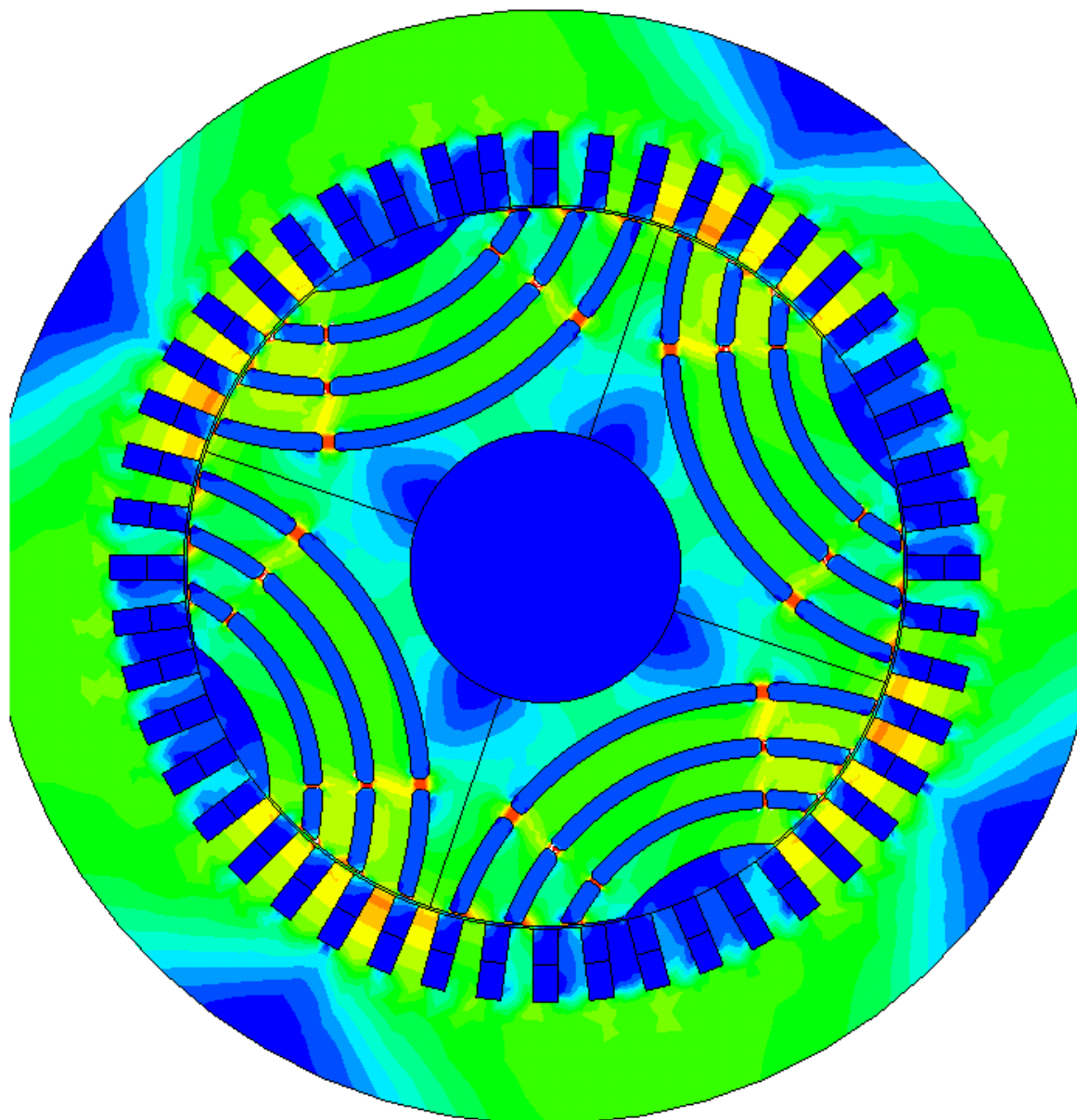


Fig. 2.3. Picture of magnetic field of the developed motor in rated mode, (Wb/m).



Magnētiskā lauka indukcija, T

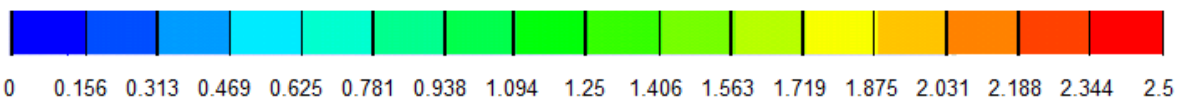


Fig. 2.4. Picture of magnetic field of the developed motor in rated load mode.

### 2.7. Traction Characteristic of the Designed Motor

Designing of the motor is followed by the calculation of parameters at different operation points, to see whether the designed motor is capable to either produce required reference torque or accelerate the trolleybus in required time.

Therefore, an algorithm is developed to calculate the parameters of Synchronous Reluctance Machine (SynRM) and to construct motor characteristics, considering the cross magnetic saturation effect. The algorithm is presented in a flow chart in Fig. 2.5 [21]. The

algorithm includes a numerical calculation part (steps: 1, 3, 4 and 5) and an FEM part (step 2). FEM is performed by defining three-phase currents in winding and solving the magnetostatics model.

The algorithm is designed for the machine mode at sinusoidal AC voltage, although in practice the SynRM is almost always coupled with a drive. Motor design calculations are usually made on the assumption that the operation is provided by a sinusoidal AC voltage [15]. The developed algorithm differs from the Kamper method [22] in that the reluctances are determined by calculating the electromagnetic torque by the FEM and according to the vector diagram of SynRM the reluctances of the armature direct axis and quadrature axis are determined. Similar algorithm for the induction machine mode determination that involves FEM calculations for the reactance computation with the voltage and the phase angle as the end criteria is presented in [23]. The developed method and calculation steps are described in more detail in publication [21].

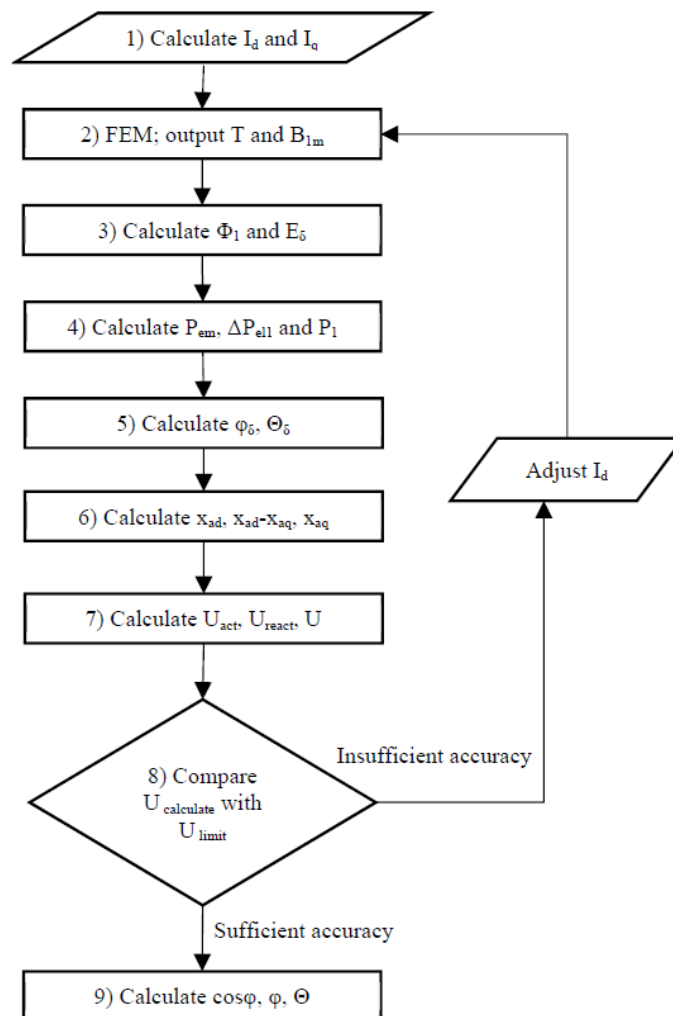


Fig. 2.5. Calculation algorithm flow-chart [21].

In outline, the algorithm has  $d$ - and  $q$ -axis currents and field frequency (rotational speed) as inputs from which other parameters are iteratively calculated up to specific accuracy. Input currents are adjusted to stay within the voltage limit.

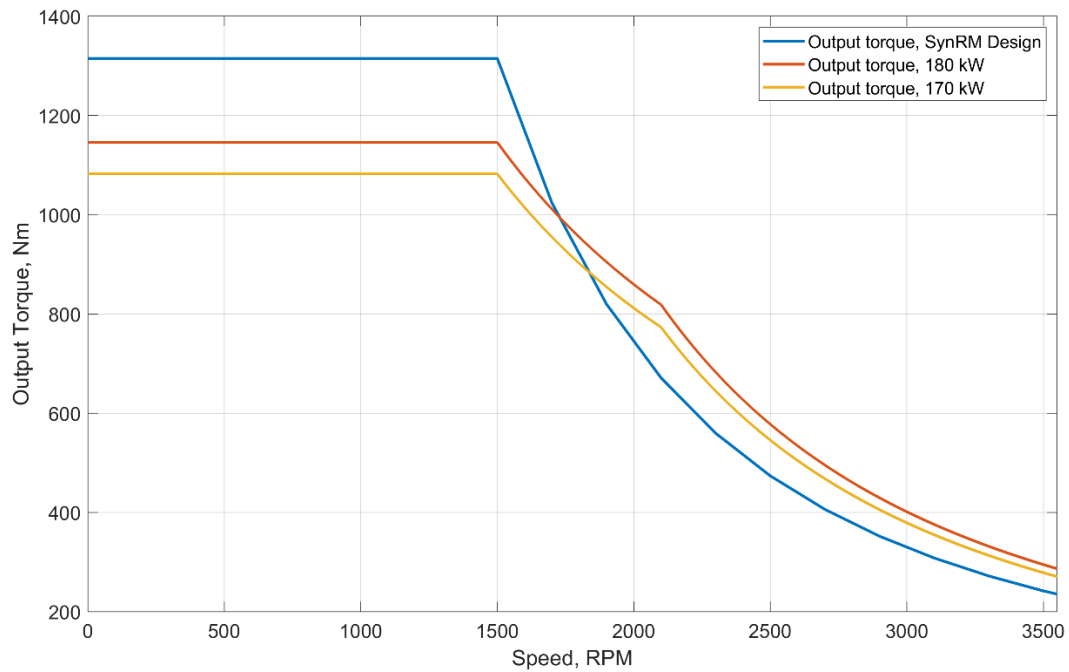


Fig. 2.6. Traction characteristic of the designed SynRM.

After the calculations, traction characteristic is obtained from 20 Hz (600 RPM) up to 120 Hz (3600 RPM, which corresponds to 65 km/h) with maximum obtainable torque limited by the rated voltage of 420 V. Fig. 2.6 presents the traction characteristic with the designed SynRM, and reference curves for reference.

### 3. Development of Control Algorithm and Model

Electric drive performance and robustness is vitally dependent on the control system. Due to the reluctance nature of the produced torque, SynRM has highly nonlinear characteristics, therefore design of its control algorithm is a challenging issue. The developed control system is based on fundamental SynRM equations, which were introduced in field-oriented control algorithm. Matlab Simulink model was created for verification of the control system.

This chapter describes the mathematical model of SynRM, control approach for SynRM and modelling of the control system in Simulink.

#### 3.1. Mathematical Model of the SynRM

Inherently SynRM cannot be operated without inverter, and primarily two control methods are used for precise control: field-oriented control and direct torque control. Both approaches provide separate control of motor magnetisation and torque. These methods rely on mathematical models of the motor in rotating reference frame. The following equations is a commonly used mathematical model of the motor [24]:

$$\begin{aligned}v_d &= R_s i_{ds} - \omega_s L_q i_{qm} + L_d \frac{di_{dm}}{dt}, \\v_q &= R_s i_{qs} + \omega_s L_d i_{dm} + L_q \frac{di_{qm}}{dt},\end{aligned}\tag{3.1.}$$

where  $i_{ds}$  and  $i_{qs}$  are stator current d- and q-axis components and  $R_s$  is stator winding resistance.

SynRM stator currents and torque producing currents are different because of iron loss, and their relation is shown in the equation (3.2.).

$$\begin{aligned}i_{ds} &= i_{dm} - \frac{1}{R_c} (\omega_s L_q i_{qm}), \\i_{qs} &= i_{qm} + \frac{1}{R_c} (\omega_s L_d i_{dm}),\end{aligned}\tag{3.2.}$$

where  $R_c$  is iron loss resistance.

The mathematical model is derived from the equivalent circuit representation of SynRM shown in Fig. 3.1 with the vector diagram of SynRM at steady-state in Fig. 3.2 [12].

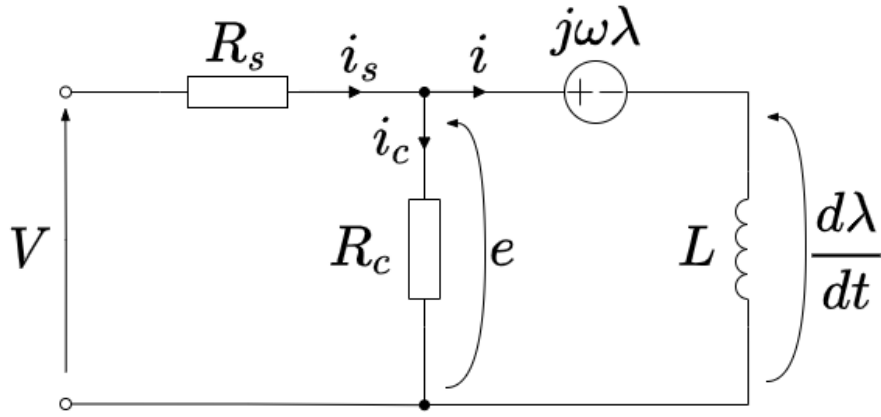


Fig. 3.1. SynRM equivalent circuit including iron loss.

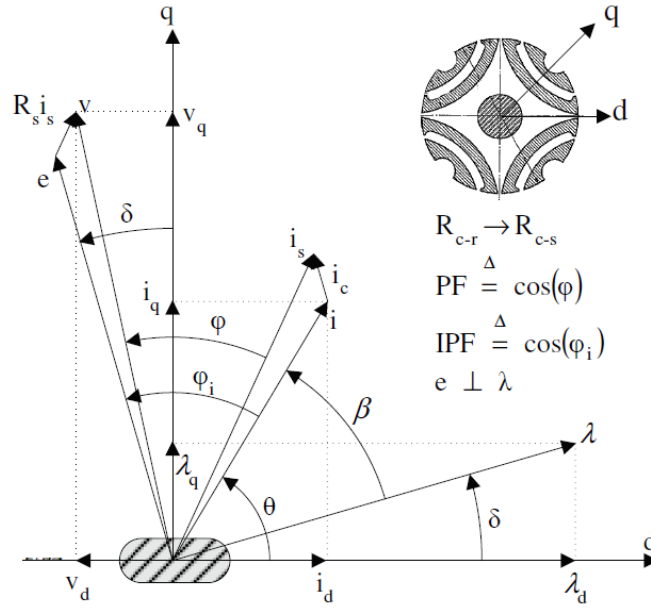


Fig. 3.2. Vector diagram of SynRM at steady-state, where  $\delta$  is load angle,  $\theta$  is current angle,  $\beta$  is the torque angle, and  $\varphi$  and  $\varphi_i$  are the angles corresponding to power factor and internal power factor respectively. They differ due iron and copper losses.

Stator flux is defined as follows in the equation (3.3.).

$$\begin{aligned} \psi &\cong \psi_d(i_d, i_q) + j \cdot \psi_q(i_d, i_q) \\ &\cong L_d(i_d, i_q) \cdot i_d + j \cdot L_q(i_d, i_q) \cdot i_q \end{aligned} \quad (3.3.)$$

The magnetising inductances are not free of saturation and cross-coupling, there they are represented as a function of both current components. In the Chapter 4.3.3 is the representation of such  $d$ - and  $q$ -axis inductances.

After the magnetizing inductances, the next most important parameters of SynRM are the machine saliency ratio  $\xi(i_d, i_q)$  that is defined according to Equation (3.4.), machine load angle  $\delta$ , current angle  $\theta$ , torque angle  $\beta$  and internal power factor angle  $\varphi_i$ . These angles, as shown in Fig. 3.2, are interconnected together by Equation (3.5.).

$$\xi(i_d, i_q) = \frac{L_d(i_d, i_q)}{L_q(i_d, i_q)} \quad (3.4.)$$

$$\theta = \beta + \delta, \quad \frac{\pi}{2} + \delta = \theta + \varphi_i \quad (3.5.)$$

The main magnetic and electric parameters of the SynRM, using the machine model based on Equations (3.3.) - (3.5.), are interconnected together through Equation (3.6.) [12].

$$\frac{-1}{\tan(\theta + \varphi_i)} = \tan \delta = \frac{\psi_q}{\psi_d} = \frac{L_q i_q}{L_d i_d} = \frac{1}{\xi} \tan \theta \quad (3.6.)$$

### 3.2. Implementation of Embedded Motor Control

The motor control system was developed on a control board with MCU TI TMS320F28335. The control unit was specially designed for an inverter with DC link voltage up to 1 kV and rated power up to 350 kW. The switching frequency of the inverter is 2 kHz.

The characteristics of the controller used in the inverter are in Table 3.1

DSC . The complete functional structure of the controller is shown in Fig. 3.3. DSC TMS320F28335 functional block diagram.

Table 3.1

DSC TMS320F28335 features

Digital Signal Controllers Type	TMS320F28335
Instruction cycle	6.67 ns (150 MHz)
Floating-point unit	Yes
3.3-V on-chip flash (16-bit word)	256K
Single-access RAM (SARAM) (16-bit word)	34K
PWM channels	ePWM1/2/3/4/5/6
32-bit QEP channels (four inputs/channel)	eQEP1/2
12-bit ADC	16 channels
Enhanced Controller Area Network (eCAN)	2 (A/B)
Serial Peripheral Interface (SPI)	1

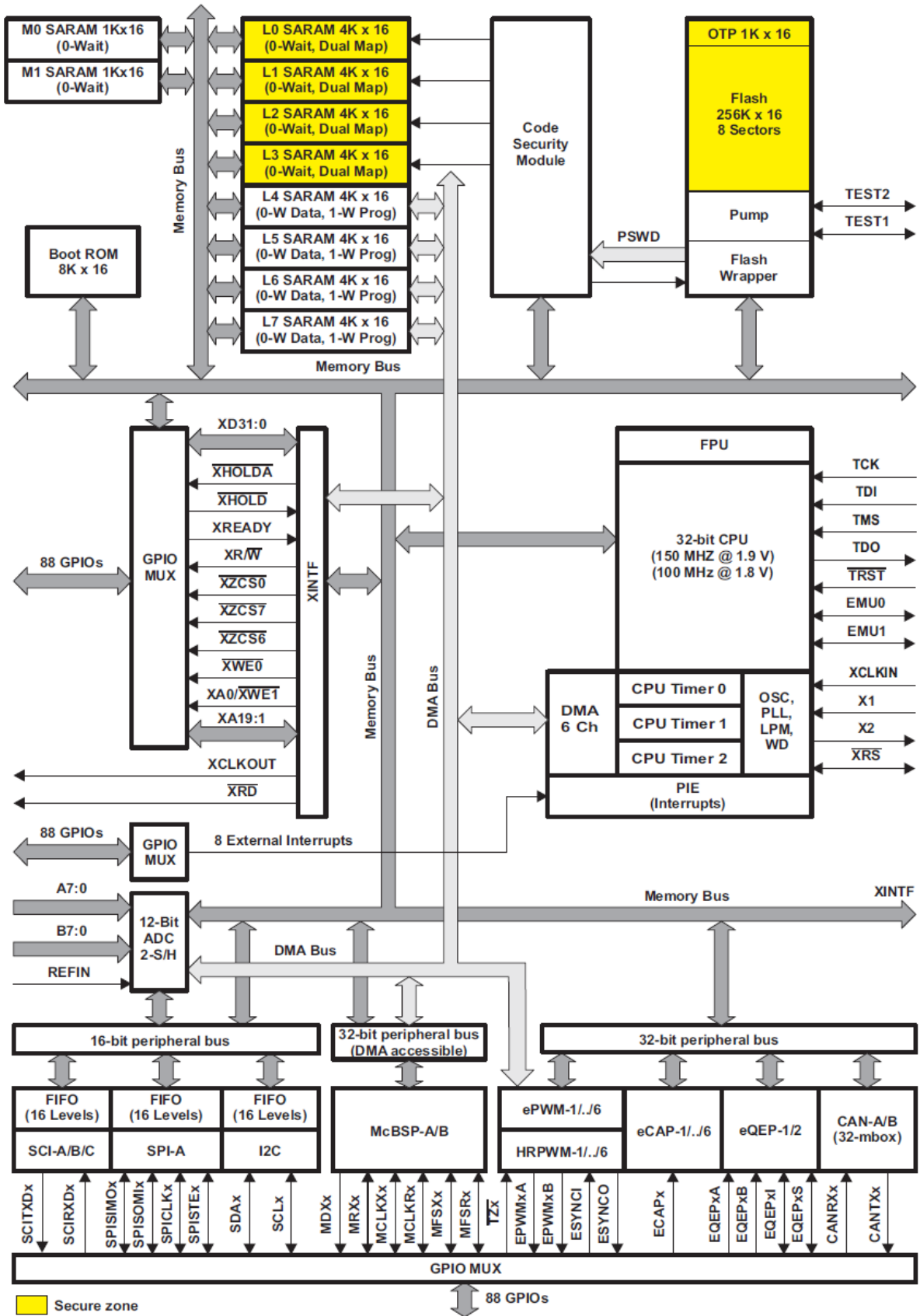


Fig. 3.3. DSC TMS320F28335 functional block diagram.

The structure of the control system is shown in Fig. 3.4. The MCU receives 7 analog current signals, one analog voltage signal and an encoder signal from speed sensor. The IGBTs control signals are generated by the ePWM module. The IGBTs driver error signals are connected to the EPWM TZ module for fast response. The SPI serial communication peripherals are configured to communicate with the resolver readout board. The CAN module is responsible for data exchange (receiving commands and transmitting data) with the control computer.

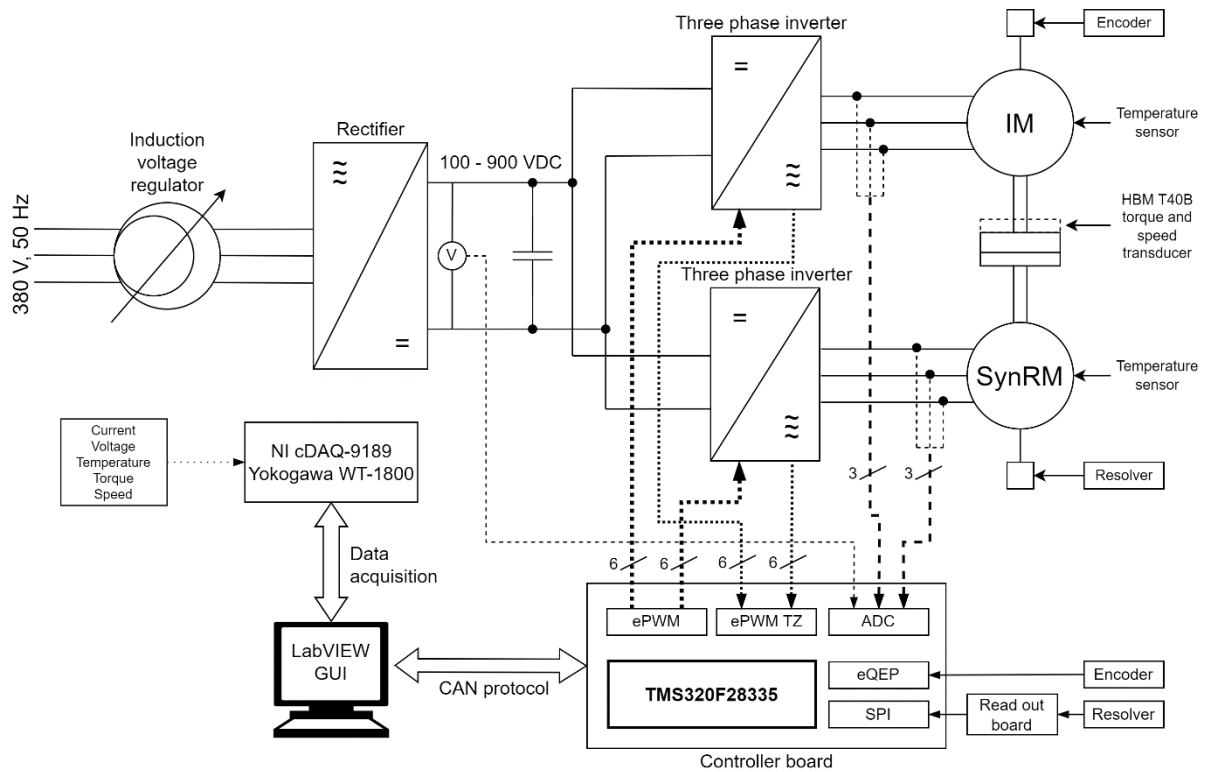


Fig. 3.4. The structure of the control system.

The built-in converter control software is written in Embedded C. The structure of the code is shown in Fig. 3.5. Motor control software flowchart. Functions from the TI Digital Motor Control [25] library were used as fundamental mathematical blocks to form the motor control code. During the research, the functions were modified to adapt to the specific application.

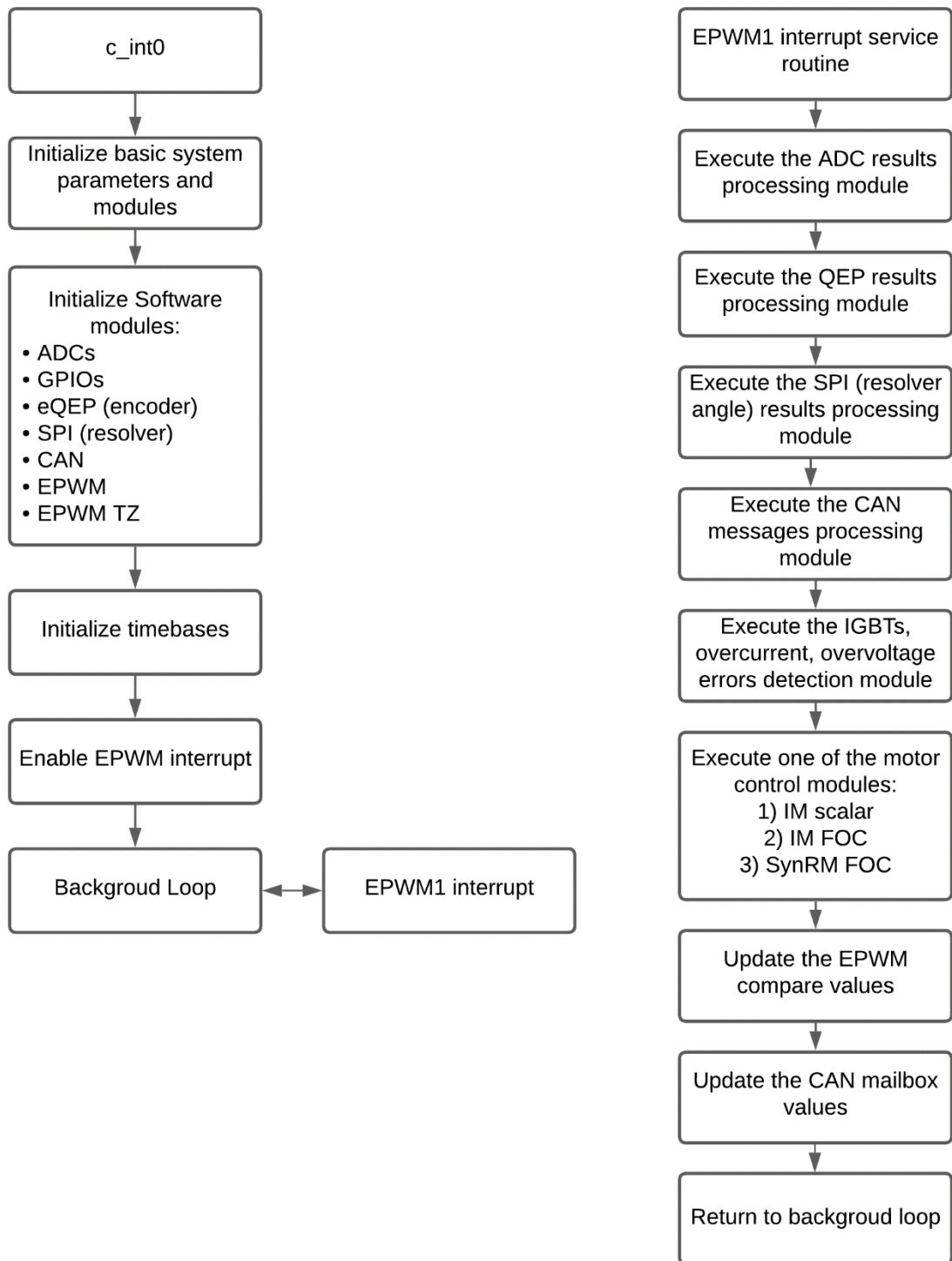


Fig. 3.5. Motor control software flowchart.

### 3.3. SynRM Control Algorithm

Modern AC motors rely on the frequency converters with direct torque control or vector control, especially in traction application. In this research the field-oriented control (vector control) is used.

Frequency converters of SynRM drives make it possible to use a rotor with flux guiding barriers for efficient synchronous operation. The rotor enables a higher saliency ratio, which improves efficiency of the motor and reduces inertia. Lower inertia improves transient response time. The SynRM stator is identical to that of an asynchronous machine, and its control system comprises similar components.

Vector control technique requires usage of the two-axis model of SynRM in the rotor reference frame. It is achieved by  $dq$ -transformations of stator currents using rotor angle information such as position or speed feedback. In case of synchronous motors, resolver is the most convenient option.

These control strategies rely on the control of current angle  $\theta$ , and the appropriate current angle is chosen based on the desired performance [14], [12].

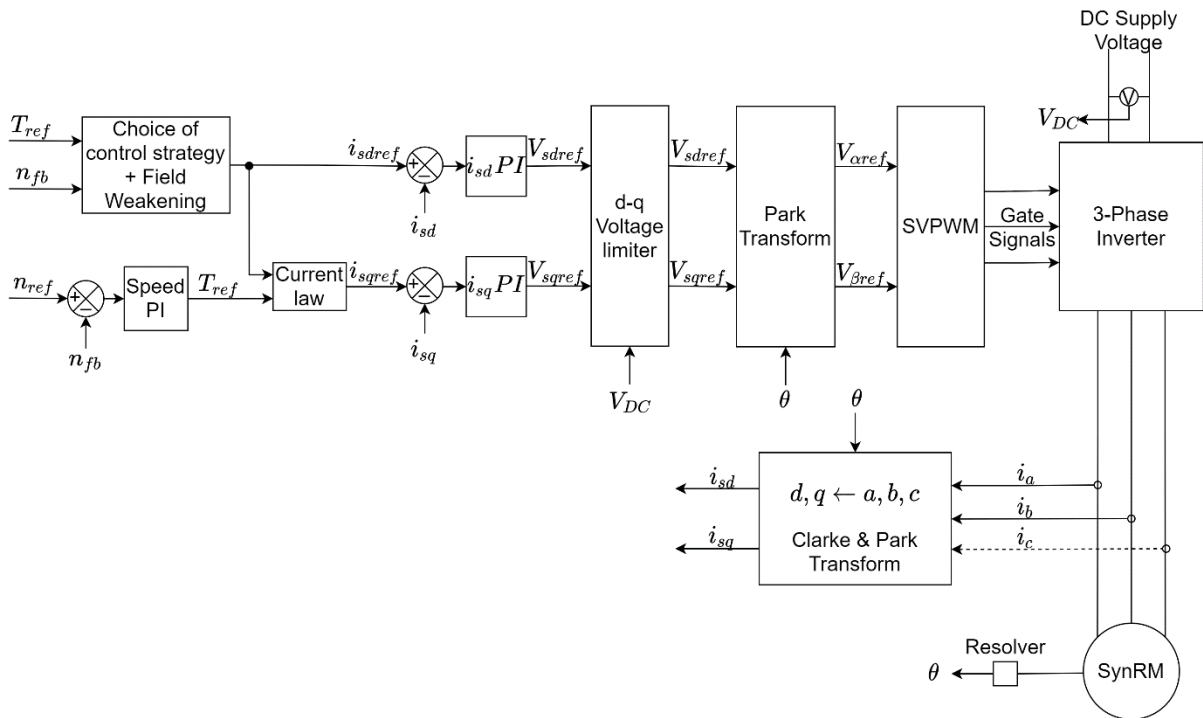


Fig. 3.6. Schematic block diagram of the vector control system for SynRM.

Fig. 3.6. Schematic block diagram of the vector control system for SynRM presents the general view of the vector control approach for SynRM, where torque control block could implement different approaches described further.

In this chapter the most used approaches to the vector control of SynRM are described [26]:

- constant d-axis current control (CDAC);
- maximum rate of change of torque (MRCT);
- maximum power factor control (MPFC);
- maximum torque per ampere control (MTPA).

### 3.3.1. Constant $i_d$ control

Constant magnetization current approach is the most simple for implementation because  $d$ -axis current is held at a constant value. SynRM remains excited at any rotation speed (until field weakening region) and current  $q$ -axis component remained for control purposes. In essence, this approach is very similar to the control of induction motors. For AC drives, the magnitude of the flux linkage using space-vector absolute values is

$$\psi_s = \sqrt{\psi_d^2 + \psi_q^2} = \sqrt{(L_d i_d)^2 + (L_q i_q)^2}, \quad (3.7.)$$

When the value of the  $i_d$  is the constant value, then  $i_q$  is derived according to the equation (3.8.):

$$i_q = \frac{\sqrt{\psi_s^2 - (L_d i_d)^2}}{L_q}, \quad (3.8.)$$

Below the rated speed, the value of  $i_d$  is kept constant, and the reference value is obtained, according to the equation (3.9.).

$$i_{dmaxref} = \frac{\sqrt{4|T_{ref}|L_d L_q}}{\sqrt{3p(L_d - L_q)}} / \sqrt{2}L_d, \quad (3.9.)$$

In the field-weakening region above rated speed, the  $i_{dref}$  component drops with the speed according to the:

$$i_{dref} = i_{dmaxref} \cdot \frac{\omega_N}{\omega_s}, \quad (3.10.)$$

### 3.3.2. Maximum Rate of Change of Torque Control

This method is based on obtaining the highest rate of change of the torque, and is achieved at the angle  $\theta$  defined in the equation (3.11.) [14], [12],

$$\theta = \arctan \xi, \quad (3.11.)$$

The reference value of the  $i_d$  current utilises the current angle and is set in accordance with equation (3.12.).  $i_q$  value is derived from that.

$$i_{dref} = \sqrt{\frac{2|T_{eref}|}{3p(L_d - L_q) \tan \theta}} \quad (3.12.)$$

### 3.3.3. Maximum Power Factor Control

Maximum power factor achieved at the value of the current angle as shown in the equation (3.13.) [14], [12]. Reference  $i_d$  and  $i_q$  values are calculated based on the same approach as shown above.

$$\theta = \arctan \sqrt{\xi}, \quad (3.13.)$$

Therefore, the maximum internal power factor is obtained based on the following expression (3.14.) [26], and as could be seen, that power factor of the SynRM is solely dependent on its value of the  $d$ - and  $q$ -axis inductances.

$$\cos \varphi_i = \frac{\xi - 1}{\xi + 1}, \quad (3.14.)$$

### 3.3.4. Maximum Torque per Ampere Control

In the ideal case, when  $L_d$  and  $L_q$  are assumed to be constant, maximum value for the  $T_{elm}/i_s$  ratio results when the angle  $\theta$  between the current and the  $d$ -axis of the rotor is  $45^\circ$ . And is obtained from the equation (3.15.),

$$\tan \theta = 1, \quad (3.15.)$$

This is accounted for by the load angle equation (3.16.) of the SynRM.

$$T_{elm} = \frac{3}{4} p(L_d - L_q) \cdot I_s^2 \cdot \sin 2\theta, \quad (3.16.)$$

In the case, when saturation is considered, MTPA current angle is shifted to values higher than  $45^\circ$  depending on the region. It happens because the main saturation effect that is affecting the  $d$ -axis inductance has to be somewhat compensated by reducing the  $d$ -axis current for a given stator current. The angle at rated current is commonly shifted from  $45^\circ$  to around  $60^\circ$  [12].

In addition to the saturation effect, MTPA current angle slightly changes because of the iron loss resistance and is mainly dependent on the rotational speed of the rotor [24].

## 3.4. Simulink Model of the Electric Drive

The first step of verification of the control system before it is used on real setup is testing with a mathematical model. Moreover, modelling could help to investigate the edge cases of operation and is able to test the drive connected to the vehicle, which is usually not achievable in the laboratory test-bench setup.

The mathematical model of the SynRM electric drive of the trolleybus is created in Matlab Simulink environment. The model is a continuation of work presented in conference paper [27].

The description of the model is divided into 4 main sections: overall high-level description, field-oriented control, model of the trolleybus and model of the electrical and mechanical systems.

### 3.4.1. High-level Overview of Algorithm

Understanding of the inner workings of the Simulink model of SynRM electric drive requires an overview of the logical connections and signal routes on the top level. This subchapter is devoted to description of such connections, while the high-level overview is shown in Fig. 3.7.

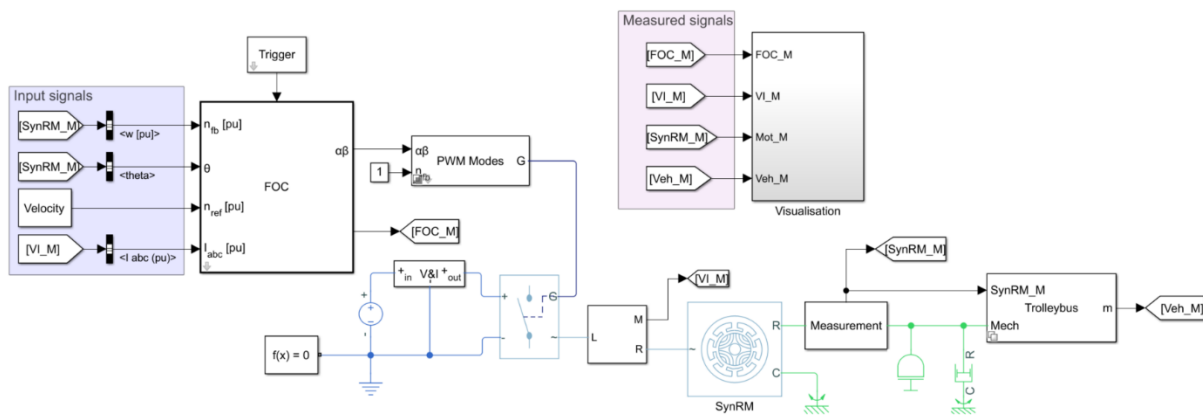


Fig. 3.7. High-level overview of electric drive model.

At the system start-up, the model is initialised with the script containing constants and look-up tables for proper operation. The used values are obtained based on the knowledge of SynRM vehicle and the test-bench setup. Furthermore, at the start-up, the motor connection could be switched between the test-bench operation (constant load in Nm) and vehicle connection.

The top-level model is organised into several subsystems or sections. Those are field-oriented controller (FOC), PWM generation for the inverter (supports several modulation approaches), traction inverter with DC voltage source, stator current and voltage measurement block, SynRM, rotor shaft measurements (rotor positions, output torque, rotor speed), and load subsystem. The load subsystem can be switched between the connection to the constant torque and vehicle.

Field-oriented control system block has 4 inputs: feedback speed, rotor position, reference speed and three phase stator currents. At start references are all zero and are updated during the simulation.

Reference speed could be set as any speed as a function of time. For road profile testing the WLTP class 1 is used. Reference speed is provided in the per unit values for the control system, and in km/h for the visualisation part.

Feedback speed is measured in  $rad/s$ , therefore conversion is needed to the per unit representation. Conversions between units are represented by formulas below.

$$n = \frac{60}{2\pi} \omega; v = \frac{3.6 \frac{D}{2} \omega}{\mu} \quad (3.17.)$$

$$v_{pu} = \frac{v}{v @ 1500RPM}; n_{pu} = \frac{n}{1500RPM}; \omega_{pu} = \frac{\omega}{\pi \cdot 50}$$

In general, all the per unit conversions are preformed based on this expression:

$$value_{pu} = \frac{value_{absolute}}{value_{conversion}} \quad (3.18.)$$

FOC block provides controller set voltage in the  $U_\alpha, U_\beta$  form and passed to the PWM generator block, space vector modulation is used mostly. Carrier frequency, as well as the FOC trigger frequency are set to the 2 kHz, the same as one used in the real DSP system on the test-bench. Subsystem outputs gate firing signal array for the inverter.

For the inverter standard three phase IGBT based form is used. It is supplied by the DC voltage source. At the input side of the inverter  $V_{DC}$  and  $I_{DC}$  are measured. Output of the inverter is a phase voltage, which supplies stator terminals of the SynRM.

Between motor and inverter are voltage and current measurements, with signal filtering and RMS calculation for the visualisation. In turn  $I_{abc}$  feedback signal is not filtered to avoid time delay for the control system. For the control system  $I_{abc}$  is converted to the per unit system.

SynRM is a standard Simscape block with parameters initialised at the start-up. Used values are obtained through laboratory testing of the existing machine.  $L_d$  and  $L_q$  values are in the matrix form as a function of both  $i_d$  and  $i_q$  each. Mechanical parameters are set externally, to see their effect is visible on the measured output torque. Mechanical parameters are inertia and viscous friction, which are also obtained during testing.

When a vehicle is connected, motor produces torque based on the difference between reference and feedback speed.

In between SynRM block and mechanical part, is the measurement subsystem. It measures angular velocity, rotor position and output torque on the shaft using ‘Ideal Rotational Motion Sensor’ and ‘Ideal Torque Sensor’ respectively. Rotor position is a feedback signal provided as an input to the control system. Output torque of the motor is an input to the Trolleybus model and visualisation.

Output of the ‘Trolleybus’ is the feedback velocity in per unit, which acts as a feedback signal to the control system, and as a ‘load’ to SynRM, being first transformed to the rad/s.

Last subsystem is the visualisation, which brings all the important signals into one place for the analysis and troubleshooting.

### 3.4.2. Field-Oriented Controller Algorithm

The control algorithm of the SynRM is hidden under the FOC subsystem, this subchapter describes the implementation of the algorithm. In the Fig. 3.8 is the Field-Oriented Controller (FOC) subsystem description.

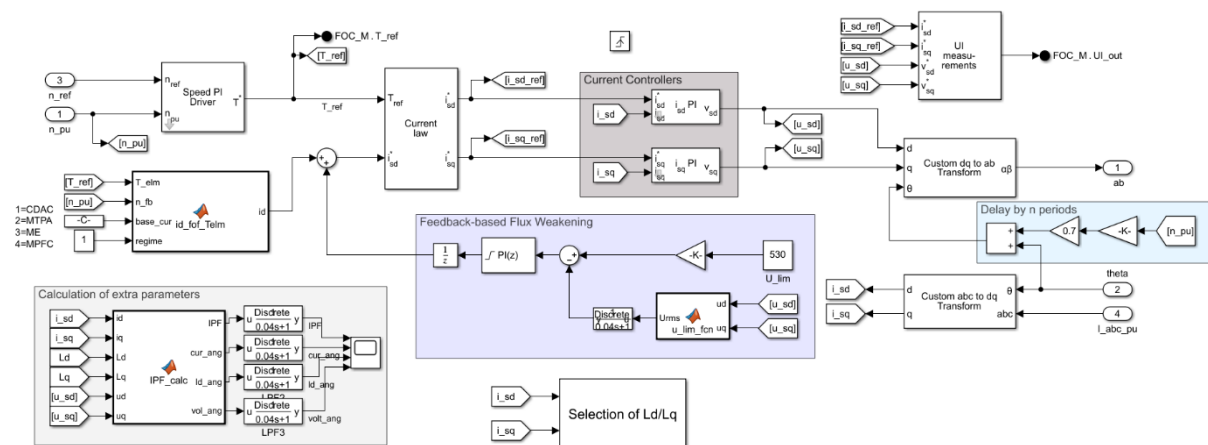


Fig. 3.8. Overview of the FOC.

As was previously mentioned, this subsystem takes 4 input signals, and has 1 output signal.

Input stator current  $i_{abc}$  is transformed to the  $i_d$  and  $i_q$  current components based on rotor position  $\theta$ , using Clarke and Park transformation matrices.

At the first stage there is a speed controller. Structure of speed controller is shown in Fig. 3.9. It is a PI-controller, which takes feedback and reference per unit speeds, and outputs reference torque in per unit as well. This subsystem has one important distinction, it uses dynamic saturation, which is governed by the limiting traction characteristic of the produced motor, which is dependent on the feedback speed.

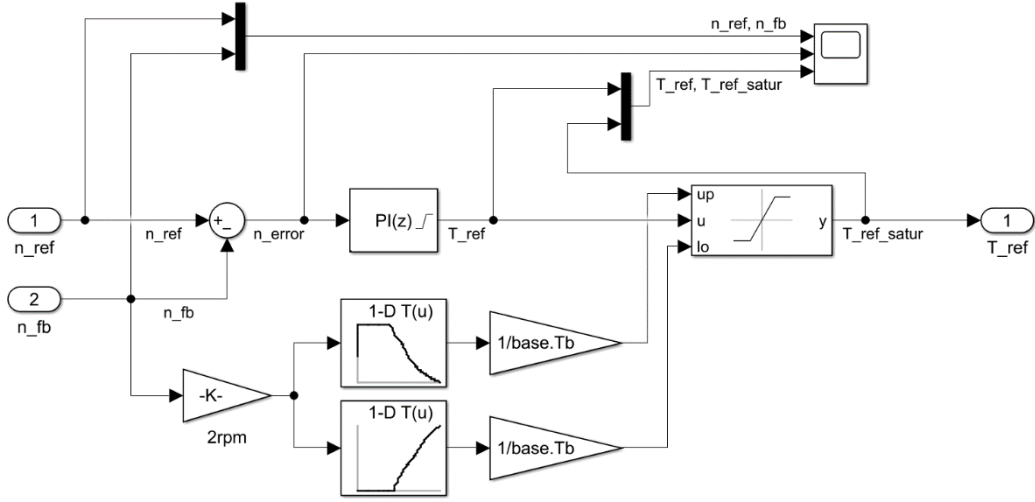


Fig. 3.9. Overview of the speed controller.

Second part of the first stage is setting of the reference d-axis current. It is set based on the chosen regime, feedback speed and feedback reference torque. There are several regimes: CDAC, MTPA, ME and MPFC. All these regimes are pre-calculated off-line based on the laboratory testing.

At the second stage ‘Current law’ the  $i_q$  is derived based on the reference torque and d-axis current. The following standard equation for the torque is used,

$$T = \frac{3}{2}p(L_d - L_q)i_d i_q. \quad (3.19)$$

Magnetising inductance components  $i_d$  and  $i_q$  are used as obtained from the laboratory tests. During the simulation they are selected from the look-up table based on the feedback  $i_d$  and  $i_q$  currents. Inductance values are in the form of 2D array as a  $L_d = f(i_d, i_q)$  and  $L_q = f(i_d, i_q)$ .

At the third stage, current controllers are used with feedback and reference  $i_d$  and  $i_q$  as inputs. For each of the current components there is a separate PI controller, all the parameters are identical. Controllers output control voltages for the inverter in the d- and q-axis form in per unit system.

Field-weakening system is feedback-based as shown in the Fig. 3.8 in blue contour. It takes controller output d- and q-axis voltages and compares them to the pre-set voltage limit. Output of the field-weakening controller is an adjustment factor for the magnetising current  $i_d$ .

Finally,  $u_d$  and  $u_q$  voltages are transformed to  $u_\alpha$  and  $u_\beta$  components using inverse Park transformation.

Last subsystem is aggregate visualisation of feedback and reference currents, and control voltage. All in d-q axis form.

### 3.4.3. Mathematical Model of the Trolleybus

Significant difference from the laboratory test-bench setup is the presence of the vehicle model, which in this case is the trolleybus. The model is based on the linear model of a moving object. The overview of the trolleybus model is shown in Fig. 3.10.

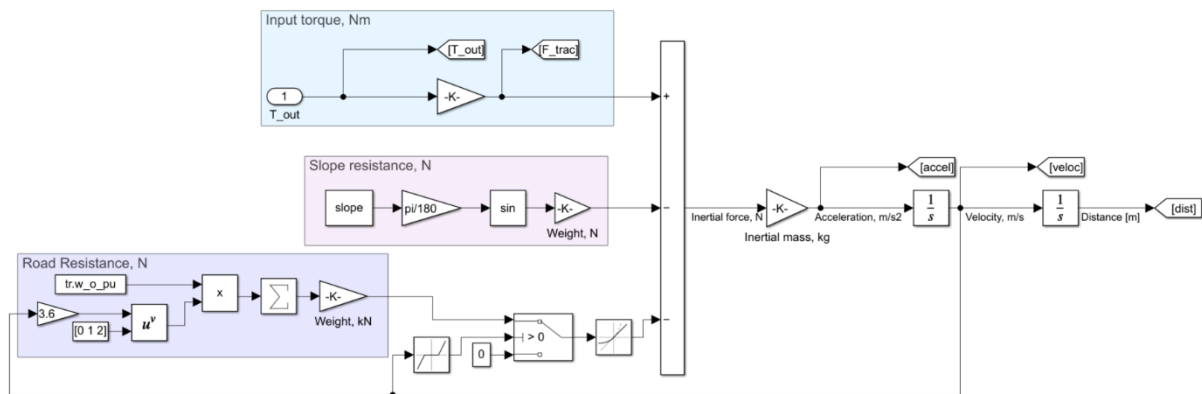


Fig. 3.10. Overview of the trolleybus model.

Vehicle dynamic performance is mainly dependent on the traction characteristic of the motor, or in other words its ability to produce output torque at a given speed. On the other hand, dynamic performance is hindered by the resistive forces, such as air, rolling, and cornering friction resistances, and different losses at power conversion stages, semiconductor converter, motor, gearbox etc.

First and foremost, it is important to state crucial relations between torque and force, and velocity on the shaft and the wheel. These values are directly related, and are shown below, to avoid confusion in description further. Equations show velocity relations and the torque/power relation.

$$\omega = \frac{2\pi}{60} n;$$

$$v = \frac{3.6 \cdot D/2 \cdot \omega}{\mu}; \quad (3.20.)$$

$$F_{wheel} = \frac{2\mu}{D} T_{shaft} \cdot \eta_{gearbox};$$

where  $n$  is angular velocity of the rotor [RPM];  $\omega$  is angular velocity of the rotor [rad/s];  $D$  is diameter of the wheel [m];  $\mu$  is gearbox conversion ratio;  $v$  is linear velocity [km/h];  $F_{wheel}$  is propulsion force on a wheel [N];  $T_{shaft}$  is torque on a shaft [Nm]; and  $\eta_{gearbox}$  is gearbox efficiency.

Coefficient 3.6 acts as a conversion between m/s and km/h (3600/1000).

From a viewpoint of dynamics, forces acting on a vehicle in motion are determined by the Newton's Second law and could be represented, as shown in Fig. 3.11 [28].

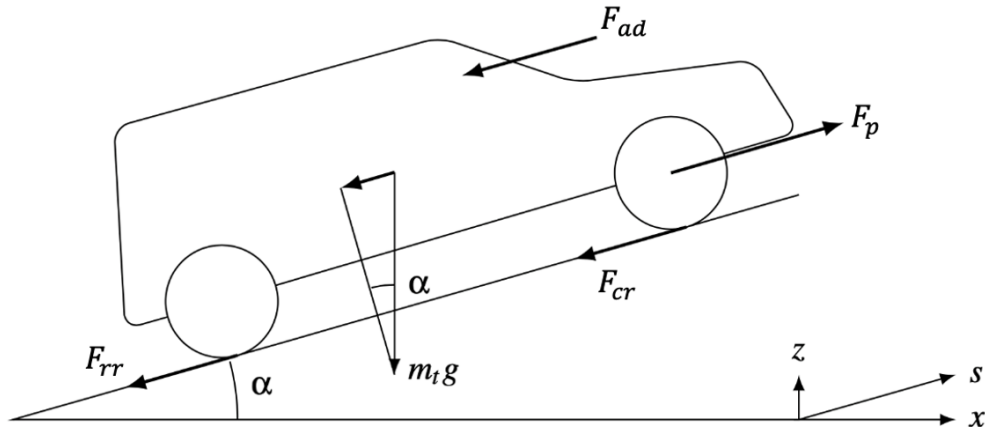


Fig. 3.11. Representation of forces acting on a vehicle in motion,

where  $F_{ad}$  is air-drag force [N];  $F_{cr}$  is cornering resistance force [N];  $F_{rr}$  is rolling resistance force [N];  $\alpha$  is the slope of the surface [%]; and  $m_t$  is total effective vehicle mass [kg].

The total effective mass of the vehicle differs from the actual mass by correcting coefficient  $1 + \gamma$ , and it represents the effect of total inertia of rotating parts. This coefficient could be obtained by estimation through tests, or by calculations knowing the vehicle structure. For the trolleybus, the correcting coefficient for inertial mass is estimated to be 0.15-0.20 [29] (in the model 0.17 is used).

As follows from the diagram the equation represents the forces acting on a vehicle [28].

$$\begin{aligned}
 m \cdot (1 + \gamma) \cdot \frac{dv(t)}{dt} &= F_p(t) - F_{res}(t) - F_{slope}(t); \\
 F_{res}(t) &= F_{ad} + F_{cr} + F_{rr}; \\
 F_{slope}(t) &= mg \cdot \sin(\alpha(t));
 \end{aligned}
 \tag{3.21.}$$

where  $\frac{dv(t)}{dt}$  is acceleration of a vehicle [ $m/s^2$ ];  $F_{res}$  is total resistive forces [N]; and  $F_{slope}$  is effect of gravity due inclination [N].

Air-drag, rolling resistance and cornering resistance have their corresponding estimative formulas, but as they are describing complex physical phenomena, it makes them difficult to estimate. In practical calculations empirically obtained dependencies are usually used to describe these forces.

Such dependency is obtained by getting vehicle up to speed, then letting it coast on a flat long straight road, with no wind. In this test deceleration is observed, and then, this speed variation is expressed using a second order polynomial to approximate the effects of these resistance forces acting on a vehicle. It is easier for calculation and could be provided by the manufacturer or obtained via testing. General approximation is shown in the following equation [28], [29], [30]:

$$F_{res}(t) = C_0 + C_1 v(t) + C_2 v(t)^2. \quad (3.22.)$$

In the case of this model, equation from the [29], [30] is taken as an approximation.

$$w = 12 + 0.004 \cdot v^2; \quad (3.23.)$$

$$F_{res} = w \cdot mg;$$

where  $v$  is km/h, and  $w$  is  $N/kN$  or a relative value per  $kN$  of force. To transform it to absolute values, it is multiplied by the weight of the vehicle.

Derivation of output signals for the control system and for the visualisation is shown partly in Fig. 3.11 and in Fig. 3.12.

Output values of velocity and displacement are consecutive integrals of acceleration velocity being integral of acceleration, and displacement  $x$  is integral of velocity.

$$v = \int a dt; \quad (3.24.)$$

$$x = \int v dt.$$

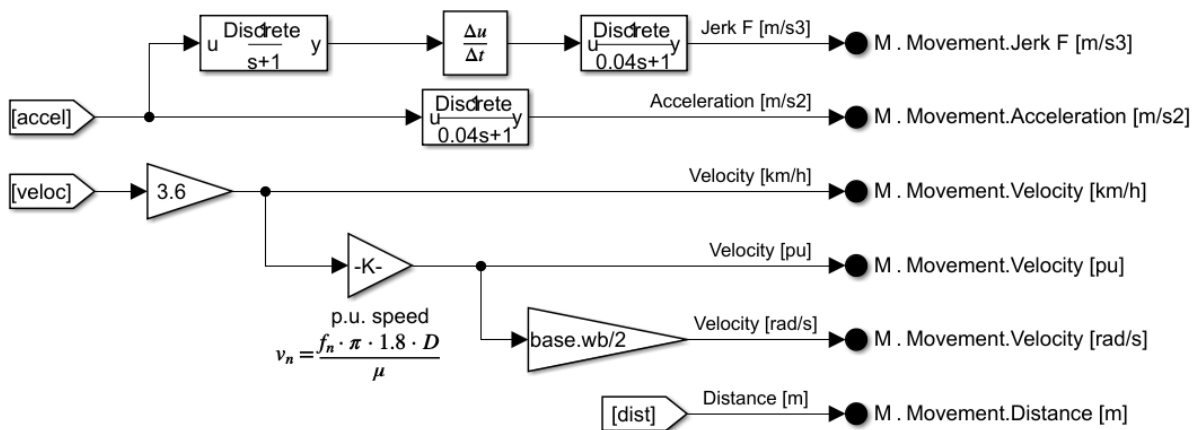


Fig. 3.12. Trolleybus model, output signal creation.

While jerk  $[m/s^3]$  is a derivative of acceleration,  $j(t) = \frac{da(t)}{dt}$ . Also, jerk is calculated with heavy filtering, to avoid excessive noise, due to the approach to calculation of derivatives by Simulink.

These calculated values are combined in an output bus signal, while velocity is transformed to the per unit system and acts as feedback output.

## 4. Experimental Investigation of SynRM Traction Drive

The accuracy and quality of the production of an electric machine is reflected in its parameters and the convergence of the results of modelling and testing. An important stage of the research is the correction of the mathematical model of the electric motor according to the test results.

This chapter describes the production process of an electric machine, the laboratory and measuring instruments, and the test results.

### 4.1. Production Process of the SynRM Traction Drive

Production of the SynRM prototype was done at JSC “RER”.

The motor consists of two main assembly units – stator and rotor.

Manufacturing of the stator of an electric motor begins with the motor housing. The housing of the SynRM prototype (shown in Figure 4-1) is welded from the smaller assembly units. The housing consists of a shell, poles, two side plates, which are interconnected by two steel channels. These parts are welded together and machined for purpose. The poles are machined for the size of steel stator sheets, necks for the end shields, and a keyway is slotted to fix the stator steel sheets inside the housing.



Figure 4-1 – SynRM Housing in Production.

Next, a core made of electrical steel sheets is pressed into the housing. The process of stator steel sheet assembly is shown in Fig. 4.2. The stator core is sandwiched between the housing collar and the segment keys welded to the outer stator ring.

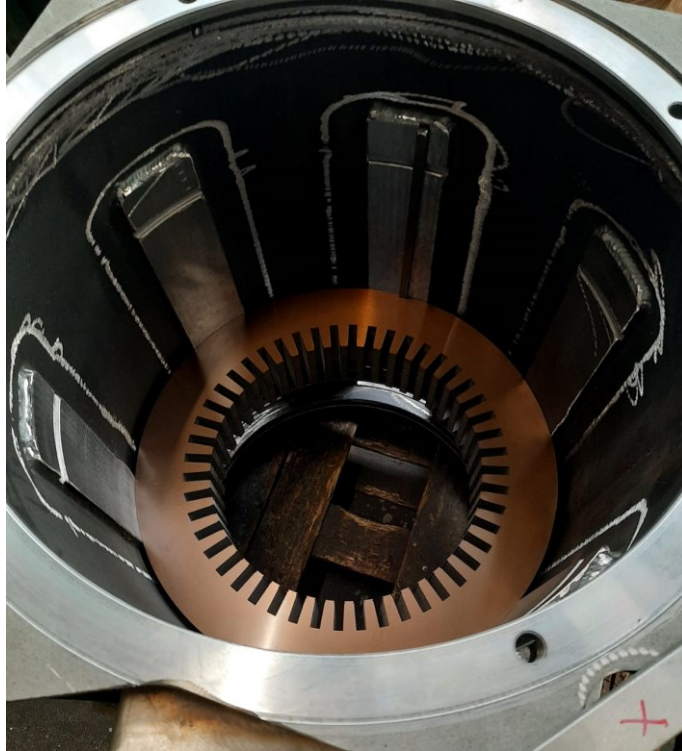


Fig. 4.2. Partially stacked SynRM stator.

After that, in the stator are placed copped coils, which are connected according to the electrical connection scheme from the design stage. Finally, the stator is impregnated with special compound for structural integrity and insulation, then dried and prepared for assembly. Fully completed stator is shown in Fig. 4.3.

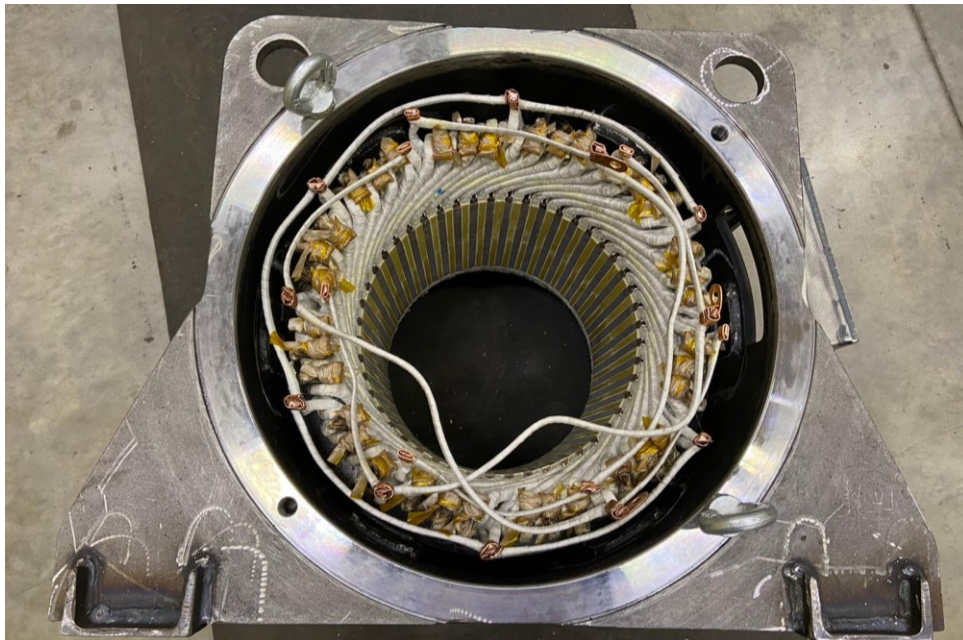


Fig. 4.3. Stator lamination stack with windings in SynRM housing.

The rotor of SynRM is a steel shaft on which the rotor steel sheets are stacked (Fig. 4.4). Since this motor is made as an experimental prototype, it was sensible to make the rotor and

stator sheets by cutting them out on a laser, and not to order expensive technological equipment in the form of stamps.



Fig. 4.4. Rotor lamination stack assembly on a shaft.

After the stacking process, the rotor is impregnated in a similar process as a stator, machined (sanded), and then the fan is installed. At the final stage, the rotor is dynamically balanced. A completed painted rotor is shown in Fig. 4.5.

Before starting the assembly, parts and assemblies of an electric machine go through a preparatory process. Are blown out of dust, and dried. The front bearing assembly is assembled on the rotor (this shield is installed on the side of the shaft cone). The bearing is fastened in this shield by means of bearing caps; the bearing itself is shrink-fit on the shaft. The second bearing is mounted on the opposite side of the rotor.

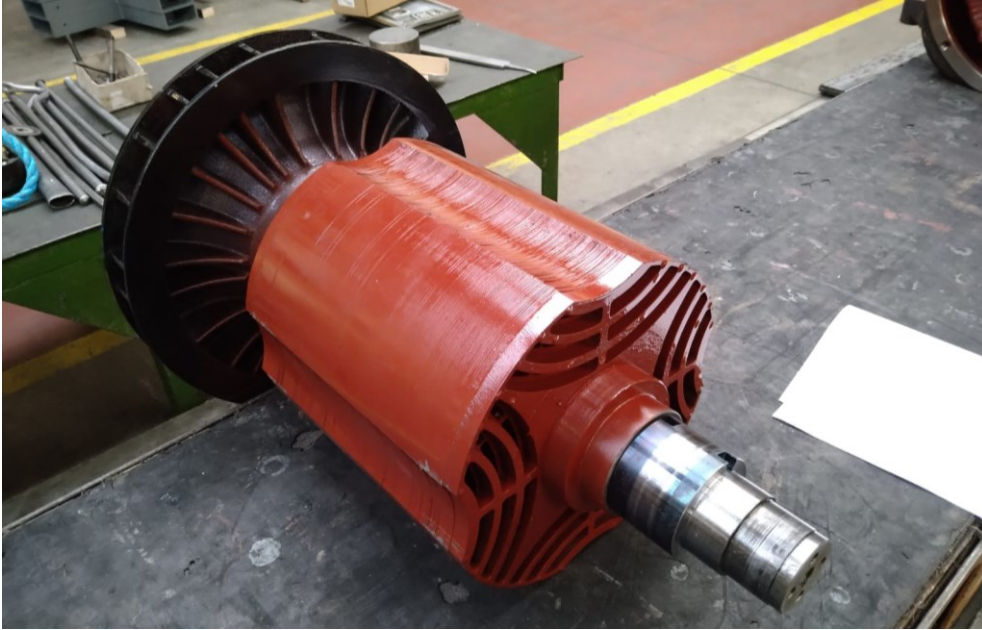


Fig. 4.5. Assembled rotor body.

The second end shield is bolted to the stator. The rotor with the end shield is slowly inserted into the stator with the help of a crane, after the rotor is placed into the stator and installed in the correct position, it is fastened. Bearing grease is not required as the bearings used are of the sealed type. They already have the required lubricant.

After that, a counting wheel for the speed sensor and the sensor itself, and an insulator are installed. After post-production testing of the motor, surfaces are prepared for painting and the motor is painted.

SynRM that has been completed and installed on a test-bench is shown in Fig. 4.6.



Fig. 4.6. SynRM traction drive on a test-bench.

## 4.2. Laboratory Testing of the Developed SynRM Traction Drive

Comprehensive laboratory testing of the designed and produced prototype is a crucial component in the research and development of the SynRM electric drive for the electric vehicle.

The tests of the manufactured sample were carried out in one of the traction laboratories of JSC “RER”. The company is the largest manufacturer of electrical equipment for transport in the Baltics. The JSC “RER” development team implements various research results in the field of electric drives. The author participated in the tests of a dump truck electrical equipment set [31], as well as in studies on vibration of electric motors of electric trains [32], [33].

### 4.2.1. Laboratory Equipment

#### *Testing Setup*

Laboratory testing of the produced SynRM prototype requires a laboratory test-bench with the corresponding measurement and control equipment.

Laboratory tests were conducted at the test-bench setup of laboratory of urban vehicle electric drives up to 1kV DC at the premises of JSC “RER” [27]. The test-bench setup is shown in Fig. 4.7, basic-scheme of the test-bench setup is shown in Fig. 4.8, and the inverter control board is shown in Fig. 4.9.

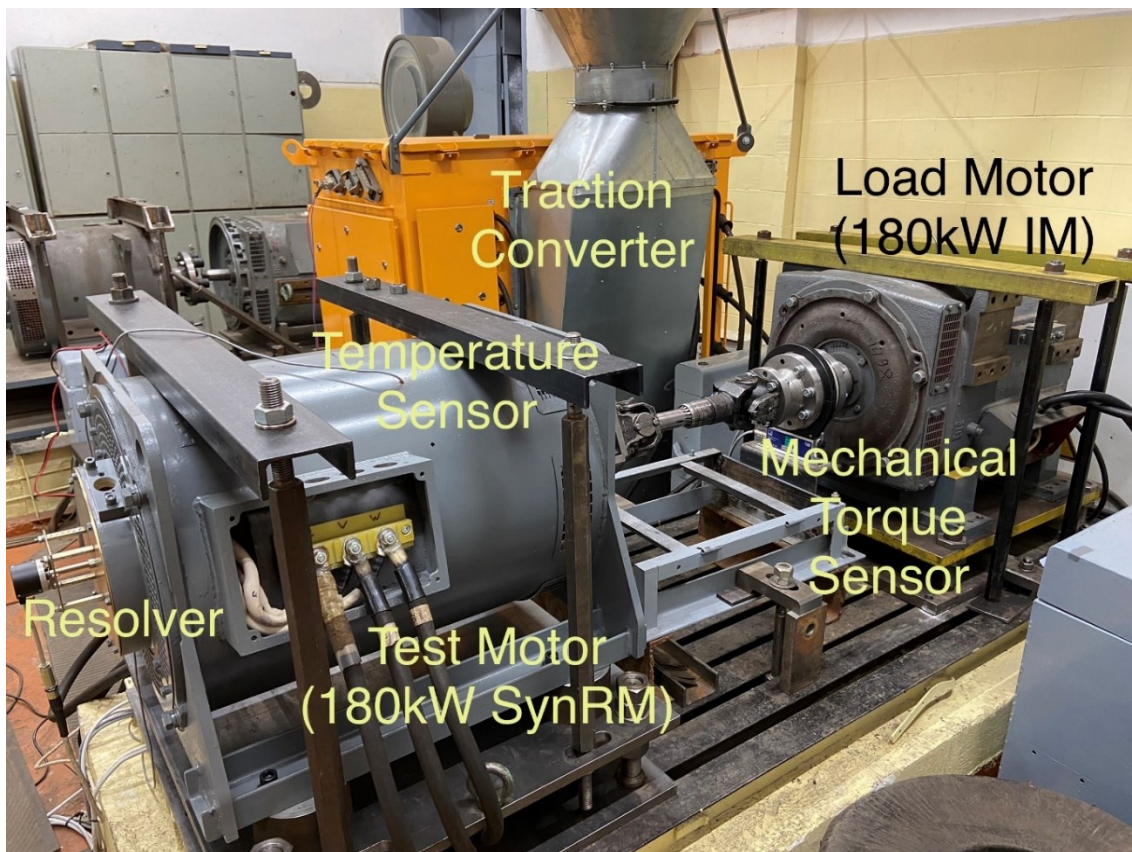


Fig. 4.7. Laboratory test-bench setup.

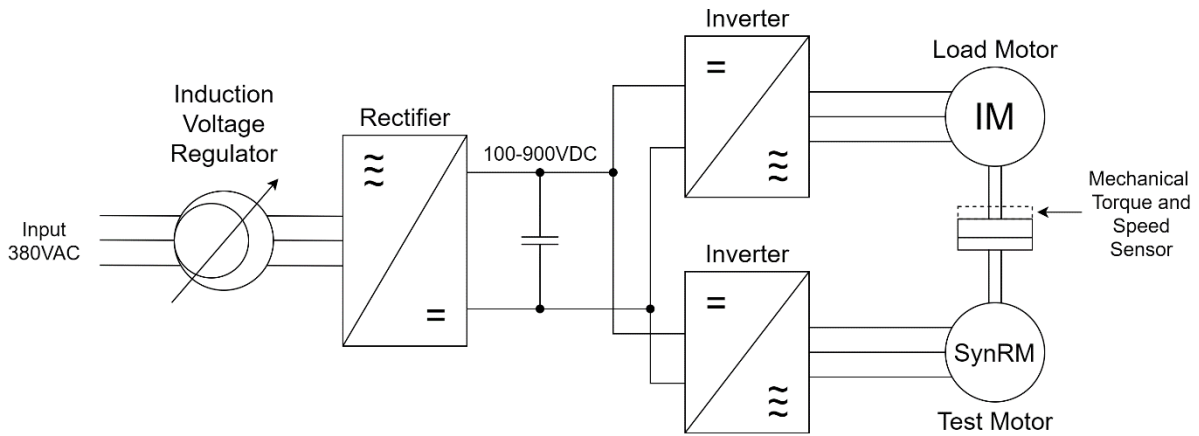


Fig. 4.8. Basic scheme of the laboratory test-bench setup.

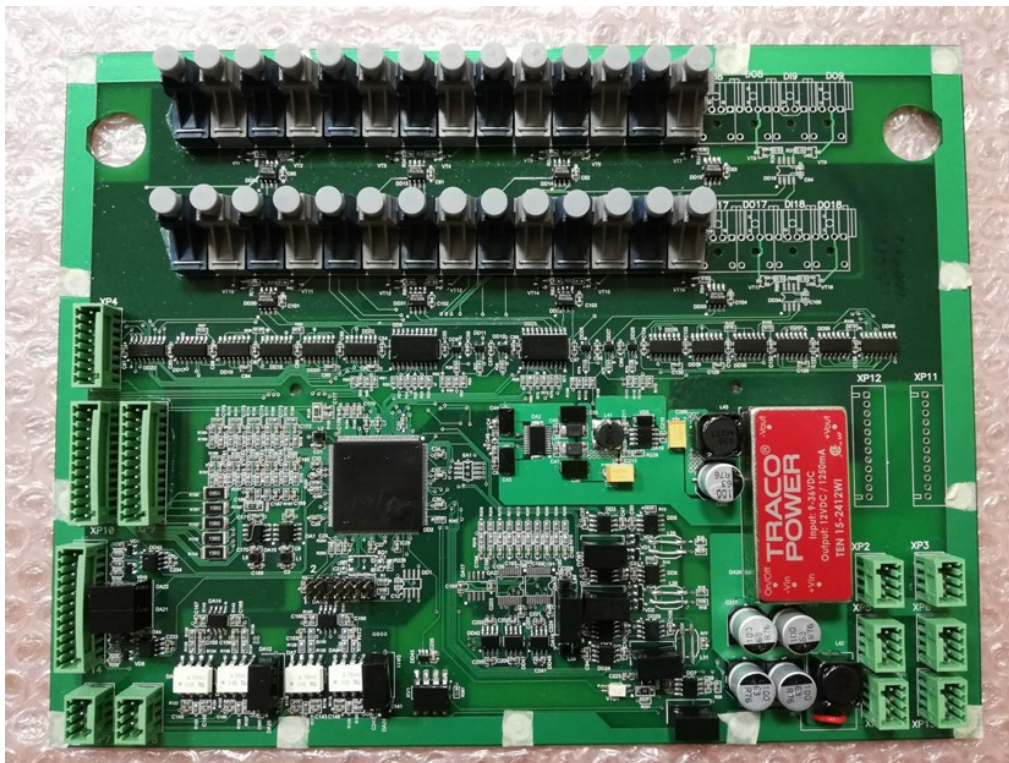


Fig. 4.9. Laboratory inverter control board MCU TI TMS320F28335.

Test and load motors are rigidly connected using a cardan joint and are mutually loaded. The motors are controlled by the traction converter supplied by the controlled DC-link voltage of up to 1kV. The control system is deployed to the TMS320F28335 digital signal processor (DSP). Control of the motors relies on the signals from the current and voltage sensors, from the resolver (rotor position sensor) for SynRM, and speed sensor for induction motor. Setting of reference parameters to the control system in the laboratory is done in graphical user interface (GUI), shown in Fig. 4.10 and communication with DSP is done using CAN bus.

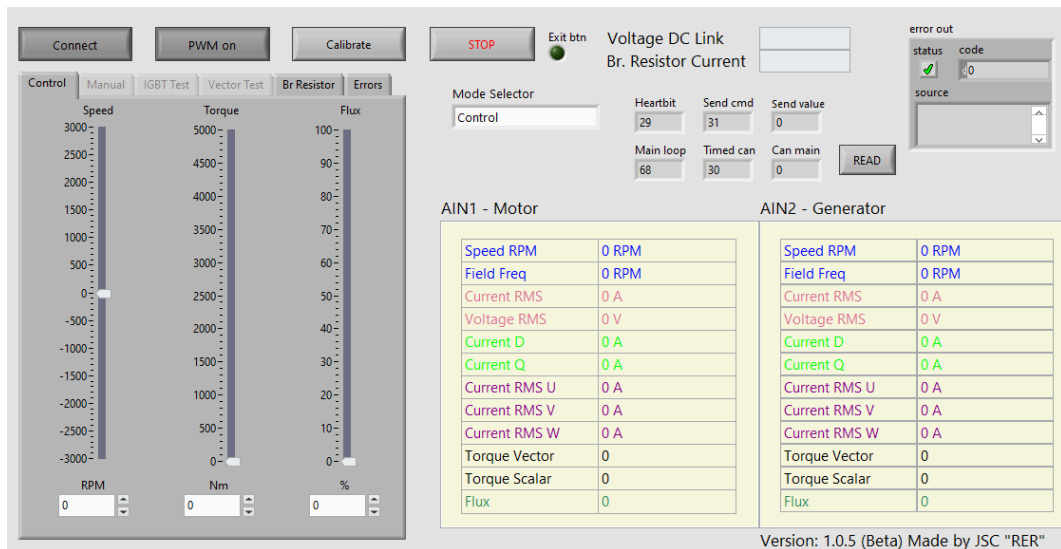


Fig. 4.10. Motor control GUI.

### *Measurement Equipment*

Besides the laboratory test-bench, there is a measurement and data analysis setup that allows to obtain, visualize and save all the data needed for research. Therefore, the quality of control and measurement results are approved by verified sensors and measuring equipment.

Output torque and rotational speed are measured using T40B 5kNm torque transducer by HBM. Current values are measured by ES2000 hall sensors by ABB. Sensors are shown in the Fig. 4.11.



Fig. 4.11. Installed torque transducer (left), installed current sensors (right).

Stator temperature is measured using PT100 temperature sensors. Sensor is located inside the stator steel close to copper conductors. Resistance of the stator windings is measured with milli-ohmmeter, for each of the pairs of windings.

Voltage is measured directly with Yokogawa WT1800 Precision Power Analyser (Fig. 4.12). This device can handle direct voltage measurements of up to 1kV. Current and voltage are logged from the power analyser with the built-in functionality.



Fig. 4.12. Yokogawa WT1800 precision power analyser.

Data pre-processing and logging from the torque flange and temperature sensor are recorded using NI measurement setup (Fig. 4.13). NI cDAQ-9189 chassis is used with NI9361, NI9215 and NI9216 modules, and the chassis is connected to the operating PC with the Ethernet connection.

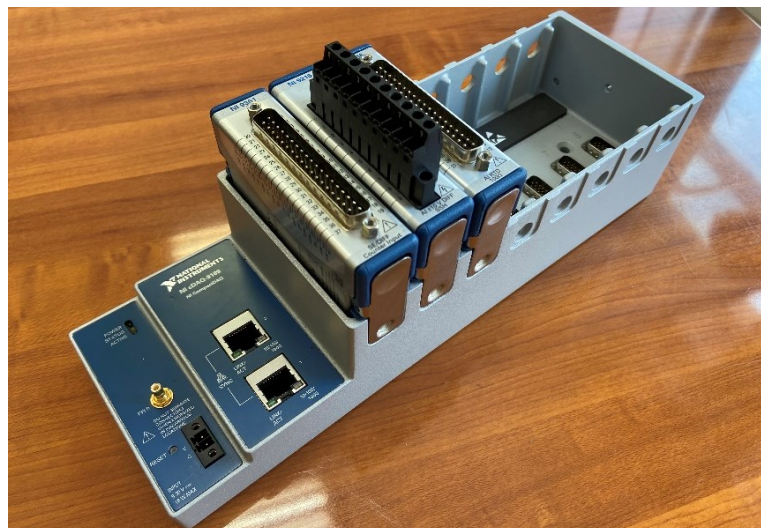


Fig. 4.13. NI measurement setup.

Signal logging is done using graphical user interface created in the LabVIEW environment. Values of torque and speed are recorded with 5kHz discretisation, while temperature with 2Hz discretisation. After the data logging phase, it is processed using automated scripts, created in Matlab.

More detailed specifications of equipment are presented in the Appendix A1.

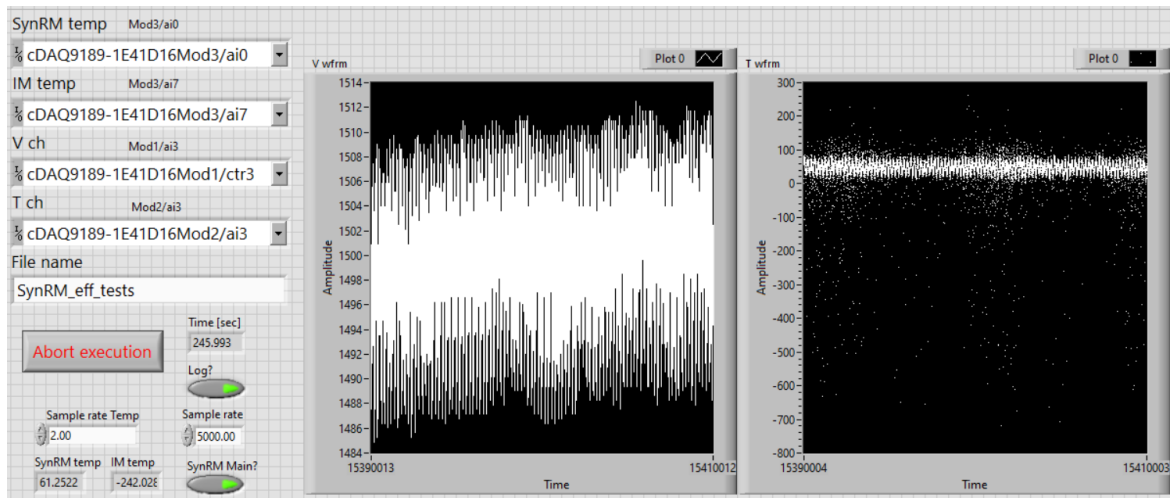


Fig. 4.14. LabVIEW data logging GUI.

#### 4.2.2. Traction Characteristic of SynRM

Proper testing of the designed and produced SynRM is done to determine its tractive limitations, at and below 420 V at different speeds.

##### *Testing at Rated Speed*

Below in Fig. 4.15 is the loading test of the SynRM at rated point of 1500 RPM at different load levels. Output torque, rotor frequency, stator RMS voltage and stator RMS current are presented in the figure. The data was recorded with the equipment described in the previous subchapter.

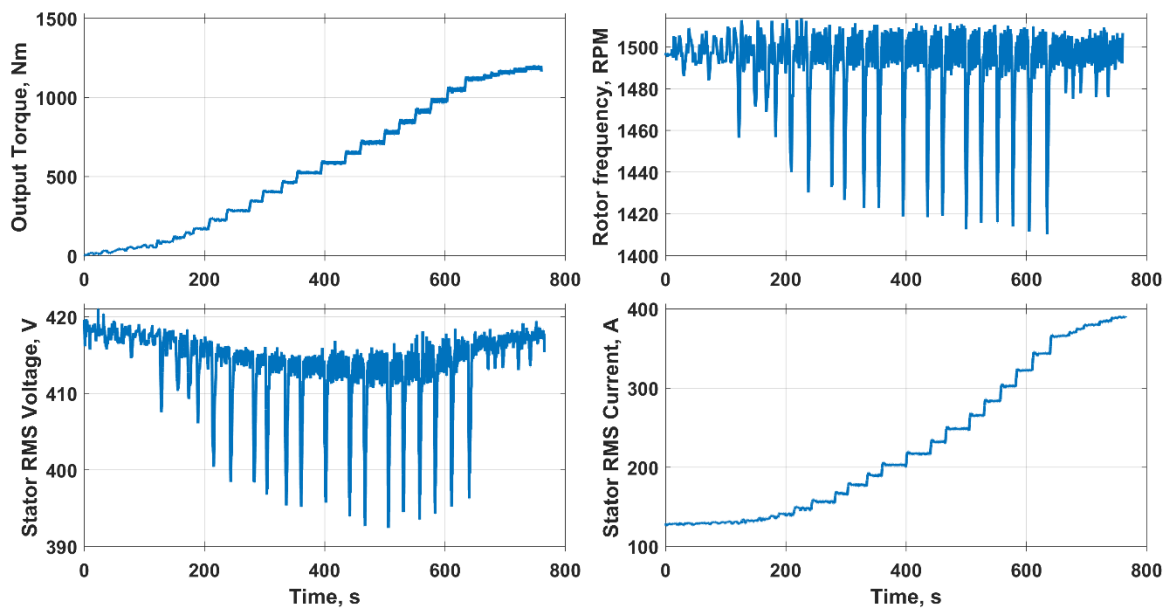


Fig. 4.15. SynRM loading test at 1500 RPM.

Table 4.1 presents the tabulated data of the above presented test. D-axis current was kept constant to keep the magnetisation at the constant level. It can be seen that maximum laboratory obtained output torque is 1186.3 Nm, above that value the motor becomes unstable and loses synchronism.

Table 4.1  
Data from the SynRM loading test at 1500 RPM

$n, RPM$	$T_{out}, Nm$	$P_{out}, kW$	$U, V$	$I, A$	$\eta, \%$	$\cos \varphi$	$i_d, A$	$i_q, A$
1499.8	14.2	2.2	418.2	128.2	34.30%	0.069	180.8	16.1
1500.6	24.2	3.8	418.2	128.5	47.20%	0.086	180.6	21.6
1499.7	40.1	6.3	417.8	129.3	59.80%	0.112	180.8	29.7
1499.4	51.3	8.1	417.7	130.0	65.50%	0.131	180.9	35.2
1500.9	58.6	9.2	417.5	130.1	68.37%	0.143	180.4	38.7
1498.3	87.6	13.7	417.0	132.5	76.73%	0.187	180.8	51.0
1498.9	113.9	17.9	416.5	134.5	81.11%	0.227	180.4	62.0
1500.3	141.2	22.2	416.3	137.2	83.74%	0.268	180.4	73.6
1499.6	170.5	26.8	415.8	140.5	86.03%	0.308	180.5	85.4
1499.7	227.4	35.7	415.3	148.0	88.89%	0.378	180.6	108.2
1499.8	284.8	44.7	414.9	156.6	90.65%	0.439	180.7	130.7
1499.2	345.1	54.2	414.4	166.8	91.95%	0.492	180.8	154.3
1499.6	403.8	63.4	414.1	177.7	92.84%	0.536	180.7	177.4
1498.9	464.2	72.9	413.7	189.8	93.53%	0.573	180.8	201.3
1499.5	525.4	82.5	413.6	202.9	93.99%	0.604	180.6	225.8
1499.3	587.8	92.3	413.5	217.1	94.41%	0.629	180.6	251.1
1498.6	650.8	102.1	413.3	232.1	94.68%	0.649	180.6	276.9
1499.2	715.5	112.3	413.5	248.4	94.88%	0.666	180.5	304.2
1498.4	780.4	122.4	413.4	265.3	95.04%	0.678	180.5	331.8
1498.5	846.6	132.9	413.8	283.5	95.10%	0.688	180.5	360.9
1498.3	912.8	143.2	414.2	302.4	95.14%	0.694	180.4	390.6
1498.4	980.3	153.8	414.9	322.4	95.14%	0.698	180.5	421.7
1498.3	1048.6	164.5	415.6	343.5	95.08%	0.700	180.4	454.1
1498.4	1117.4	175.3	416.7	365.7	95.00%	0.699	180.4	487.7
1498.0	1131.2	177.5	416.8	370.4	94.96%	0.699	180.4	495.0
1497.7	1144.8	179.5	417.1	374.6	94.99%	0.699	180.5	501.2
1499.0	1159.3	182.0	417.5	379.8	94.92%	0.698	180.4	509.0
1498.8	1172.7	184.1	417.7	384.4	94.87%	0.698	180.4	516.1
1499.1	1186.3	186.2	418.0	389.1	94.83%	0.697	180.4	523.1

### ***Rated Point Comparison***

The designed motor and produced motor are compared at the rated point for the correspondence with each other at different parameters.

Table 4.2 presents the comparison at rated point (1500 RPM) and the rated output power (180 kW) of the designed motor. It shows that the efficiency of the design and prototype is very similar, while power factor is lower, leading to increase in required stator current. Additionally, magnetising current  $i_d$  is lower in the prototype to achieve the same value of supply voltage, meaning that inductances of the machine are slightly different.

Table 4.2

Comparison of designed and prototype SynRM at rated point

<b>Parameter</b>	<b>Unit</b>	<b>Design</b>	<b>Prototype</b>
Supply current	$I_1 [A]$	392.4	374.6
Supply voltage	$U_1 [A]$	420	417.1
Power factor	$\cos \varphi$	0.663	0.699
Supply power	$P_{in} [W]$	189200	189034
Mechanical power	$P_{out} [W]$	179144	179546
Rotor angular velocity	$n [RPM]$	1500	1498
Mechanical torque	$T_{out} [W]$	1141	1144.8
Stator winding losses	$\Delta P_{el1} [W]$	5637	4409
Iron losses	$\Delta P_{mag} [W]$	2873	2390
Mechanical losses	$\Delta P_{mech} [W]$	544	810
Additional load losses	$\Delta P_{add} [W]$	1002	1890
Total losses	$\Sigma \Delta P [W]$	10056	9488
Efficiency	$\eta [\%]$	94.69	94.99
$d$ -axis current	$i_d [A]$	205.8	180.5
$q$ -axis current	$i_q [A]$	526	501

Comparison of the designed and produced SynRM at different loads at 1500 RPM is shown in Fig. 4.16.

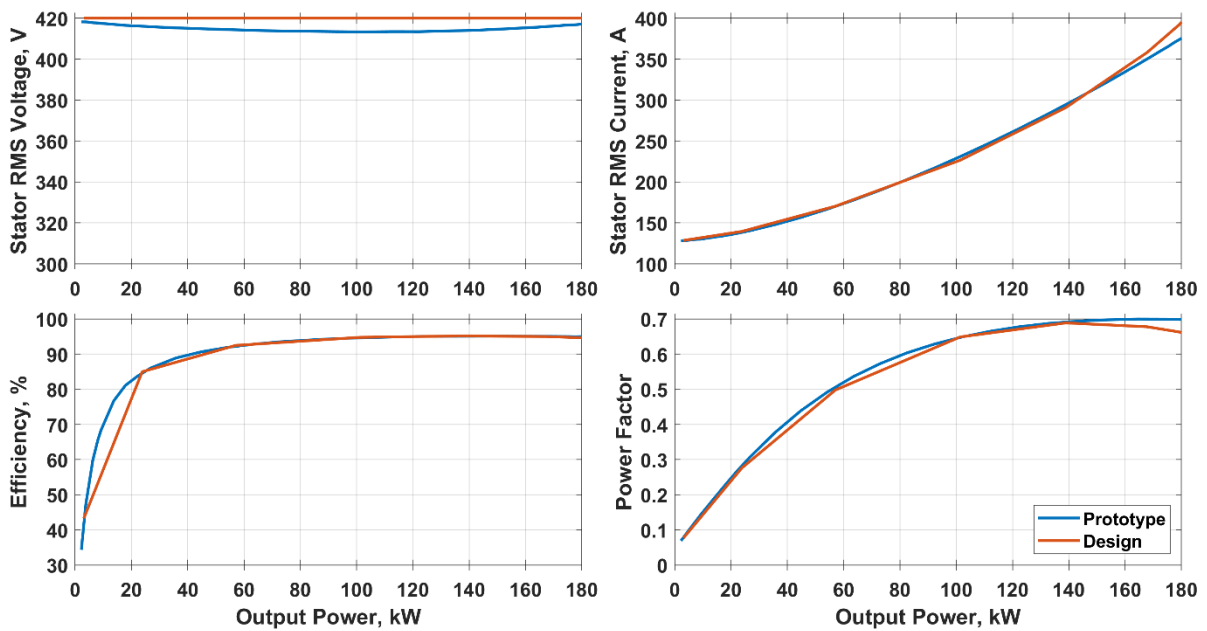


Fig. 4.16. Comparison of designed and produced SynRM.

**Traction Characteristic**

The produced SynRM was tested below 1500 RPM for required and slightly higher torque, while above 1500 RPM it was tested at 420 V up to the maximum achievable torque. Fig. 4.17 presents is the traction characteristic comparison of designed, produced and reference torque characteristics.

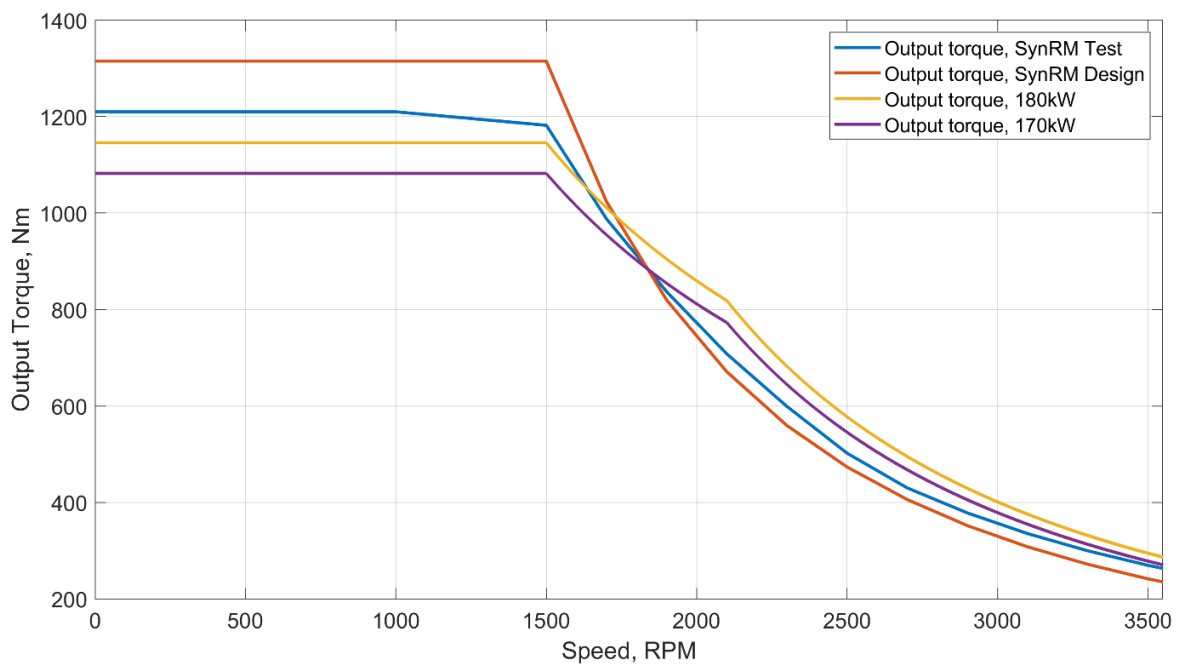


Fig. 4.17. SynRM test, design, and reference output torque curves.

Table 4.3 is the comparison of trolleybus performance of designed and produced performance.

Table 4.3

Comparison of trolleybus performance with designed and produced SynRM

	Designed SynRM	Produced SynRM
	Horizontal road	
Time to 45 km/h, s	17.36	17.32
$a_{max}$ [ $m/s^2$ ]	1.19	1.09
Residual force at 60 km/h	3.7%	16.8%
Top speed, km/h	60.7	63.1
	12 ‰ Inclination	
Time to 45 km/h, s	21.98	21.37
$a_{max}$ [ $m/s^2$ ]	1.09	0.99
Residual force at 54 km/h	–	6.0%
Top speed, km/h	52.9	54.8

From the calculation could be seen that motor design was optimised for the rated point with high efficiency, while it had very steep maximum torque reduction at speeds above rated. It is still able to achieve maximum speed and required time, but residual force requirement is not met.

Produced motor on the other hand, has very similar performance, being able to achieve required time and speed, while also sustaining above 10% residual force. Given difference, even though maximum torque of the designed machine is higher, since produced motor has less steep maximum torque reduction above rated speed.

Output torque of the designed motor above rated speed follows  $T_{out} \propto \left(\frac{1}{n}\right)^2$  rule, while tested prototype has lower power factor of  $T_{out} \propto \left(\frac{1}{n}\right)^{1.8}$ .

### 4.3. Laboratory Investigation of SynRM Parameters

Full mathematical model of the motor is derived for the usage in the Simulink model of the electric drive. Additionally, knowledge of the SynRM model helps to derive more optimal control approach.

### 4.3.1. Mechanical Losses

Mechanical losses are a consequence of bearing friction losses and windage losses of rotating rotor [13]. And there are number of ways to determine mechanical losses of the rotating machine experimentally.

One of them is deceleration test [34], which provides dry torque and friction coefficient of the machine. This test is useful when these specific dry torque and friction coefficient values are of importance for specific application. But as this test has been conducted several times on several machines, it is not the most reliable and has big margin of error, as these values are very small, especially the dry torque, which could be in order of only several Nm.

Another approach, especially when laboratory setup has output torque sensor, is to measure friction torque at several different values of speed with unloaded machine. After that make second order polynomial curve fitting. Second order polynomial is the most common dependency [13].

Output torque is a sum of total friction losses for both machine on a test-bench, but due to both machines are of the same rated power and with ventilator coupled to the shaft, losses are assumed to be equal for each of machines, there for half from the measured value.

Fig. 4.18 presents processed values of the torque and speed in blue dots, and second order polynomial approximation in red.

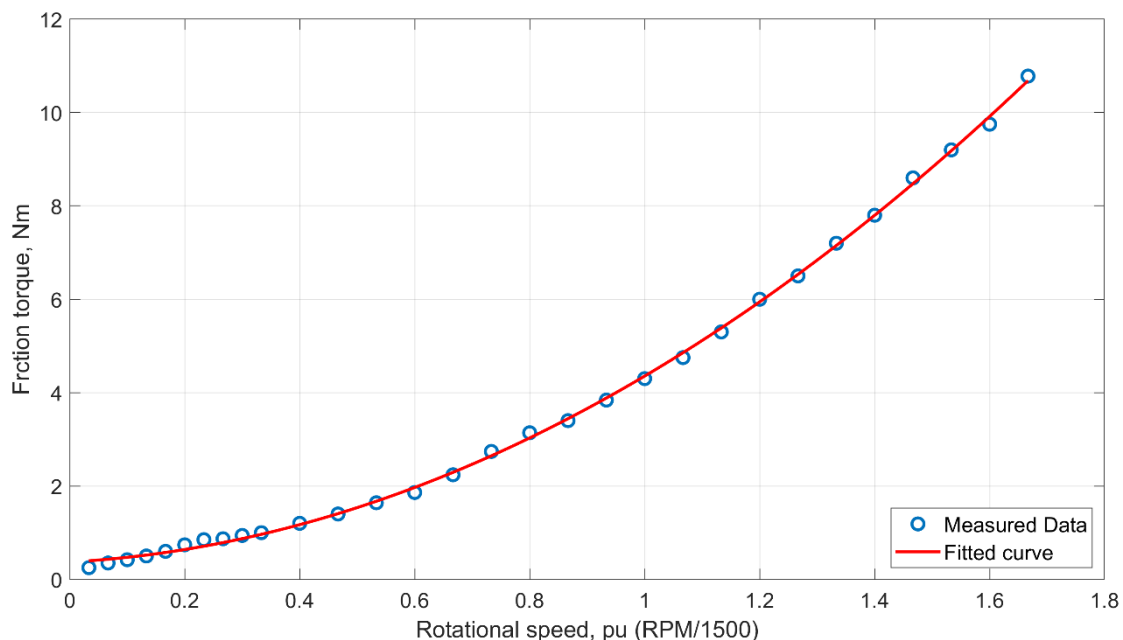


Fig. 4.18. Mechanical losses of the SynRM.

Second order polynomial fitting is done with the Curve Fitting Toolbox of Matlab. Fitted model used is  $T_{mech} = p_1 \cdot n_{pu}^2 + p_2 \cdot n_{pu} + p_3$ . Approximation coefficients are

$p_1 = 3.304; p_2 = 0.68; p_3 = 0.3708$  with 95 % confidence bounds. And goodness of fit is  $R^2 = 0.9993$ , which is very accurate.

#### 4.3.2. Stator Winding Resistance

Stator winding resistance is an important value, to accurate mathematical modelling of the machine, and later calculation of the inductance values.

Value is measured using the milli-ohmmeter at the room temperature stator windings and the value is brought to the 20 °C. The measurements are taken for each of three phases (winding pairs), average value is taken and divided by 2 to get resistance of a single winding.

The value of the resistance of the one phase winding brought to 20 °C is  $R_S = 9.6 \text{ m}\Omega$ .

#### 4.3.3. D- and q-axis Inductances

The most important values for the control and modelling of SynRM are  $d$ - and  $q$ -axis inductances ( $L_d$  and  $L_q$  correspondingly). For many mathematical models parameters at rated point are sufficient, but for traction applications it is crucial to know values at all points of inside traction characteristic, and/or inside torque limit at specified voltage.

Therefore, it is very important to obtain accurate  $L_d$  and  $L_q$  values and their dependences on magnetic saturation and cross-saturation. Testing shows the dependency on both currents in a form of  $L_d = f(i_d, i_q)$  and  $L_q = f(i_d, i_q)$ .

Testing of SynRM to produce accurate values of inductances is done by loading it with another machine and setting  $i_d$  current to a range of different values. Changing of both currents at one value of torque, produces dependency on both. And based on literature sources, inductances values depend only on currents, and not on rotational speed [12]. Thus, testing was decided to make at rated rotational speed of 1500 RPM.

Obtainment using above mentioned approach is possible due to state equations of SynRM, which are shown below [9], [24].

$$\begin{aligned} v_d &= R_s i_d - \omega_s L_q i_q + L_d \frac{di_d}{dt}; \\ v_q &= R_s i_q + \omega_s L_d i_d + L_q \frac{di_q}{dt}; \end{aligned} \quad (4.1.)$$

where  $v_{d/q}$  is  $d$ - $q$ -axis voltage;  $i_{d/q}$  is  $d$ - $q$ -axis stator current;  $\omega_s$  is synchronous electrical angular velocity.

Derivative part is neglected because measurement is done in a steady-state regime. And when all the values are known, except  $L_d$  and  $L_q$  in a system of two equations, derivation of inductances is straightforward.

To accurately calculate inductance values, stator winding resistance  $R_s$ ,  $d$ - and  $q$ -axis stator current and voltage components and angular velocity are required.

$R_s$  is measured, and it is adjusted based on the winding temperature, measured during the operation. Angular velocity is measured using encoder at the shaft. Current components are obtained from the logs of the control system, which are decoupled stator currents values from current sensors using the rotor position from the resolver measurements.

Three phase stator currents are measured directly, while voltage values are not measured directly, but recorded from the control system output ( $u_d, u_q$ ). During laboratory testing these values were proven to be unreliable, and voltage angle could drift away. Therefore, reconstruction based on measured active and reactive powers is done, as shown in equations below.

$$P_{in} = \frac{3}{2}(i_d u_d + i_q u_q); \quad (4.2.)$$

$$Q = \frac{3}{2}(i_d u_q - i_q u_d);$$

where  $P_{in}$  is active input power;  $Q$  is reactive input power.

Calculated  $L_d$  and  $L_q$  dependencies are shown in Fig. 4.19 and Fig. 4.20.

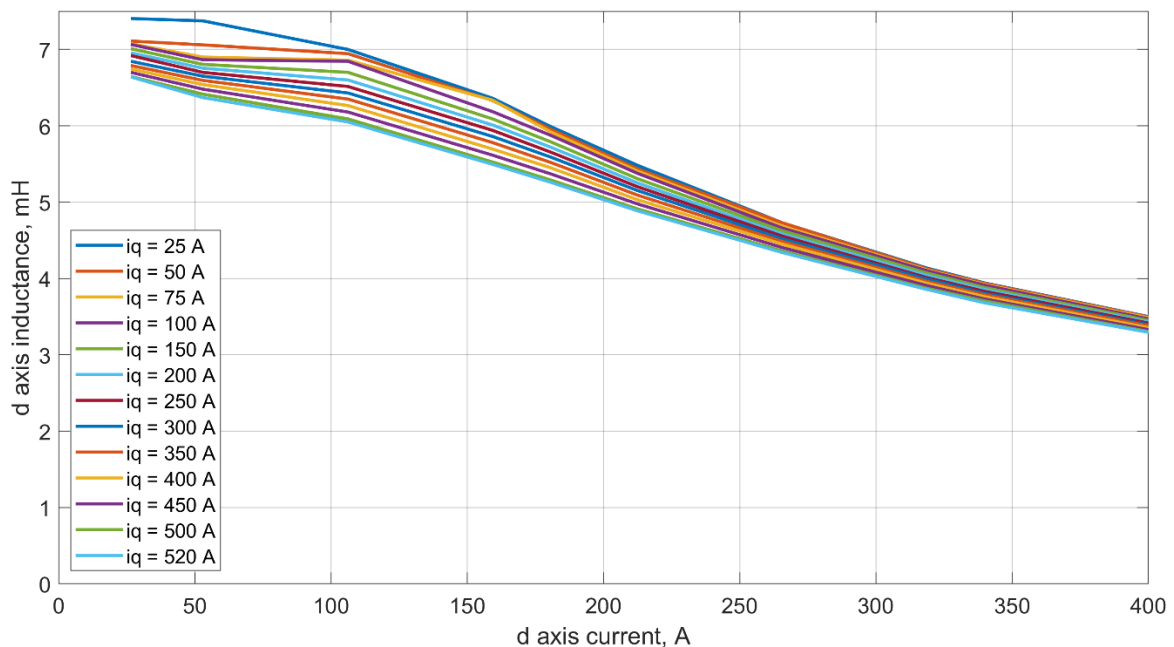


Fig. 4.19. D-axis inductance curve.

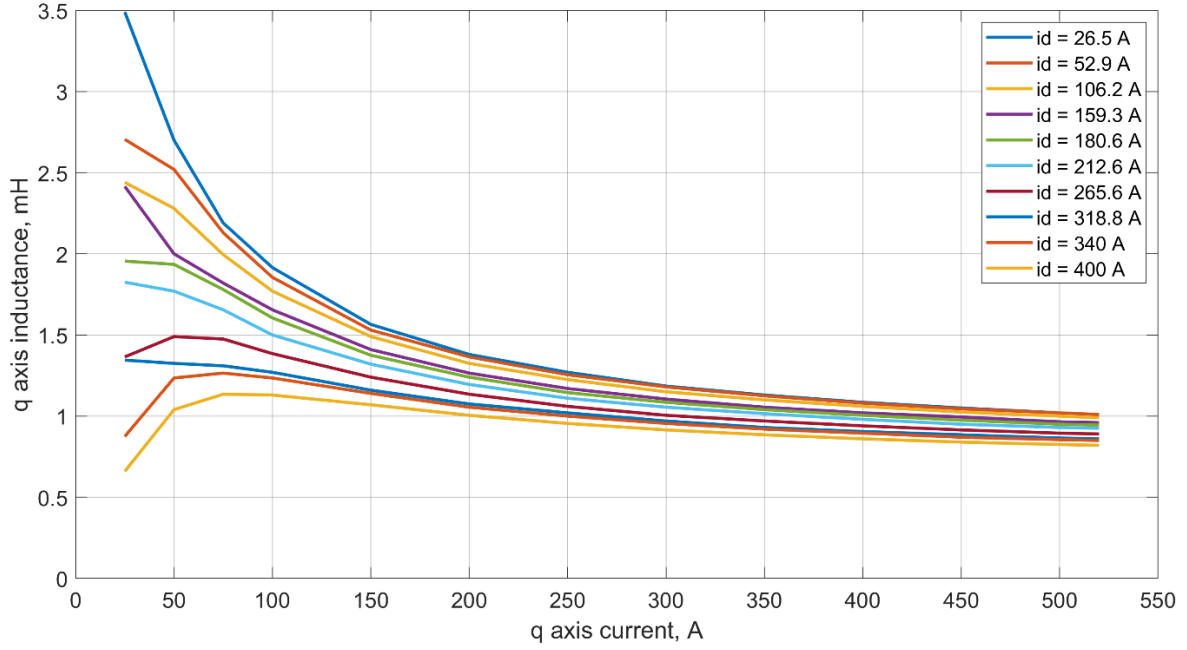


Fig. 4.20. Q-axis inductance curve.

#### 4.3.4. Thermal testing of SynRM

One of the requirements of the SynRM at the design stage was S2-60 min operating regime. Therefore, thermal test should be carried out for the produced prototype to establish whether the motor could be used in such operating regime without overheating.

SynRM was tested for heating at rated speed (1500 RPM) and load (180 kW or 1145.9 Nm) for 1 hour. Motor was loaded by the 180 kW IM from near room temperature environment. At the beginning temperature was 29.1 °C. After 1 hour, end temperature was 88.7 °C.

Based on the measured values, exponential approximation was performed to find numerical value of temperature time constant.

Approximation is done, based on the following expression [35], with coefficients shown below.

$$\tau = (\tau_{max} - \tau_{beg}) \cdot \left(1 - e^{-\frac{t}{T}}\right) + \tau_{beg} \quad (4.3)$$

Where  $\tau_{max} = 105.1 \text{ }^{\circ}\text{C}$  – expected steady-state temperature;  $T = 40.3 \text{ min}$  – time constant;  $\tau_{beg} = 26.92 \text{ }^{\circ}\text{C}$  – expected temperature at the beginning of the test.

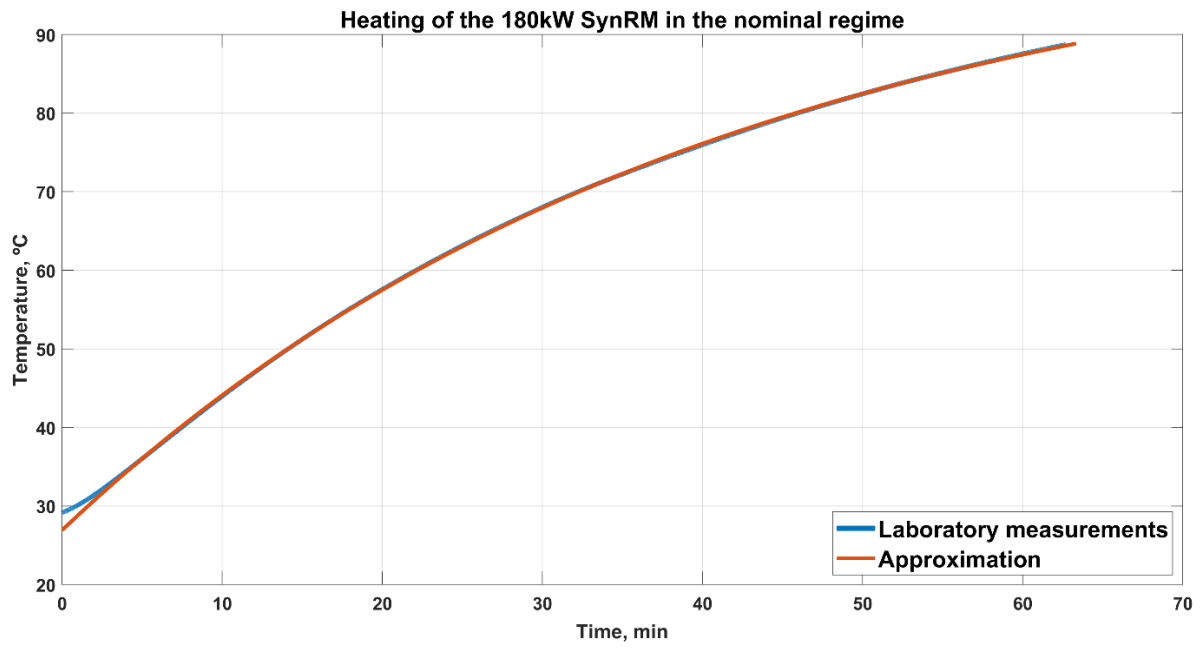


Fig. 4.21. Thermal test curve of SynRM.

Fig. 4.21 presents the laboratory temperature measurement and corresponding approximation. Approximations fits measured data perfectly with the R-squared of 1.

## 5. Verification of SynRM Control System Performance in Traction Drive

Verification of the control system performance allows to make conclusions about the developed product and provides information for future improvements. Verification is carried out by laboratory and model testing in different steady-state and transient regimes. Model testing allows to predict the control system performance on real vehicle in the edge cases, to assure stable operation.

The performance of SynRM traction drive is also compared to the conventional IM traction drive.

### 5.1. Investigation of SynRM and IM Performance in Traction

#### 5.1.1. Comparison of Maximum Torque Capabilities

The maximum torque coefficient indicates the ability of the electric motor to deliver the required torque at a reduced supply voltage. In vehicles powered by a DC traction grid, this indicator is critically important, since the grid voltage can be reduced by 30 % of the rated during operation.

Laboratory testing of SynRM showed (Fig. 4.17) that the electric motor provides the required rated torque, up to a rated speed of 1,500 RPM, and does not meet the requirements in the field-weakening regime.

For comparison, Fig. 5.1 shows the rated reference and theoretical maximum traction characteristics of the used 180kW induction motor for the trolleybus.

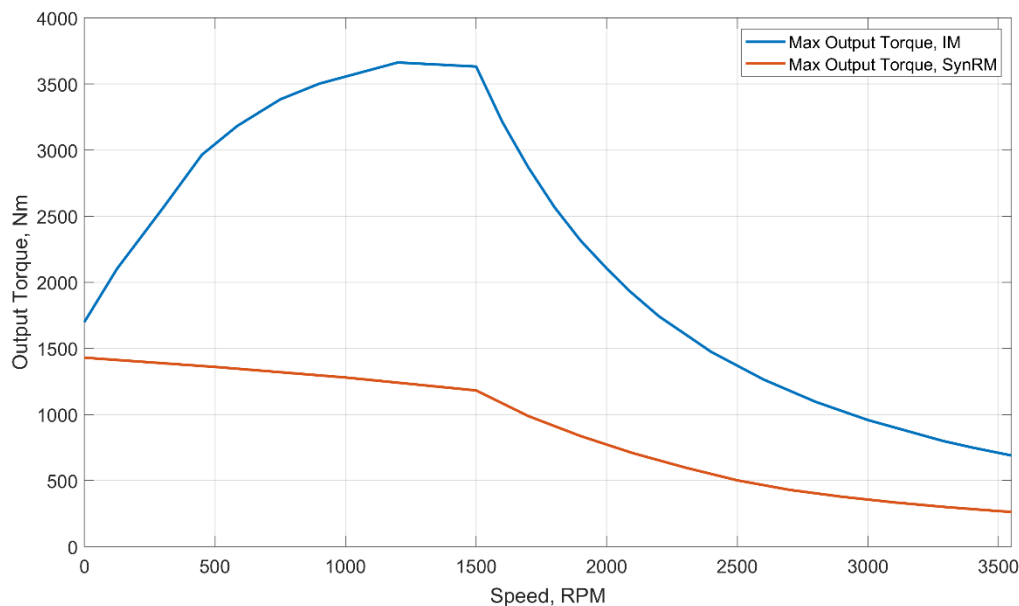


Fig. 5.1. Maximum output torque of 180 kW IM.

It can be seen that the maximum torque is significantly higher than the maximum torque of SynRM. In addition, in the field-weakening regime, the induction motor can provide the required torque, with a 50 % reserve at the maximum required speed.

### 5.1.2. Comparison of Efficiency Indicators

For the research of electric drives electric motor efficiency is important parameter. For traction applications, it is convenient to use the efficiency map since the motor operates in different modes while the vehicle is moving. Full process description was published in the RTUCON 2021 conference [36]. Created efficiency maps in the later chapter are used for the accurate calculation of losses in the urban driving cycle for motors comparison.

Efficiency of each of the motors is obtained experimentally. Efficiency is calculated as a ratio of output power on the shaft and input power on the motor terminals.

$$\eta = P_{out}/P_{in} \quad (5.1.)$$

Output power is derived from the output torque and rotational speed.

$$P_{out} = T_{out} \cdot \omega_m \quad (5.2.)$$

Input power was measured using the Yokogawa WT1800 from stator line current and voltage, while output power was measured as a product of output torque on the shaft and rotational speed. Full description of the laboratory testing, and measurement setup was discussed in the Chapter 4.2.1.

Efficiency maps of IM and SynRM show significant contour lines representing efficiency values in percent, with colour bar to the right showing the colour coding of each graph. Each of the efficiency values is brought to 150°C.

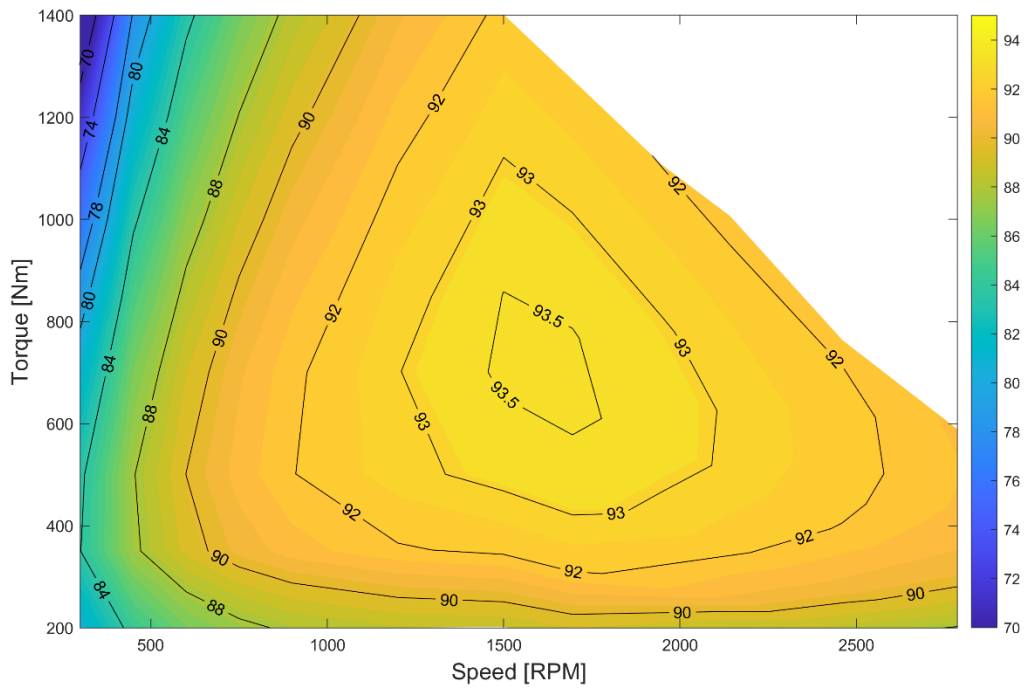


Fig. 5.2. Efficiency map of IM with  $i_d = const.$

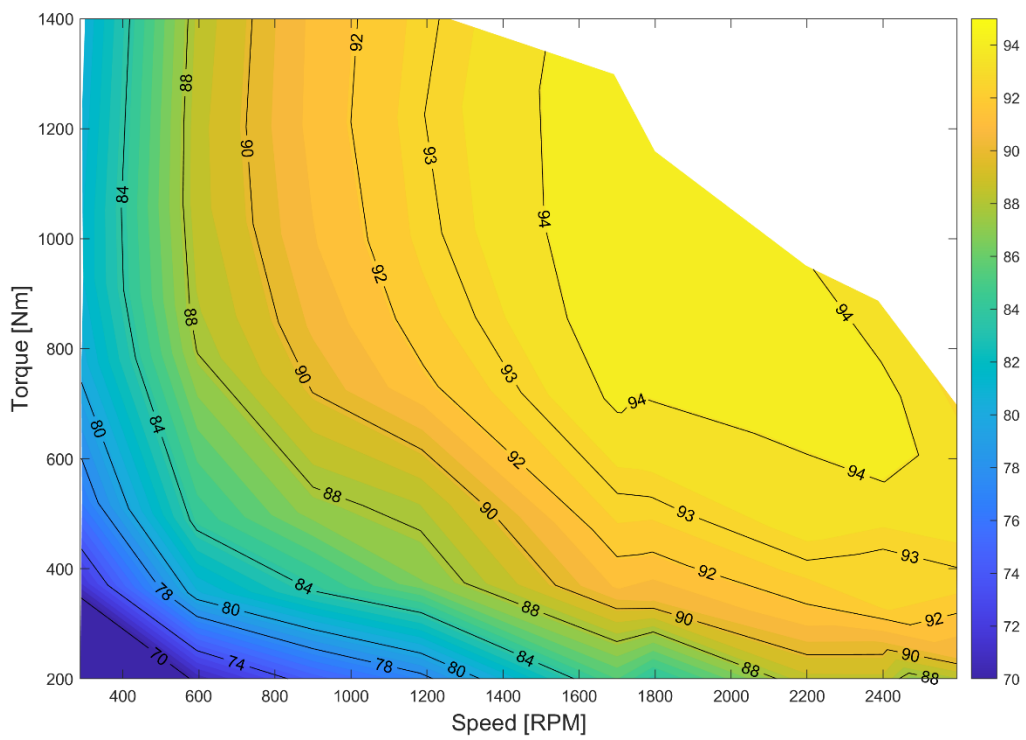


Fig. 5.3. Efficiency map of SynRM with  $i_d = const.$

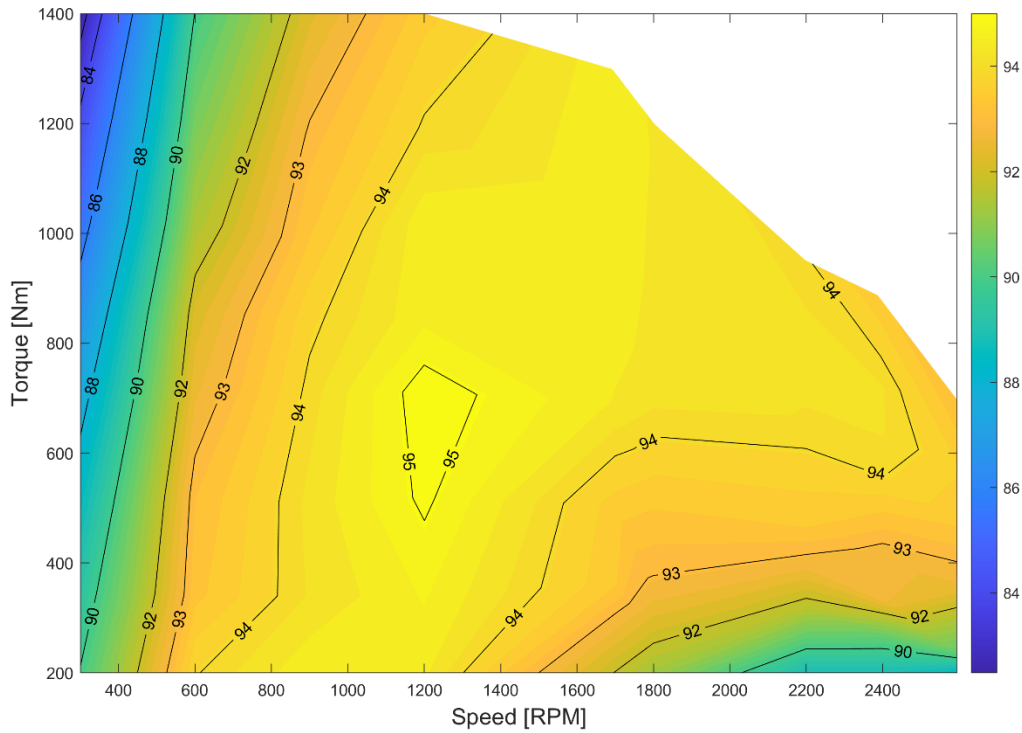


Fig. 5.4. Efficiency map of SynRM with MTPA.

***Efficiency maps with  $i_d = const.$***

Initial comparison of IM and SynRM efficiency maps is done using the identical approach, i.e. with constant  $d$ -axis current control. This is done to compare the motors with the same control.

The results are presented in Fig. 5.2 and Fig. 5.3. The tests were performed both below the rated point and above it in the field-weakening regime.

It can be seen that SynRM performs worse at lower load levels up to approximately 700 Nm at a whole speed range. But above the rated point closer to the rated power, SynRM becomes more efficient.

This is a preliminary comparison, so to establish the performance with the same control approach. As would be seen further this is far from optimal, where MTPA control is presented as a viable option to improve motor performance.

***Control approach comparison of the SynRM***

As was seen from the previous test, SynRM with constant  $d$ -axis control falls behind the IM in efficiency at lower load levels. To combat that, MTPA control strategy is used to improve the performance of the machine below the voltage limit.

Fig. 5.3 and Fig. 5.4 show the comparison of SynRM efficiency maps utilizing two different control strategies: constant  $d$ -axis current and MTPA controls. MTPA is used up to 520 V limit, which is the rated voltage of the machine. When the MTPA control becomes unachievable, it is switched to  $i_d = const.$

It can be seen that at all operational points, where usage of MTPA is possible, efficiency of the machine is improved considerably. Moreover, the efficiency map of the SynRM with MTPA control is much flatter, with the minimum of 82.48 % at measured 300 RPM and 1400 Nm, and the maximum of 95.21 %. Whereas  $i_d = const$  control falls to the minimum of 60 % at measured 300 RPM and 200 Nm, with the maximum of 94.71 %.

In contrast, IM falls to 66.53% at measured 300 RPM and 1400 Nm, with the maximum of 93.61%.

### 5.1.3. Distribution of IM and SynRM losses

Efficiency maps provide overall view and visual comparison of the motors in whole working range. More detailed information for thorough analysis of motors is obtained by means of distribution of losses with each of the control strategies.

Fig. A2.1 (Appendix A2) shows the constituent parts of losses of IM and SynRM with constant  $d$ -axis control at rated load. For more detailed numerical comparison rated point is chosen for three scenarios. Summary of the results is presented in Table 5.1.

Table 5.1  
Distribution of motor losses in steady-state at rated point

Parameter	Unit	IM	SynRM CDAC	SynRM MTPA
Stator current	V	529	522	481.2
Stator current	A	229.4	370.5	350.6
Power factor	p.u.	0.905	0.575	0.664
Input power	W	197276	193657	191451
Rotational speed	RPM	1500	1500	1500
Output power	W	180000	180000	180000
Output torque	Nm	1145.9	1145.9	1145.9
Stator Cu losses	W	4688	6176	5501
Rotor Cu losses	W	4055	-	-
Iron losses	W	5760	4863	3354
Additional losses (1% of input power)	W	1973	1937	1915
Mechanical losses	W	800	681	681
Total losses	W	17276	13657	11451
Efficiency	%	91.24	92.95	94.02

SynRM does not have rotor copper loss, as rotor is comprised only of stamped sheets of electrotechnical steel.

For the constant  $d$ -axis current control rated magnetization of  $\cong 520$  V is chosen, while MTPA is selected as stated above. MTPA control lowers the magnetization of the iron core, consequently substantially lowering iron loss of the motor, and lower current hence lowers stator copper losses. At lower rotational speeds difference in iron loss becomes more prominent, therefore improving the efficiency of SynRM.

While having superior efficiency, SynRM has important drawback to consider, which is substantially lower power factor, as seen in the table. The lower power factor is a physical limitation and needs to be coped with, and it depends on the ratio of inductances, which is dictated by the geometry and material of rotor [5].

$$\cos \varphi = f \left( L_d(i_d, i_q) / L_q(i_d, i_q) \right) \quad (5.3.)$$

Lower power factor in turn requires higher current to be drawn from the power converter, which inflicts higher stress on the switching devices, increasing switching losses.

#### 5.1.4. Comparison of Power Factor

Power factor values have also been taken across the entire speed range. As can be seen from the graph in Fig. 5.5,  $\cos \varphi$  in SynRM it is significantly inferior to IM. The power factor of IM is  $\cos \varphi = 0.67 - 0.7$ , and of SynRM is  $\cos \varphi = 0.85 - 0.9$ . This difference is based on the physical properties of the machine, and a lower power factor was expected at the design stage based on theoretical calculation.

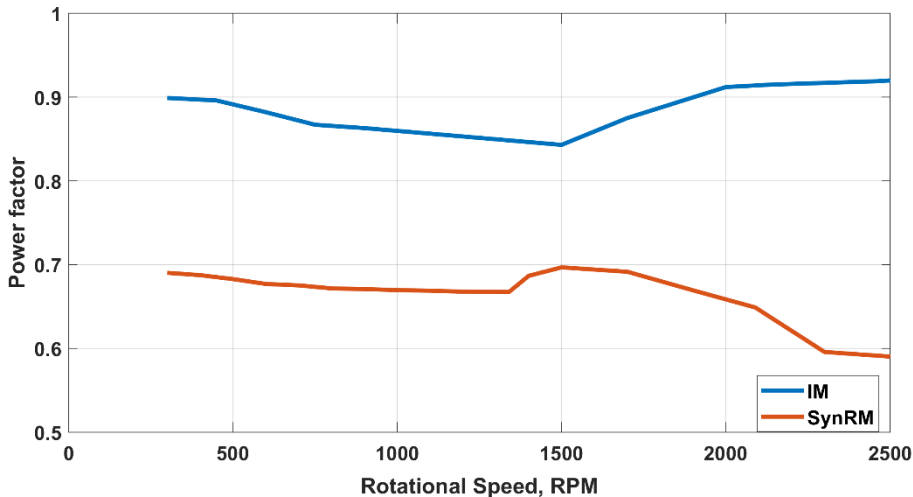


Fig. 5.5. Comparison of motor power factor.

### **5.1.5. Summary of the comparison**

Recently, many studies have been conducted comparing the characteristics of SynRM and IM [37], [38], [39]. However, in the mentioned studies, general industrial electric motors were used, and the issue of traction capabilities was not analysed. This research examines all the parameters required for traction applications.

After laboratory tests and comparative analysis, it can be concluded that the main advantage of the developed and produced synchronous-reluctance motor, compared to the induction motor, is efficiency. The efficiency of the developed motor is high, and its characteristic is much flatter not only at and near the rated point, but also in other regimes of operation.

On the other hand, the desire to increase efficiency negatively affected the torque margin of SynRM. To ensure the required torque, it was necessary to raise the magnetic induction in the iron, relative to the induction of IM, which is the main way of forming the torque in SynRM. As a result, SynRM provided the required torque up to rated speed but failed to meet the additional requirements for the traction application of electric motors. Insufficient torque margin degrades the dynamic performance of the vehicle in operation and leaves very low residual force at maximum speed.

Low power factor is another disadvantage of SynRM. The power factor does not affect the performance or efficiency of the motor but requires more current on the stator windings. As a result, it leads to increased losses in the frequency converter, as well as increases the requirements for the maximum current of the electric drive system. The disadvantage may be less important if the rest of the electric drive equipment has high efficiency.

## **5.2. Performance of the SynRM Traction Drive Simulink Model**

For verification of Simulink model performance several tests were carried out. Direct comparison to the laboratory tests is done at rated speed with different loads, and at different speeds at constant load. Additionally, the trolleybus performance was evaluated based on dynamic requirements.

### **5.2.1. The rated rotational speed test**

This test was carried out at a rated speed of 1500 RPM using constant d-axis current control, thus keeping voltage almost constant. Torque was set to 4 reference values of 0, 200, 730, and 1200 Nm. Visual representation of the test results is shown in Fig. 5.6, and steady-state numerical values are shown in Table 5.2.

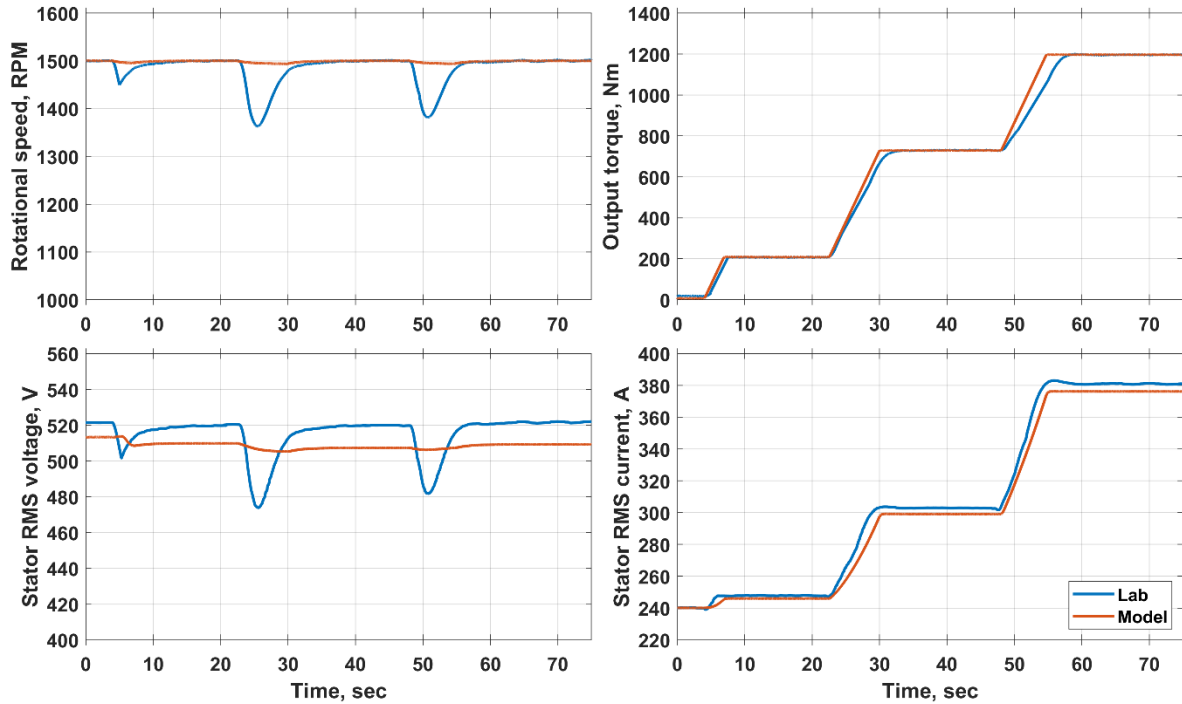


Fig. 5.6. Laboratory and test performance characteristics at the rated speed.

Simulink model was set to the same references; therefore, speed and torque are achieved with no difference. While voltage and current were slightly different, voltage different does not exceed 2.5 %, and current difference was 1.5 %. Small difference was achieved due to accurate laboratory testing of the motor under test. Further improvement to the mathematical model could be done by considering transient processes, which on the other hand requires more sophisticated calculation approaches.

Table 5.2  
Steady-state Values of the Rated Speed Test

Reference Torque	0		200		730		1200	
	Lab	Model	Lab	Model	Lab	Model	Lab	Model
Speed	1500.5	1500	1500.5	1500	1500.5	1500	1500.5	1500
Torque	6.5	18.3	207.1	207.8	730.4	728.8	1196.3	1197
Voltage	521.4	513.4	519.8	509.9	519.9	507.3	521.3	509.3
Current	240.2	240.1	247.7	246.1	303.0	299.2	381.0	376.2

### 5.2.2. Test at different speeds

This test was carried out at a constant load and at different speeds of 300, 500, 700, 900, 1100, 1300, and 1500 RPM. Constant  $d$ -axis current control approach was used for this performance analysis.

Simulink model was set to the same reference as on a laboratory test-bench setup. Results show that model voltage values do not exceed 5.8 % difference between laboratory tests, with the average difference of 1.6 %, while being constantly lower than laboratory measurements. Similarly, current values do not exceed 6.4 % difference between laboratory tests, with the average difference of 2.6 %, while being constantly lower than laboratory measurements. Error outlier is at the lowest speed of 300 RPM and is supposedly due the way of RMS calculation in Simulink at low values of duty cycle.

Visual representation of the test results is shown in Fig. 5.7, and steady-state numerical values are shown in Table 5.3.

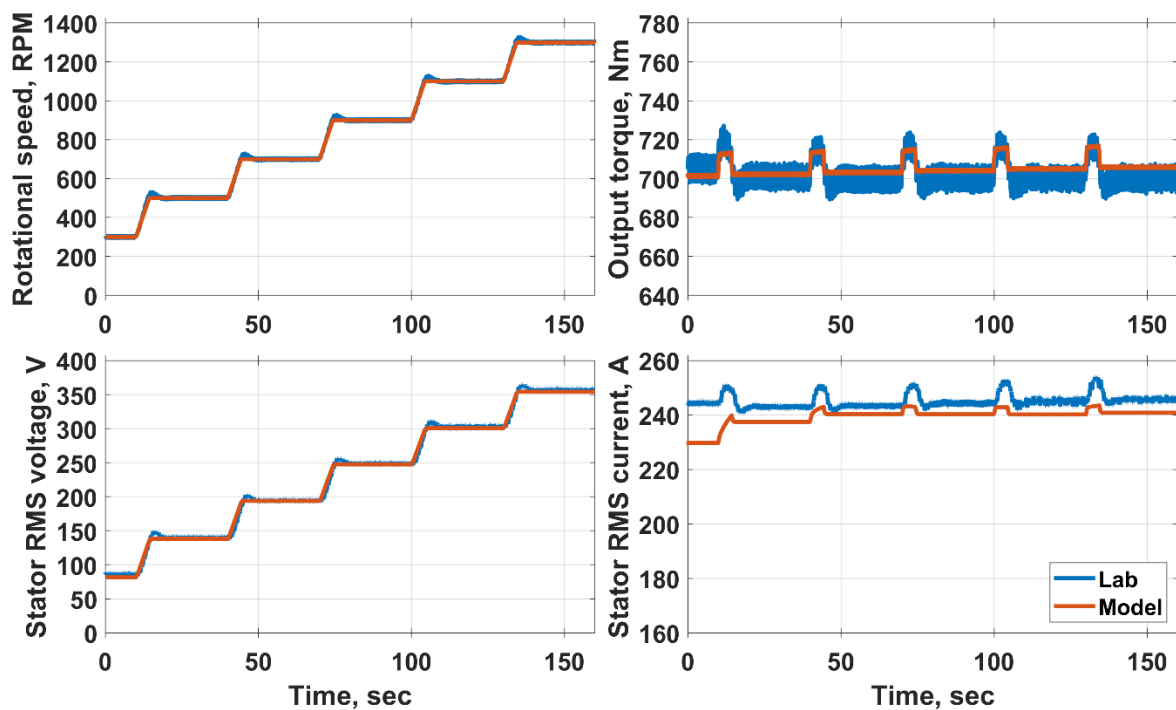


Fig. 5.7. Laboratory and test performance characteristics at constant torque,

Table 5.3 has following abbreviations: L is laboratory, M is Simulink model,  $n_{ref}$  is reference speed in RPM,  $n$  is speed in RPM,  $T$  is output torque in Nm,  $V$  is voltage in V, and  $I$  is current in A.

Table 5.3

Steady-state values of the constant torque test

n ref	300		500		700		900		1100		1300	
	L	M	L	M	L	M	L	M	L	M	L	M
n	300	300	500	500	700	700	900	900	1100	1100	1300	1300
T	705	701	701	702	700	703	700	704	700	705	700	706
V	86.3	81.7	140	138	195	194	249	248	303	301	357	354
I	244	230	243	238	243	240	244	240	245	240	246	241

### 5.2.3. Acceleration till the maximum speed

The test for acceleration to the maximum speed is carried out to test the ability to hold the maximum traction characteristic and whether the fully loaded trolleybus can achieve the dynamic requirements.

The speed reference is set to 60 km/h. Fig. 5.8 presents the output characteristic during the test. It can be seen that acceleration to 45 km/h takes 17.15 seconds, which is inside of the maximum allowable time (Subchapter 1.1). Furthermore, the maximum speed of 60 km/h is successfully achieved with the residual force of 12.2 % ( $T_{out\ max}$  at 60 km/h is 254 Nm,  $T_{out}$  at 60 km/h is 223 Nm). During acceleration rated voltage is sustained close to 420 V, with the peak of 428.3 V during overshoot.

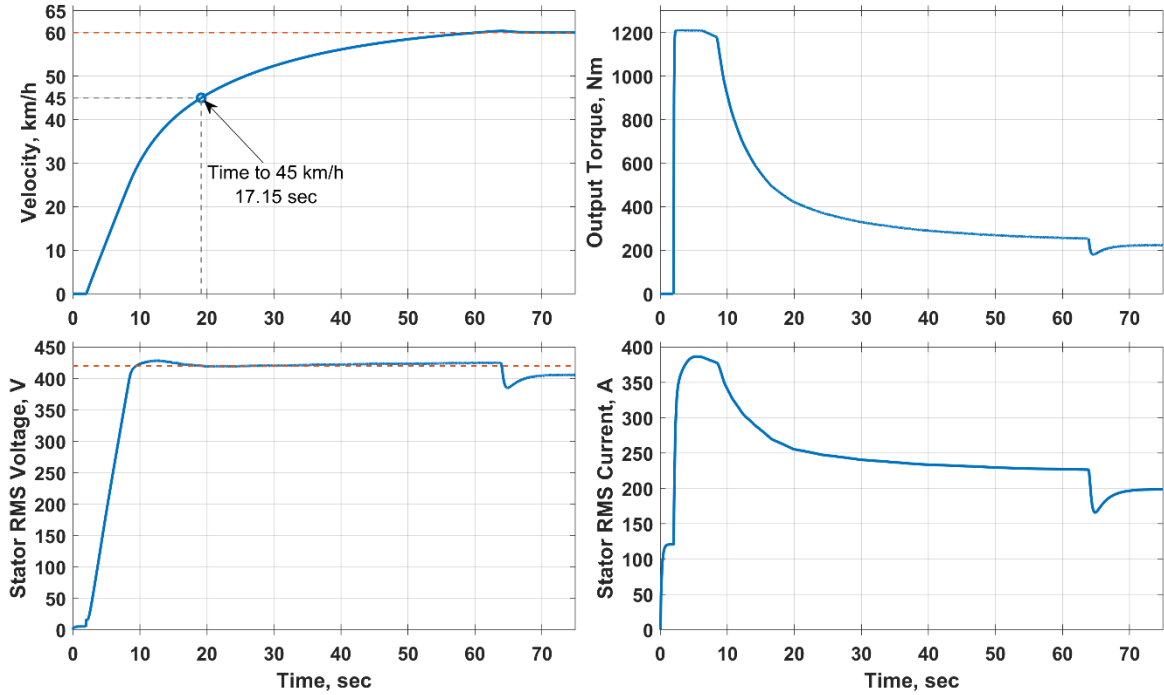


Fig. 5.8. Acceleration to the maximum speed, output characteristics

Acceleration (shown in Fig. 5.9) is dependent on the output torque, and the torque is limited by the traction characteristic. And as it can be seen that acceleration does not go above the limit of  $1.2 \text{ m/s}^2$ , as required. Peak acceleration is  $1.18 \text{ m/s}^2$ , with the average of  $1.1 \text{ m/s}^2$  at the constant torque region.

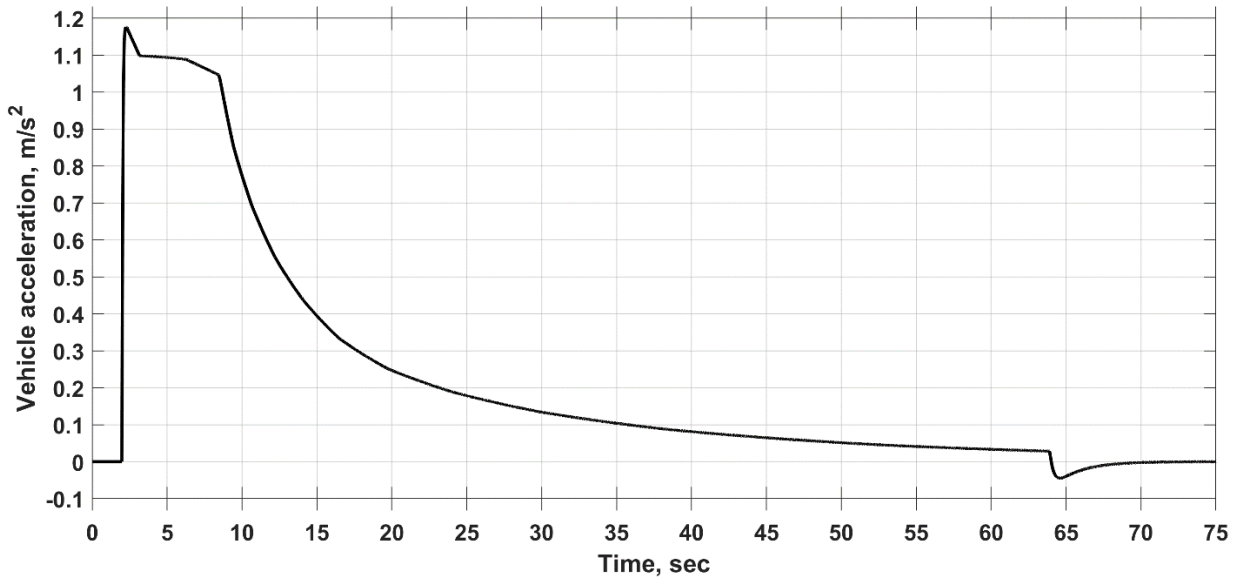


Fig. 5.9. Acceleration graph during the maximum speed test

#### 5.2.4. Performance of the model

Performance of the Simulink traction drive model is tested with a standardized freely available road profile. For model testing the Worldwide Harmonized Light Vehicles Test Procedure defined by the United Nations Economic Commission for Europe [40] was chosen.

This test represents mixed use in an urban environment. Also, this test was selected because it is freely available for urban use, and trolleybus power to mass ratio is appropriate for the use with Class 1 [40].

##### *Dynamic indicators*

Performance simulation is based on class 1 low phase profile. It was carried out to show the dynamics of the vehicle in urban environment. Below in the Fig. 5.10 is the reference speed of the full WLTP Class 1 low phase road profile, which is followed by the vehicle.

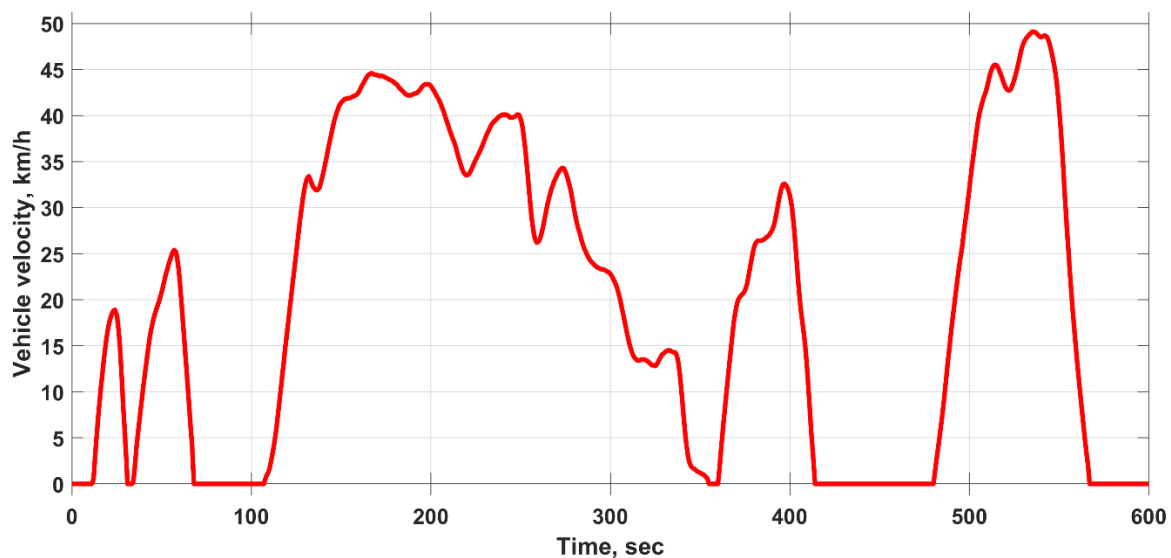


Fig. 5.10. WLTP road profile speed reference

Electric traction drive model is tested both with SynRM with CDAC and MTPA approach, and with IM with CDAC approach.

At first it is important to analyse identical indicators of simulations, which should be achieved with any appropriate motor to follow the road profile reference. These are output torque necessary to keep the reference speed, and therefore instantaneous acceleration of the vehicle at the point in time.

Vehicle acceleration is shown in Fig. 5.11, while torque utilisation is shown in Fig. 5.12. It can be seen that at most of the time motor is working inside the limiting traction characteristic, with only two stretches of road, where maximum is achieved.

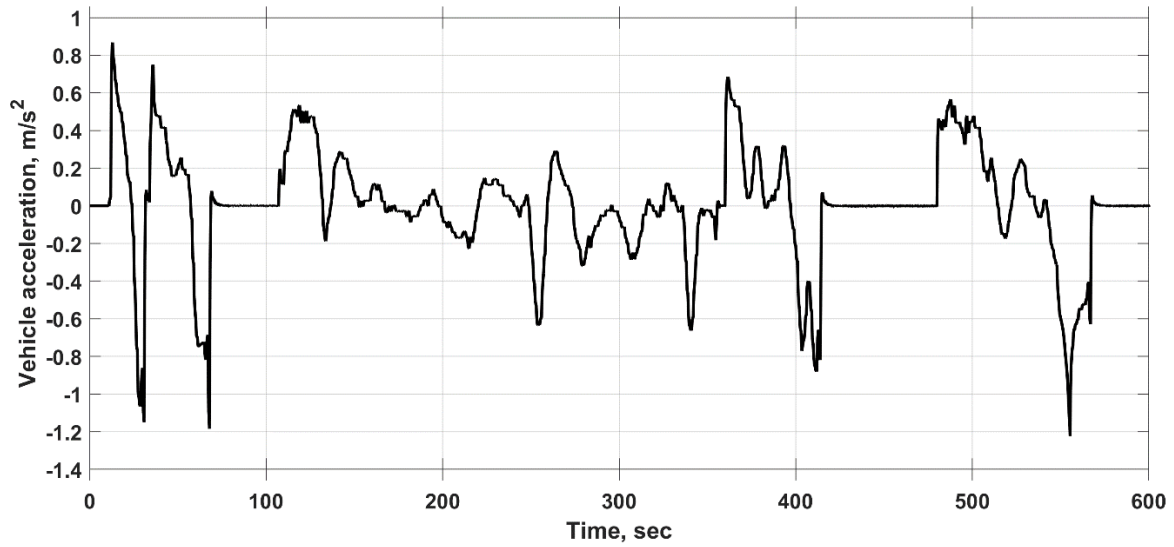


Fig. 5.11. Road profile modelling vehicle acceleration.

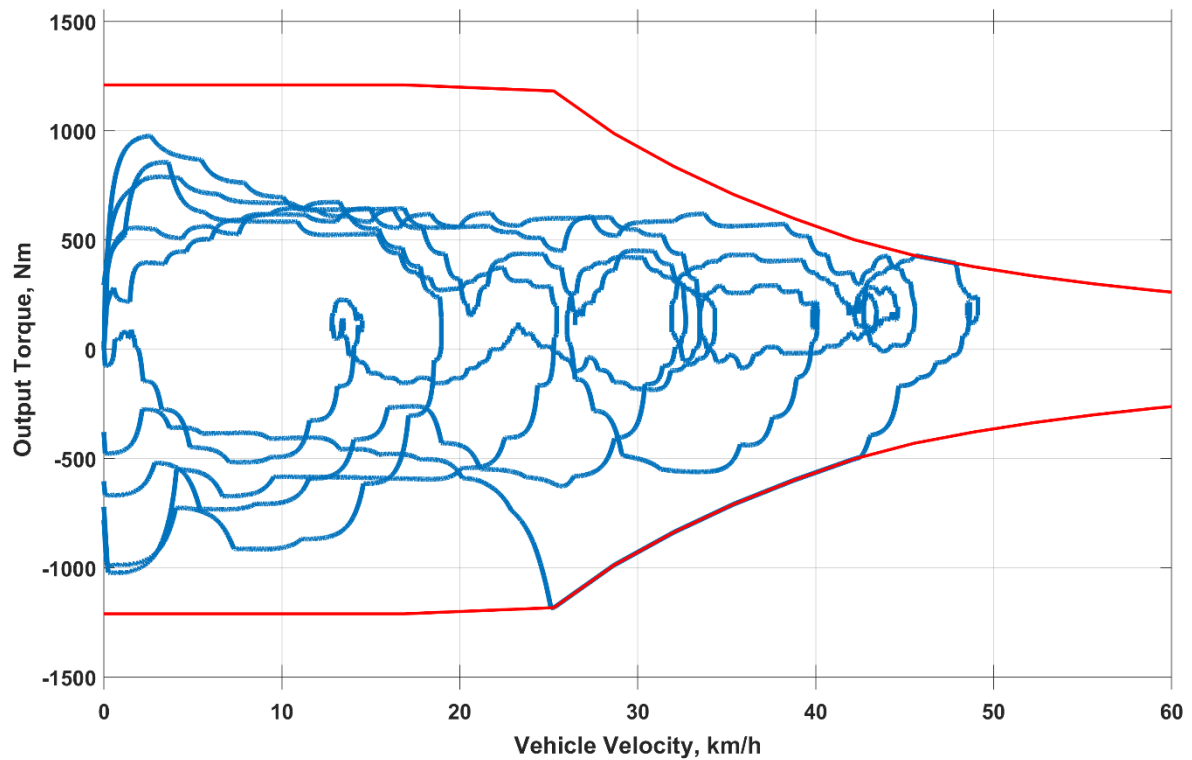


Fig. 5.12. WLTP torque utilisation.

Achieving limiting traction curve makes motor unable to keep up with the reference speed, as seen in Fig. 5.13. At small stretch of road (549 – 557 seconds period), motor output speed dipped by 1.81 km/h compared to the speed reference. While at all other points speed difference did not exceed 0.54 km/h.

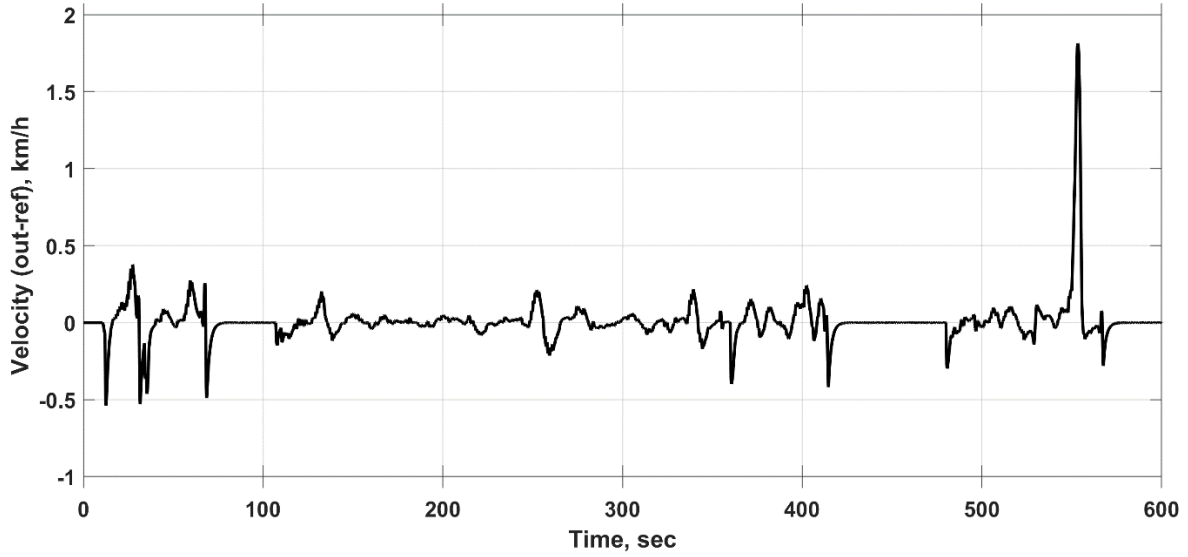


Fig. 5.13. Speed difference (output - reference)

### ***Motor comparison***

Due to different approaches to the control of the motor performance indicators are different, while following the same speed reference.

Output power (kW), output torque (Nm), RMS stator current (A), efficiency and internal power factor (IPF) are shown in the Appendix A2. Efficiency calculation is based on interpolation of experimentally obtained efficiency maps from Chapter 5.1.2, while IPF for SynRM is calculated based on equation (3.5.). And for the IM is calculated based on input active and reactive power equations (5.4.).

$$\begin{aligned}
 P &= \frac{3}{2} (i_d u_d + i_q u_q) \\
 Q &= \frac{3}{2} (i_d u_q - i_q u_d) \\
 \cos \varphi_i &= \frac{P}{\sqrt{P^2 + Q^2}}
 \end{aligned} \tag{5.4.}$$

From the modulation results could be seen that with the MTPA approach efficiency and IPF is kept at more stable value, allowing to optimise losses, and therefore input energy from the converter side. While IM has substantially higher power factor.

### ***Energy consumption***

Below in the

Table 5.4 is the total energy consumed during the driving cycle in kWh. Braking energy is not accounted for recuperation and is just assumed to be converted to heat. Converter efficiency is set to  $\eta_{conv} = 97.5 \%$ .

Table 5.4  
Energy during WLTP cycle

	Value [kWh]
Energy at the wheel	4.04
Input energy (SynRM CDAC)	4.69
Input energy (SynRM MTPA)	4.49
Input energy (IM CDAC)	4.67

From the results of total consumed energy it can be seen that energy loss in the motor with the converter is 0.65 kWh for SynRM CDAC, while for SynRM MTPA it is 0.45 kWh, meaning that 30.7 % reduction of motor loss could be achieved only with the control approach, with sustained level of dynamic performance.

The traction drive with the induction motor shows almost the same energy consumption as with CDAC SynRM (3.2% more than with SynRM) and 40 % bigger energy loss difference compared to the SynRM with MTPA.

## Conclusions

As a result of the research, an experimental prototype of the traction SynRM was developed in the dimensions of the existing IM. Firmware has been developed to control the drive. The operation of the control system was tested on a Matlab Simulink mathematical model. To confirm the results of calculations and simulations, laboratory tests were carried out.

Laboratory tests of SynRM showed a high convergence of the results with the calculated values at the rated speed. The main difference was in the stator current, which indicates a mismatch between the values of  $L_d$  and  $L_q$  at the rated speed. Determination of the inductance values is the most difficult design task, since it can strongly depend on the homogeneity and accuracy of the parameters of the magnetic circuit material, as well as on the quality of the motor assembly.

The torque limit values obtained during testing in the entire speed range also differ from the projected ones due to the discrepancies between the projected inductance curves  $L_d(I_d)$  and  $L_q(I_q)$  and the measured ones. The tests have shown lower values of the maximum torque at rated voltage, but higher in the field weakening mode. During laboratory tests the  $L_d(I_d, I_q)$  and  $L_q(I_d, I_q)$  curves were taken to correct the calculated coefficients. Further design iterations will be carried out, considering the specifics of materials and manufacturing deviations.

The SynRM control system was developed in the Matlab Simulink environment and tested on a real laboratory inverter. The field-oriented control (FOC) algorithm was adopted as a basis. The control system uses the instantaneous values of stator currents and the angle of the rotor position to form a reference of voltage values. To accurately determine the torque, the values of  $L_d(I_d)$  and  $L_q(I_q)$  were entered into the control system using look-up tables. Regulation of currents, torque and speed is carried out using PI controllers. During simulation and in laboratory conditions, the control system reliably and stably fulfilled the commands in the torque-control and the speed-control modes. The developed control system made it possible to implement all the planned tests necessary to confirm the operability and stability of the drive.

Simulation of the dynamics of the trolleybus movement with the developed SynRM showed that the drive meets the acceleration requirements when driving on a slope at rated voltage. The drive performs all specified accelerations and decelerations in the WLTP cycle. The disadvantage of this SynRM is a small margin for the maximum torque, which especially affects the performance of the drive when supply voltage drops below rated value. Even though, according to the requirements of the WLTP test cycle, the maximum torque is never reached, actual operation mode may be more severe.

When comparing SynRM and classic IM, the increase in efficiency declared during the design was confirmed during the tests. At the rated speed, the efficiency increased by 2%. In a region below rated speed, the SynRM degrades the efficiency much more slowly than the IM efficiency. In turn, the power factor of SynRM is reduced relative to IM by 0.2, which increases the stator and inverter currents. When the efficiency of the inverter is high, the difference in power factor should not significantly affect the overall efficiency of the drive.

As a result of the research, it can be concluded that an electric drive based on SynRM can be an alternative to IM. However, in the initial design, it is important to consider the low critical torque reserve and low power factor.

## List of References

- [1] *WHITE PAPER Roadmap to a Single European Transport Area – Towards a competitive and resource efficient transport system*, <http://eur-lex.europa.eu/LexUriServ/LexUriServ.do?uri=COM:2011:0144:FIN:EN:PDF.>, 2011.
- [2] J. Larminie and J. Lowry, *Electric Vehicle Technology Explained*, 2nd Edition, Wiley, 2012.
- [3] “Possibilities of energy demand reduction in trolleybus transportation,” CIVITAS, Brno, 2014.
- [4] W. Backhaus, A. Bätzner, J. Kohout, E. Lenz, R. Kayser and D. S. Röhlig, “Knowledge Brief, Infrastructure for In Motion Charging Trolleybus System,” Knowledge Brief of UITP, the International Association of Public Transport, Brussels, July, 2021.
- [5] R. R. Moghaddam, S. Nategh, J. Islam and A. Boglietti, “Different Traction Motor Topologies Used in E-Mobility : Part II: Magnet-based Solutions,” in *2020 International Conference on Electrical Machines (ICEM)*, 2020.
- [6] E. Bostanci, M. Moallem, A. Parsapour and B. Fahimi, “Opportunities and Challenges of Switched Reluctance Motor Drives for Electric Propulsion: A Comparative Study,” *IEEE Transactions on Transportation Electrification*, vol. 3, no. 1, pp. 58-75, March 2017.
- [7] Heidari, H.; Rassölkin, A.; Kallaste, A.; Vaimann, T.; Andriushchenko, E.; Belahcen, A.; Lukichev, D.V., “A Review of Synchronous Reluctance Motor-Drive Advancements,” *Sustainability*, 2021.
- [8] J. K. Kostko, “Polyphase reaction synchronous motors,” *Journal of the American Institute of Electrical Engineers*, vol. 42, no. 11, pp. 1162-1168, 1923.
- [9] G. Abad, *Power Electronics and Electric Drives for Traction Applications*, Chichester: Wiley, 2017, p. 630.
- [10] K. Gulbis, U. Brakanskis, E. Kamolins, M. Gorobečs, A. Potapovs, K. Sejejs, J. Zarembo and V. Burenin, “Analysis of Test Results of Developed Synchronous Reluctance Motor for Public Transport Application,” *Latvian Journal of Physics and Technical Sciences*, 2021.

- [11] A. Potapovs, U. Brakanskis, M. Gorobecs, K. Gulbis, E. Kamoliņš, K. Sejejs, V. Burenin, J. Zarembo, "180 kW Synchronous Reluctance Motor for Mass Transit Electrical Traction Application," in *23rd European Conference on Power Electronics and Applications (EPE'21 ECCE Europe)*, Brussels, Belgium, 2021.
- [12] R.-R. Moghaddam, *Synchronous Reluctance Machine (SynRM) in Variable Speed Drives (VSD) Applications*, Stockholm: The Royal Institute of Technology, 2011, p. 260.
- [13] J. Pyrhonen, T. Jokinen and V. Hrabovcova, *Design of Rotating Electrical Machines*, Chichester: Wiley, 2014, p. 584.
- [14] J. Pyrhonen, V. Hrabovcova and R. S. Semken, *Electrical Machine Drives Control*, Chichester: Wiley, 2016, p. 504.
- [15] I. Boldea, *Reluctance Synchronous Machines and Drives*, Oxford: Clarendon Press, 1996.
- [16] I. Boldea and S. A. Nasar, *The Induction Machines Design Handbook*, CRC Press, 2009.
- [17] И. П. Копылов, *Электрические Машины: Учебник для вузов*, Москва: Энергоатомиздат, 1986.
- [18] A. Vagati, M. Pastorelli, G. Franceschini and S. C. Petrache, "Design of Low-Torque-Ripple Synchronous Reluctance Motors," *IEEE Transactions on Industry Applications*, vol. 34, no. 4, 1998.
- [19] A. Vagati, "Synchronous Reluctance Electrical Motor Having A Low Torque-Ripple Design". Patent 5818140A, 6 October 1998.
- [20] T. A. Lipo and T. Matsuo, "Rotor design optimization of synchronous Reluctance machine," *IEEE Transaction on Energy Conversion*, vol. 9, no. 2, 1994.
- [21] K. Gulbis, U. Brakanskis, E. Kamoliņš and J. Zarembo, "Parameter Calculation Method of Synchronous Reluctance Motor Including Cross Magnetic Saturation," in *2020 IEEE 61th International Scientific Conference on Power and Electrical Engineering of Riga Technical University (RTUCON)*, Riga, Latvia, 2020.
- [22] M. Kamper, A. F. Volsdhenk, "Effect of rotor dimensions and cross magnetisation on  $L_d$  and  $L_q$  inductances of reluctance synchronous machine with cageless flux

- barrier rotor,” in *IEEE Proceedings - Electric Power Applications, Volume 141, Issue 4*, July 1994.
- [23] A. Podgornovs and R. Geidarovs, “Induction machine mode determination using vectograms and magnetic field calculation results,” in *2017 IEEE 58th International Scientific Conference on Power and Electrical Engineering of Riga Technical University (RTUCON)*, Riga, 2017.
- [24] K. Yahia, D. Matos, J. O. Estima and A. J. M. Card, “Modeling synchronous reluctance motors including saturation, iron losses and mechanical losses,” in *2014 International Symposium on Power Electronics, Electrical Drives, Automation and Motion*, Ischia, 2014.
- [25] “Digital Motor Control. Software Library: Target Independent Math Blocks,” Texas Instruments, Inc. C2000 Systems and Applications, 2013.
- [26] A. J. P. Ortega, *Design and Comparison of Induction Motor and Synchronous Reluctance Motor for Variable Speed Applications: Design Aided by Differential Evolution and Finite Element Analysis*, The Ohio State University, 2013.
- [27] V. Burenin, J. Zarembo, A. Žiravecka and L. Ribickis, “Model of Laboratory Test Bench Setup for Testing Electrical Machines,” in *2020 IEEE 61th International Scientific Conference on Power and Electrical Engineering of Riga Technical University (RTUCON)*, Riga, Latvia, 2020.
- [28] A. Sciarretta and A. Vahidi, *Energy-Efficient Driving of Road Vehicles*, Cham: Springer International Publishing, 2020, p. 294.
- [29] Л. Байрыева и В. Шевченко, *Электрическая тяга. Городской наземный*, Москва: Транспорт, 1986, p. 206.
- [30] В. Розенфельд и И. Исаев, *Теория Электрической Тяги*, Москва: Транспорт, 1995, p. 294.
- [31] I. Dvornikovs, M. Marinbahs, J. Zarembo, E. Groza and K. Ketners, “Investigation of traction motor dynamic using computer simulation and method of mutual loading of two pair motors,” in *2019 16th Conference on Electrical Machines, Drives and Power Systems (ELMA)*, Varna, Bulgaria, 2019.
- [32] G. Kobenkins, M. Marinbahs O. Sliskis, V. Burenin, J. Zarembo, “Carry Out of Strength Tests of Geared Motor Box as Part of a Frequency-Controlled Traction

- Electric Drive,” in *17th Conference on Electrical Machines, Drives and Power Systems (ELMA 2021)*, Sofia, Bulgaria, 2021.
- [33] G. Kobenkins, M. Marinbahs, V. Burenin, J. Zarembo, A. Bizans, O. Sliskis, “Determination of the Level of Own Vibration of Geared Motor Boxes in Industrial Conditions,” in *2021 IEEE 62st International Scientific Conference on Power and Electrical Engineering of Riga Technical University*, Riga, 2021.
- [34] F. Giri, *AC electric motors control: advanced design techniques and applications*, Chichester: John Wiley & Sons Ltd, 2013, p. 555.
- [35] М. П. Костенко и Л. М. Пиотровский, *Электрические Машины, ч. 2, Машины Переменного Тока, т. II*, Ленинград: Энергия, 1973.
- [36] V. Burenin, J. Zarembo, O. Krievs and L. Ribickis, “Comparison of Synchronous Reluctance Motor and Induction Motor Efficiency Maps for Traction Application,” in *RTUCON 2021*, Riga, Latvia, 2021.
- [37] H. Kärkkäinen, L. Aarniovuori, M. Niemelä, J. Pyrhönen and J. Kolehmainen, “Technology comparison of induction motor and synchronous reluctance motor,” in *IECON 2017 - 43rd Annual Conference of the IEEE Industrial Electronics Society*, 2017.
- [38] A. V. Zakharov, S. I. Malafeev and A. L. Dudulin, “Synchronous reluctance motor: Design and experimental research,” in *2018 X International Conference on Electrical Power Drive Systems (ICEPDS)*, 2018.
- [39] A. Rassolkin, H. Heidari, A. Kallaste, T. Vaimann, J. P. Acedo and E. Romero-Cadaval, “Efficiency Map Comparison of Induction and Synchronous Reluctance Motors,” in *2019 26th International Workshop on Electric Drives: Improvement in Efficiency of Electric Drives (IWED)*, 2019.
- [40] United Nations, “Worldwide Harmonized Light vehicles Test Procedure, Addendum 15,” United Nations, 2019.

## A1. Appendix

### Laboratory Equipment

Name of laboratory equipment	Type	Measuring range / Accuracy
Torque flange	K-T40B-005R-MF-S-M-HU2-A-U	±5kNm / 0.05
Current Sensor	ABB ES2000F	±2200A / ≤ ±0.5
Temperature probe, PT100	TSA-1RD.T9. 5.30.2SL.M1.B.3	-50°+200°C / B
Power Analyzer	Yokogawa WT1800	0-1000V, 0-5A / ≤ 0.5 (depends on the mode)
8-Slot Chassis	NI cDAQ-9189	-
8-Ch Counter Input Module	NI 9361	0-5V differential, 0-24V single ended
4-Ch Voltage Input Module	NI 9215	±10 V
8-Ch 100Ohm RTD Analog Input Module	NI 9216	0-400 Ohm
Power Supply	NI PS-15	24-28 VDC
Voltage Inverter	ШПСУ-90 (JSC RER)	1000V, 400kW
Induction Voltage Regulator	ИР-2 (JSC RER)	Up to 1kV

## A2. Appendix

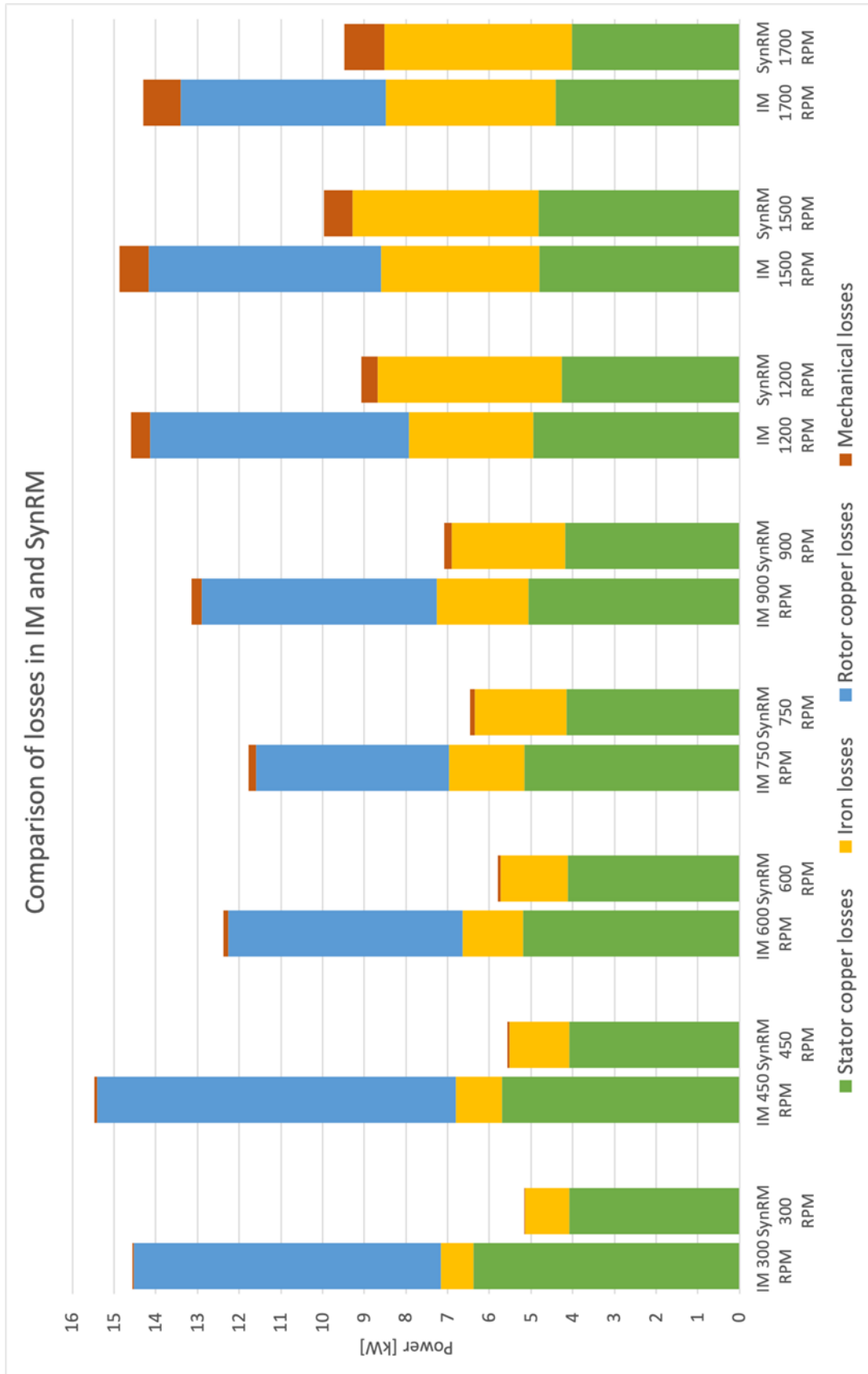


Fig. A2.1. Comparison of constituent parts in motor losses.

### A3. Appendix

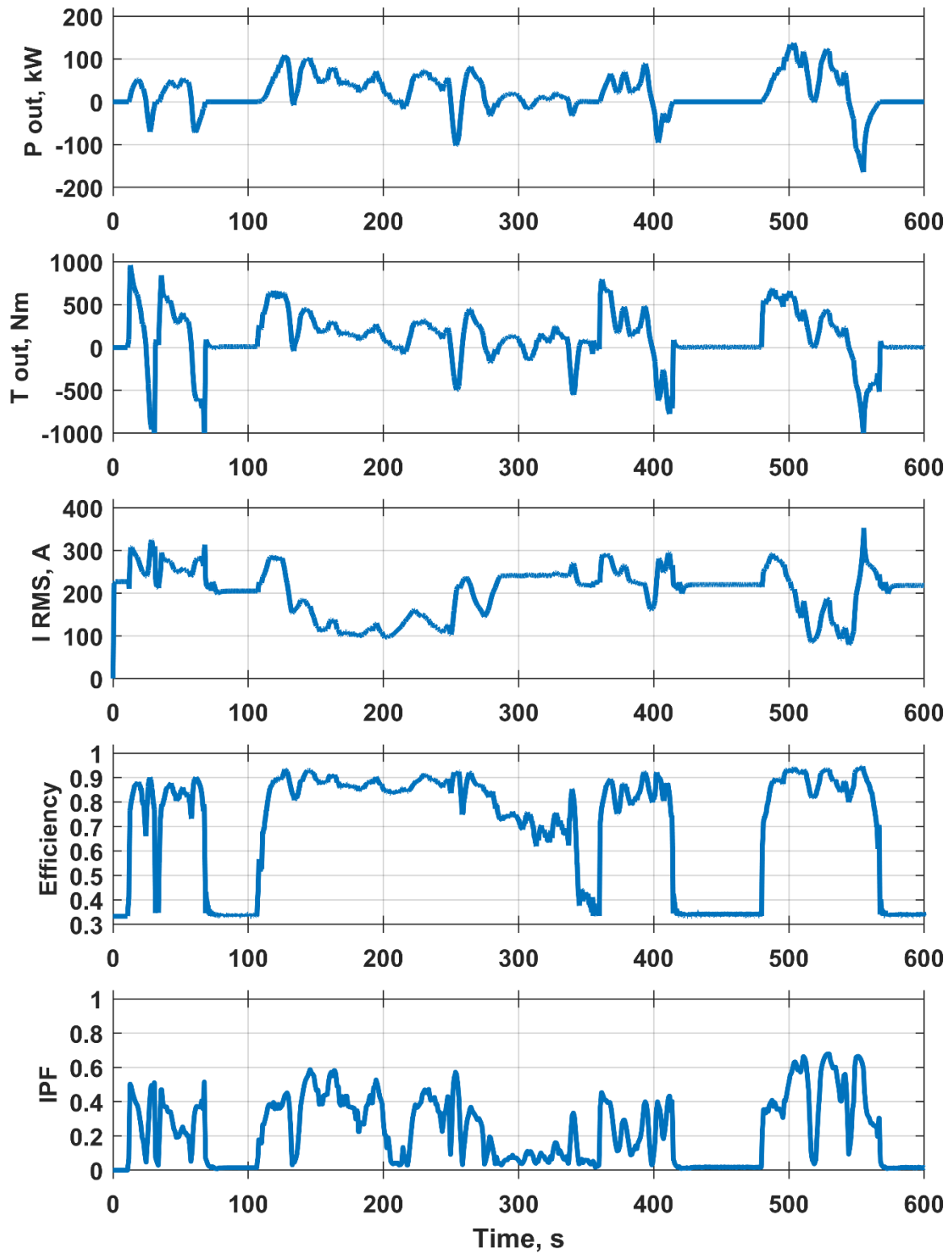


Fig. A3.1. SynRM parameters with CDAC under WLTP Class 1 low phase.

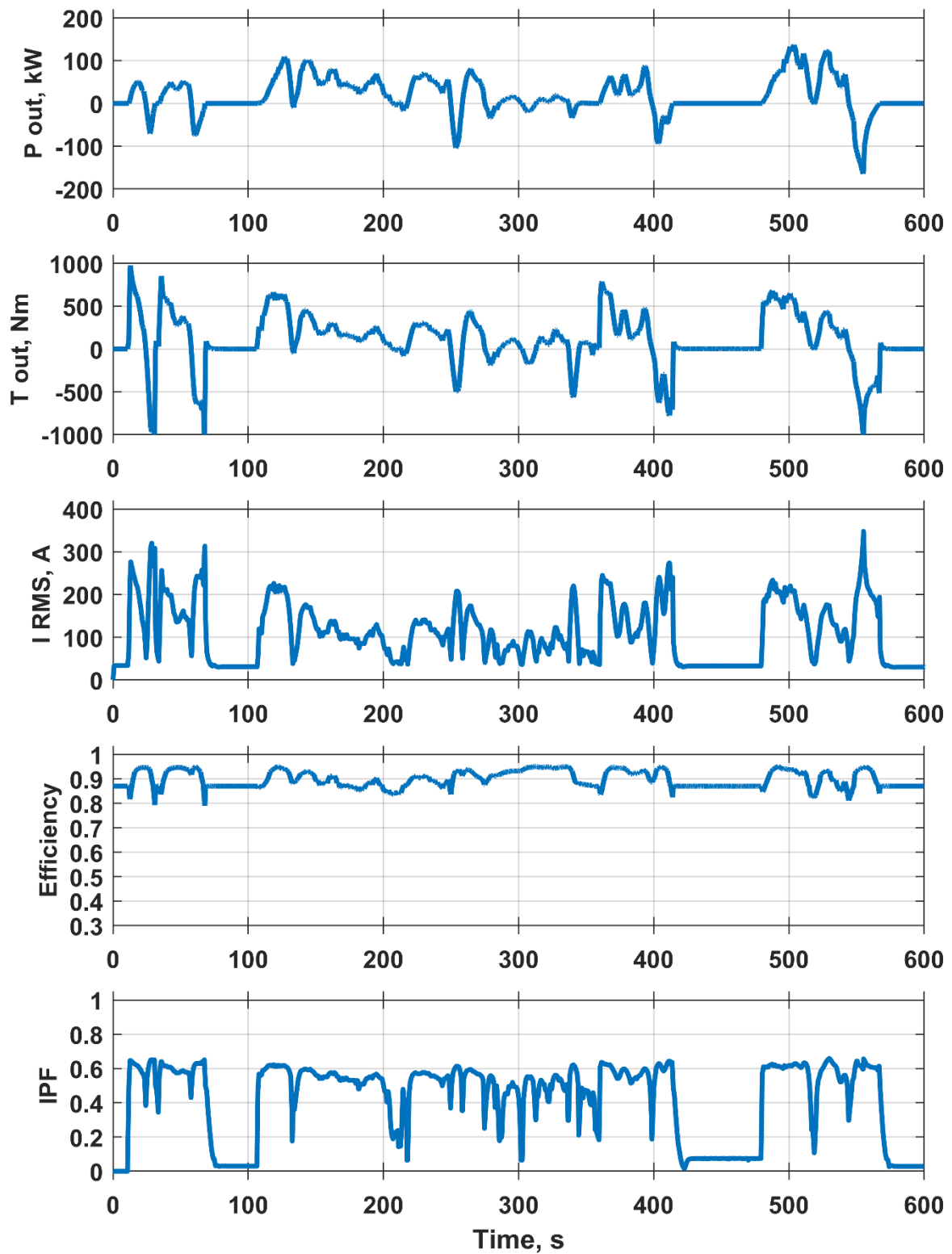


Fig. A3.2. SynRM parameters with MTPA under WLTP Class 1 low phase.

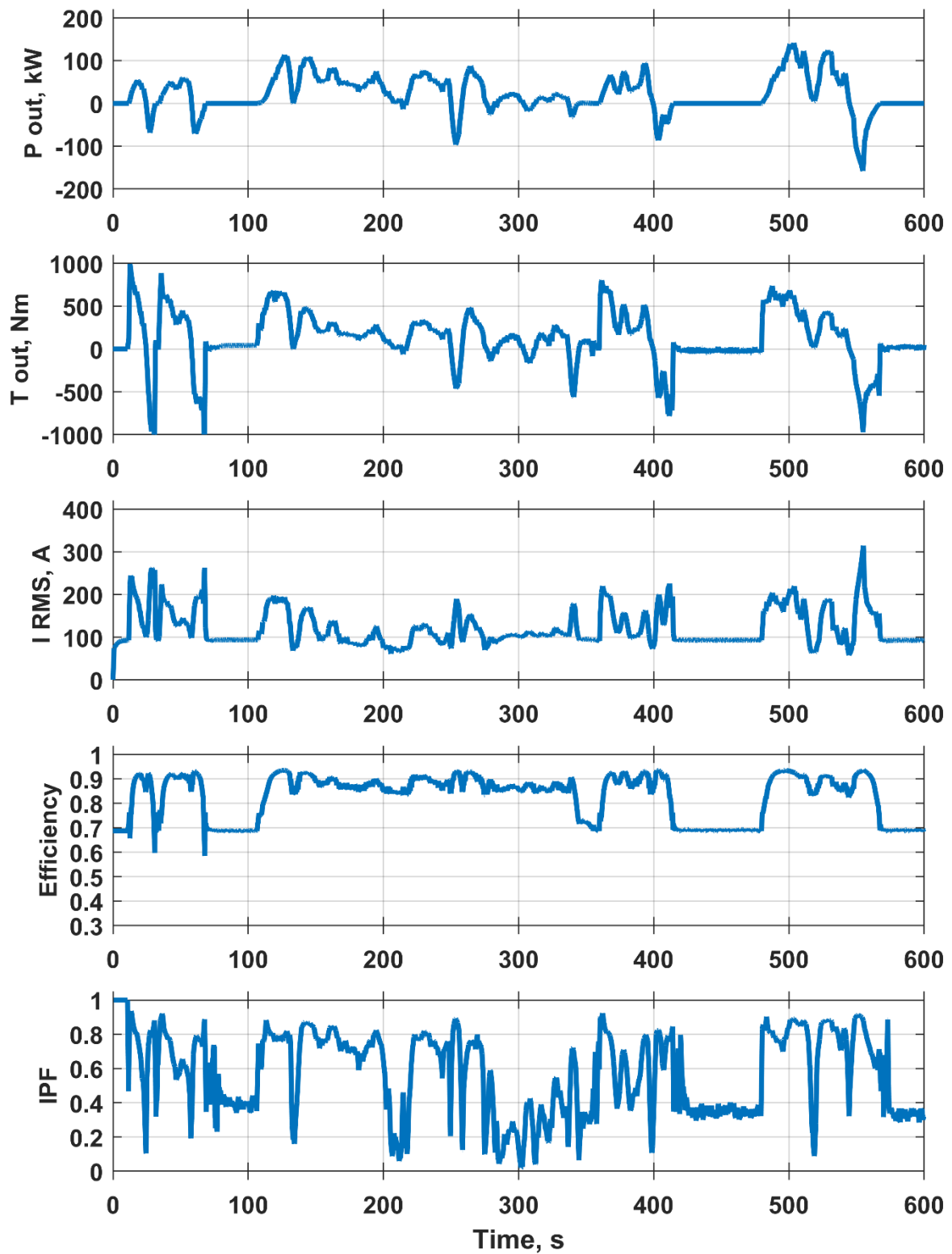


Fig. A3.3. IM parameters with CDAC under WLTP Class 1 low phase.